University of Torino
Department of Molecular Biotechnology and Health Sciences
Molecular Biotechnology Center "Guido Tarone"

Molecular Medicine Ph.D. program
XXXVI cycle, academic years 2020/2024

The Role of the RAC1-Regulating Proteins ARHGAP15 and ARHGEF6 in the Development of Forebrain GABAergic INs

Ph.D. Candidate:
Carla Liaci

Supervisor:
Prof. Giorgio Roberto Merlo, University of Torino, Department of Molecular Biotechnology and Health Sciences

Doctoral Examination Committee:
Prof. Luciano Conti, University of Trento, Department of Cellular, Computational and Integrative Biology - CIBIO
Prof. Anna Cariboni, University of Milano, Department of Pharmacological and Biomolecular Sciences

Torino
November 11, 2024

Summary

My doctoral research focused on investigating forebrain development in gene-disruption models with altered RAC1 GTPase pathway activity. Specifically, I studied the effects of mutations in two key regulatory proteins of RAC1 GTPase, ARHGAP15 and ARHGEF6, on neurogenesis, migration, and differentiation dynamics.

The second chapter presents the results of a study aimed at investigating the effects of *Arhgap15* ablation, a gene encoding a specific negative regulator of RAC1, on the migration and maturation of cortical GABAergic INs (CINs) during mouse development. This study revealed that ARHGAP15 exerts a nuanced negative regulation on RAC1-dependent cytoskeletal remodeling, crucial for morphological maturation and directional control during CIN migration, ultimately influencing their laminar distribution and inhibitory function (Liaci et al., 2022) .

Chapter 3 delves into the role of ARHGEF6, a positive regulator of RAC1, in both mouse and human forebrain development. Mutations in ARHGEF6 are causally linked to non-syndromic intellectual disability (ID) MRX46 (OMIM: 300436). The study showed that *Arhgef6-KO* mice exhibit a significant reduction in hippocampal GABAergic INs (INs), particularly in the CA2 and CA3 regions, along with impairments in IN maturation. To explore the human context, we generated *ARHGEF6-KO* human induced pluripotent stem cells (hiPSCs). hiPSC-derived ventral organoids were utilized to assess alterations in ARHGEF6-KO related to cell proliferation, differentiation, and survival. Studies on dorsal-ventral assembloids demonstrated that *ARHGEF6-KO* INs exhibit a distinct migration phenotype, contributing to the reduction of the number of INs reaching the dorsal compartment. Overall, these results suggest that the observed defects in the number of GABAergic INs at the hippocampal level may arise from three primary factors: impaired progenitor proliferation and differentiation capacity, decreased survival, and migration defects.

Collectively, these findings reinforce the previously established link in the literature between ID and alterations in forebrain GABAergic system development. Our data further highlight the critical role of the RAC1 pathway in regulating the proliferation, differentiation, and migration of progenitors and INs.

Acknowledgments

I would like to thank my mentor, Professor Giorgio Roberto Merlo, for his constant support and unwavering belief in my ability to succeed as a scientist. You once told me that when you first got into developmental biology, you thought it was the most beautiful thing ever. Now I think you were absolutely right.

I would like to thank Professors Giorgia Quadrato and Luciano Conti for their invaluable contribution to my education. Your guidance and teachings have enabled me to achieve significant milestones. I am deeply grateful to you.

I would like to express my sincere gratitude to my committee member, Professor Anna Cariboni, for her availability, assistance, and kindness.

I would like to express my sincere gratitude to all my lab mates who contributed to this work: Mattia Camera, Jean-Paul Urenda, Lucia Prandi, Beatrice Savarese, Simona Rando, Giovanni Catapano, and Van Truong (Jennifer). Mattia and JP, your brilliance and passion are truly inspiring. I am fortunate to have shared much of my work with you.

I would also like to thank all my friends and colleagues, particularly Luca, Pietro, Federico, Rebecca, Lorenzo, Giovanni, Ilaria, Ingrid, Gabriele, Giulia, and Jojo. I feel incredibly lucky to have met you all during this journey. You made these years so much more meaningful.

And finally, I would like to thank my family, Delfina, Luigi, and Massimiliano, and my dearest Chiara, Alessia, Mirea, Manuela, and Simone, for their undying love and support.

Contents

Chapter 1
Introduction

1.1 Cytoskeleton functions in neuronal development

During development, neurons migrate to find synaptic partners and establish the complexity of the neuronal wiring. Neurite extension and navigation are possible thanks to the formation of the growth cone, a sensory-motile structure at the tip of the growing axon directed by chemotaxis (Kahn & Baas, 2016). The structure of the growth cone is characterized by a dynamic periphery, in which actin filaments extend and retract to explore the surrounding environment, and by a more stable center that forms the axonal shaft (Lowery & Vactor, 2009). The interplay between microtubule assembly and actin dynamics is then essential for axonal elongation. The polarity of microtubules, essential for the directional transport of proteins and organelles (Maday et al., 2014), allows the sliding movement that supports axon formation, as tubulin monomers are continuously transported at the leading edge of the growth cone (E. Tanaka & Sabry, 1995). Microtubules' and actin filaments' polymerization result from the addition of α/βtubulin and glomerular actin (G-actin), respectively (Lewis et al., 1997). The rate of filament elongation and morphogenesis depends on the concentration and availability of monomers but also on the presence of proteins that regulate the assembly/disassembly kinetics and those responsible for increasing the level of complexity for higher-order network structures (Johnson & Jope, 1992). While microtubules are the stiffest components of the cytoskeleton and can switch between a stably growing state and a rapidly shrinking one, actin filaments are less rigid and more organized, supporting the overall structure and allowing the motility of the leading edge (Pollard & Borisy, 2003). It is assumed that growth cones are already provided with all the proteins necessary for synaptogenesis during their search for contacts (Haydon & Drapeau, 1995). The protrusion of filopodia finger-

like structures retract upon contact with the postsynaptic cell to form a vestigial presynaptic terminal. These filopodia are characterized by a less tight bundle that is more dynamic compared to the architectural stability of conventional filopodia (Korobova & Svitkina, 2010). This dynamism is required to let the nascent spine be perfectly aligned between the presynaptic active zone and the postsynaptic density (PSD). Juxtaposition is possible thanks to the presence of cell adhesion molecules that provide perfect docking geometries between the two membranes in the synaptic cleft (Südhof, 2018). The actin cytoskeleton is involved in spine morphogenesis, as it controls changes in spine shapes. Immature dendritic spines show linear and thin-like structures, but, after contacting the presynaptic terminal, actin filaments begin to cluster and enlarge the contact surface to form a mature spine with a mushroom-like shape (Yoshihara et al., 2009a). This is conceivable thanks to actin-related proteins that generate branched filaments, such as the ARP2/3 complex, balanced with capping proteins, such as CAPZ, to restrict their elongation and actin severing proteins, such as ADF/cofilin, that enhance filament disassembly (Spence & Soderling, 2015). In addition, several scaffold proteins contribute to the maturation of dendritic spines controlling actin dynamics, *e.g.*, PSD95, SHANK, and SRCIN1 (also known as p140Cap) (Repetto et al., 2014; Sala et al., 2001; Yusifov et al., 2021). Synapses are not static formations. They undergo changes in postnatal life, while carrying out specific activities, *e.g.*, learning, and in specific periods, *e.g.*, synaptic pruning during adolescence. Synaptic plasticity takes place in an activity-dependent manner: LTP is the result of strengthened synapses after high-frequency stimulation from the presynaptic terminal, while long-term depression (LTD) is a decrease in synaptic activity after low-frequency signals (Huganir & Nicoll, 2013). For LTP, the presence of NMDA-type glutamate receptors in the membrane of the postsynaptic cells allows the insertion of new AMPA receptors in response to high-frequency stimuli. The localization of these ionotropic, excitatory glutamate receptors leads to an increase in the postsynaptic current and consequently to a stronger connection in a positive feedback loop. Both AMPA receptors' and NMDA receptors' trafficking relies on the actin cytoskeleton (Allison et al., 1998; C. H. Kim & Lisman, 1999; Zhou et al., 2001).

1.2 The core regulation of actin dynamics

Alterations in neurites and spine morphology, as well as in neuronal migration properties, have been consistently associated with intellectual disability (ID) and other neurodevelopmental disorders (NDDs) that include ID as a main and recurrent phenotype (Irwin et al., 2000). These developmental features rely on the proper actin cytoskeleton dynamics, as neurite outgrowth, axonal migration, synaptogenesis, and synaptic plasticity are the result of three main processes: fibrous-actin (F-actin) dynamics (elongation/severing/branching), actin–myosin

contractility, and F-actin coupling with the extracellular matrix (Kozma et al., 1997; Smith, 1994). All three processes are regulated by a complex protein network in which the Rho-family small GTPases RAC1, CDC42, and RHOA emerge as hubs (**Figure 1**).

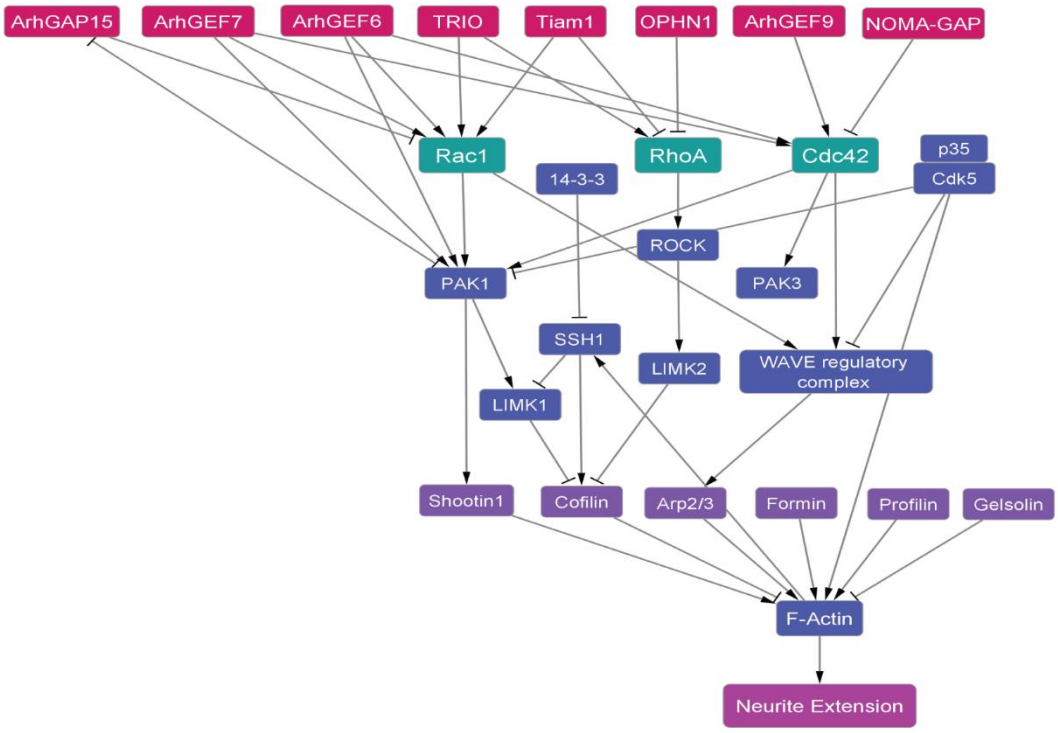

Figure 1: PPI network of the best-characterized components of the Rho GTPase signaling RAC1, RHOA, and CDC42. Boxes represent the nodes (proteins), while the arrows indicate the edges (interactions). GTPases are reported in green, their GEFs and GAPs in red, their effectors in blue, and actin-binding or actin-modifying proteins in purple. Edges can be either "activator" (arrowheads) or "inhibitor" (blunted lines). The "neurite elongation" node represents the phenotypic outcome.

1.2.1 Rho GTPases and Effectors

This section illustrates in detail the key components of the signaling pathway responsible for the control of the dynamics of the actin cytoskeleton, focusing on the biochemical and cellular role of each protein and its links with neurological and cognitive deficits in human and animal models.

RAC1: RAC1 is a key regulator of neurite elongation, axon migration, synaptic function, and synaptic plasticity, as it promotes neurite outgrowth [85], spine

formation and stabilization (Tashiro et al., 2000), and clustering of AMPA and NMDA receptors in the postsynaptic memane (Duffney et al., 2013), and it is essential for long-term synaptic plasticity in the hippocampus, which is the molecular mechanism at the base of learning and memory formation (Martinez & Tejada-Simon, 2011). Formation and stabilization of integrin-dependent adhesion sites at membrane protrusion require local RAC1 activation followed by local RAC1 inactivation (S. Woo & Gomez, 2006). Moreover, the expression of constitutively active RAC1 inhibits NGF-induced neurite outgrowth, indicating that tight spatiotemporal regulation of RAC1 signaling is required for optimal neurite outgrowth. Seven de novo missense RAC1 variants have been reported in patients with mild to severe ID (Lelieveld et al., 2016; Reijnders et al., 2017). Among them, two function as dominant-negative alleles (p.Cys18Tyr and p.Asn39Ser), while one is a constitutively active allele (p.Tyr64Asp) (Reijnders et al., 2017). For the other mutations, it is not clear if they generate dominant-negative alleles or if they could result in a condition of haploinsufficiency. Interestingly, the p.Cys18Tyr variant prevented GTP-mediated activation of RAC1 and prevented overexpression of the mutated RAC1 from inhibiting the induction of LTP in the hippocampus (Tian et al., 2018). In mice, the deletion of Rac1 in the ventricular zone of the telencephalon resulted in ventricles enlargement, impaired migration of median ganglionic eminence-derived INs, and impaired projection of commissural and corticothalamic axons. Interestingly, primary Rac1-deficient neurons had increased neurites formation and branching, indicating that RAC1 may be dispensable for neuritogenesis per se (L. Chen et al., 2007).

CDC42: CDC42 plays a critical role in neurite outgrowth, neuronal migration, and dendritic spines formation and maturation (Wong et al., 2001). It is also essential for the establishment of neural polarity, as it promotes axon formation and elongation by regulating ADF/cofilin activity at the growth cone and by promoting microtubules stability through DPYSL2 (dihydropyrimidinase-like 2) (Garvalov et al., 2007; Li et al., 2021). Eight CDC42 de novo missense mutations have been reported in 13 unrelated patients showing several developmental abnormalities, including ID and dysmorphic facial features (Motokawa et al., 2018; Takenouchi et al., 2016). In vitro studies and experiments involving C. elegans showed that these mutations result in proteins with altered activity and/or impaired target interactions, with some mutations acting as a gain of function and others acting as hypomorphs. Notably, one missense mutation of CDC42, which has been described as a de novo mutation in one individual and inherited mutation in three related individuals, resulted in a hypomorphic allele associated with several developmental phenotypes, but not with ID (Martinelli et al., 2018). Overall, the complex and heterogeneous

set of developmental abnormalities associated with CDC42 mutations may reflect different functional consequences of the single mutations. Brain-specific Cdc42-KO mice die soon after birth and show a reduced cortical mass and a widespread loss of axonal tracts (Garvalov et al., 2007). The effects of CDC42 depletion in the postnatal brain have been assessed using *Cdc42*$^{flox/flox}$, Camk2a-CRE mice, in which CRE recombinase is expressed in cortical pyramidal neurons and hippocampus starting from P16-P19. These mice showed reduced spine density and LTP in the hippocampus, together with memory deficits (I. H. Kim et al., 2014).

RHOA: Broadly speaking, the effects of RAC1 and CDC42 signaling on neurite outgrowth and dendritic spine formation are antagonized by RHOA signaling (Kozma et al., 1997; S. Woo & Gomez, 2006; Yamaguchi et al., 2001). RHOA activity inhibits the formation of integrin-dependent adhesions (Penzes et al., 2013), promotes neurite retraction by activating myosin 2a (Hirose et al., 1998; Jalink et al., 1994; Kubo et al., 2008; Pilpel & Segal, 2004), and negatively regulates spine formation and maintenance (Pilpel & Segal, 2004). Interestingly, KCTD13 (potassium channel tetramerization domain containing 13) and CUL3 (cullin 3), two genes linked to NDDs, are involved in RHOA ubiquitination (Y. Chen et al., 2009; G. N. Lin et al., 2015; T. Wang et al., 2016), and RHOA inhibition rescues synaptic transmission, learning, and memory defects in Kctd13-KO mice (Escamilla et al., 2017; Martin Lorenzo et al., 2021). These findings are consistent with the notion that RHOA dysregulation itself is linked to NDDs.

PAK1: Six PAK proteins have been identified in mammals. Based on their sequence homology, PAKs are classified into two groups, the first including PAK1, PAK2, and PAK3 and the second including PAK4, PAK5, and PAK6. All six PAKs are expressed in the nervous system with a different spatio-temporal pattern, with PAK1 and 3 being the most studied in the context of neuronal function (Zhang et al., 2022). Active RAC1 and CDC42 bind to the CRIB region of PAK1, relieving its autoinhibition and promoting its kinase activity (Manser et al., 1994). PAK1 plays a critical role in both synaptic function and axon migration. Pak1-KO mice show impaired LTP at hippocampal CA1 synapses, reduced enrichment of F-actin at dendritic spines, and impaired NMDA-dependent ADF/cofilin phosphorylation (Asrar et al., 2009). Both overexpression and inhibition of PAK1 in the mouse developing brain led to profound defects in the migration of cortical neurons (Causeret et al., 2009). In humans, gain of function missense variants in PAK1 have been associated with ID, macrocephaly, and seizures (Horn et al., 2019; Ohori et al., 2020). Interestingly, deficits in the PAK1 pathway may partially explain the impaired migration of GABAergic neurons in DS patients (Huo et al., 2018).

PAK3: Differently from PAK1, which is activated by both RAC1 and CDC42, PAK3 is mainly activated by CDC42 (Kreis et al., 2007). Mutations of PAK3 are associated with XLID (Duarte et al., 2020; Qian et al., 2020). Two PAK3 variants responsible for severe ID and corpus callosum agenesis (G424R and K389N) were shown to suppress kinase activity, increase the interaction between PAK3 and the guanine exchange factor ARHGEF6 (Rac/Cdc42 guanine nucleotide exchange factor 6, also known as α-PIX), and inhibit cell migration (Duarte et al., 2020). Another variant (R67C) inhibits the binding of PAK3 to CDC42, impairing PAK3 activation (Kreis et al., 2007). In mice, the latter variant impacts cognitive functions and adult hippocampal neurogenesis (Castillon et al., 2020). Likewise, Pak3-KO mice have no apparent defects in the actin cytoskeleton, but showed impaired hippocampal LTP, together with learning and memory deficits (Meng et al., 2005).

LIMK1: LIMK1 (LIM domain kinase 1) is a serine–threonine kinase that possesses two LIM domains, a PDZ domain, and a C-terminal kinase catalytic domain (Okano et al., 1995). LIMK1 is a key downstream target of RAC1 signaling and is activated by PAK1 by phosphorylation at the Thr-508 residue (Edwards et al., 1999). Dominant-negative LIMK1 inhibits RAC1-stimulated lamellipodial protrusion (N. Yang et al., 1998), CDC42-induced filopodia formation, and RHOA-mediated stress fibers formation in Cos-7 cells (Sumi et al., 1999). Neurons of Limk1-KO mice showed reduced growth cone size and altered dendritic spine morphology (Meng et al., 2005). In humans, heterozygous deletion of 27 genes, including LIMK1, results in Williams syndrome, a complex developmental disorder characterized by ID and impaired long-term memory (Hoogenraad et al., 2004). Interestingly, *Limk1*+/− mice also showed impaired long-term memory, together with reduced late-LTP in the hippocampus (Pröschel et al., 1995), indicating the LIMK1 haploinsufficiency in Williams syndrome patients may be causally related to memory defects. Unlike LIMK1, which is specifically expressed in the nervous system and enriched at mature synapses, LIMK2 is ubiquitously expressed (Pröschel et al., 1995; J. Y. Wang et al., 2000), although it has been less studied. In the neuronal context, there is evidence for the role of LIMK2 in neurite outgrowth and neuronal migration (Andrews et al., 2013; Tastet et al., 2012).

ROCK: ROCK (Rho-associated coiled-coil containing protein kinase) is activated by active RHOA (Ishizaki et al., 1996; Matsui et al., 1996). Two ROCK isoforms exist: ROCK1, which is prominently expressed in non-neuronal tissues such as liver and testis, and ROCK2, which is mainly expressed in brain and skeletal muscle (Nakagawa et al., 1996). ROCK activity stabilizes actin filaments by activating LIMK, which in turn inactivates ADF/cofilin (Maekawa et al., 1999;

Ohashi et al., 2000); on the other hand, ROCK promotes actomyosin contractility and stress fibers formation by phosphorylating MLC9 (myosin light chain 9) at Ser19, the same residue phosphorylated by MLCK (myosin light chain kinase) (Amano et al., 1996), and by phosphorylating MBS, the regulatory subunit of myosin light chain phosphatase (Katoh et al., 2001; Kimura et al., 1996). A nonsense variant of ROCK was identified in an ID patient (Bowling et al., 2017). The pharmacological inhibition of actomyosin contractility inhibits actin retrograde flow and actin filaments' severing and promotes neurite outgrowth in the early stages of neuronal polarization (Kollins et al., 2009; Medeiros et al., 2006), indicating that RHOA opposes neurite elongation by stimulating actomyosin contractility. Notably, PAK1 inhibits MLCK (Sanders et al., 1999), suggesting that RAC1 and RHOA act antagonistically on actomyosin contractility.

Cdk5-p35: CDK5 (cyclin-dependent kinase 5) is activated by binding with the specific protein partners CDK5R1 (cyclin-dependent kinase 5 regulatory subunit 1, also known as p35) and CDK5R2 (also known as p39) (Tang et al., 1995; Tsai et al., 1994). CDK5 is important for neuronal migration, neurite outgrowth, axon guidance, and synaptogenesis during brain development and for synaptic plasticity during adulthood (Hawasli et al., 2007; Hisanaga & Endo, 2010). CDK5 controls cytoskeleton remodeling by regulating Rho GTPases and by stabilizing actin filaments through p35-mediated-binding to F-actin (He et al., 2011). CDK5 functions as a balance factor, as it can both facilitate RHOA-mediated growth cone collapse or dendritic spine retraction through phosphorylation of NGEF (neuronal guanine nucleotide exchange factor, also known as ARHGEF27) (Fu et al., 2007) or inhibit these processes by phosphorylating CDKN1B (cyclin-dependent kinase inhibitor 1B) and prevents RHOA activation by guanine exchange factors (GEFs) (Besson et al., 2004; Kawauchi, 2015). Similarly, CDK5 activates RAC1 via phosphorylation of KALRN (kalirin RhoGEF kinase) to promote dendritic spine stabilization (Xin et al., 2008) or inhibits RAC1 activation via phosphorylation of a RASGRF2 (Ras protein-specific guanine nucleotide releasing factor 2) or PPP1R9A (protein phosphatase 1 regulatory subunit 9A, also known as neurabinI) (Causeret et al., 2007; Kesavapany et al., 2004). CDK5 can also indirectly regulate CDC42-mediated dendrite outgrowth and extension via phosphorylation of NTR (neurotrophic receptor tyrosine kinase 2) (Cheung et al., 2007). In a mutation screening, novel silent mutations in CDK5 and p35 were identified: three intronic variations and four heterozygous variations in a cohort of 360 patients with non-syndromic ID, suggesting that these mutations and polymorphisms may contribute to ID phenotype (Moncini et al., 2016).

1.2.2 GAPs and GEFs

Small GTPases cycle between a GTP-bound active state and a GDP-bound inactive state. The most important regulators of small GTPases are GTPase-activating proteins (GAPs), which promote GTP hydrolysis, GEFs, which promote activation by inducing the release of GDP and the binding of GTP, and guanine **dissociation** inhibitors, which prevent GDP dissociation (Cherfils & Zeghouf, 2013).

OPHN1: OPHN1 is an F-actin binding protein ubiquitously expressed in the central nervous system in both glial cells and neurons, where it mainly localizes at the tip of growing neurites, growth cones, and dendritic spines (Fauchereau et al., 2003; Khelfaoui et al., 2007). It shows GAP activity towards RHOA, and, to a lesser extent, towards RAC1 and CDC42 (Billuart et al., 1998; Fauchereau et al., 2003; Khelfaoui et al., 2007). In humans, LOF mutations in OPHN1 cause syndromic XLID, in which ID is associated with epilepsy, ventriculomegaly, and cerebellar hypoplasia (Bergmann et al., 2003; Nuovo et al., 2021). Ophn1-KO mice recapitulate some aspects of the human phenotype, such as social, behavioral, and cognitive impairments, as well as ventricular enlargement and susceptibility to seizures (Busti et al., 2020; Khelfaoui et al., 2007). At the cellular level, Ophn1-KO mice show hyperexcitability of the hippocampal network, associated with a reduced number of hippocampal GABAergic INs, impaired dendritic spine maturation, and short-term synaptic plasticity (Busti et al., 2020; Khelfaoui et al., 2007). Moreover, OPHN1-deficient human iPSCs showed decreased neurogenic potential and impaired neurite elongation (Compagnucci et al., 2016).

ARHGAP15: ARHGAP15 (Rho GTPase activating protein 15) is a RAC-specific GAP protein, expressed in both excitatory and inhibitory neurons of the adult hippocampus and cortex. It is a negative regulator of RAC1/RAC3 activity, and its loss results in the hyperactivation of the RAC1 pathway (Zamboni et al., 2016). ARHGAP15 comprises a pleckstrin homology domain, which mediates its membrane localization and consequent activation via binding to the PI3K product phosphatidylinositol 3,4,5-trisphosphate (Zamboni et al., 2016). *Arhgap15*-KO mice showed altered neuritogenesis and synaptic density, resulting in increased spike frequency and bursts, accompanied by poor synchronization. Its loss mainly impacts IN-dependent inhibition. Adult *Arhgap15*-KO mice showed defective hippocampus-dependent functions such as working and associative memories (Zamboni et al., 2016). In humans, the loss of ARHGAP15 has been reported in a rare variant of Mowat– Wilson disease, which is characterized by severe

neurological deficits, severe ID, speech impairment, and ASD (Mulatinho et al., 2012; Smigiel et al., 2010).

NOMA-GAP: ARHGAP33 (Rho GTPase activating protein 33, also known as NOMAGAP) is a multi-adaptor protein with GAP activity, and it is a major negative regulator of CDC42 (Rosário et al., 2007). NOMA-GAP has been shown to be essential for NGF-stimulated neuronal differentiation through the inhibition of CDC42 signaling and regulation of the ERK5-MAPK signaling (Rosário et al., 2007). *Noma-gap*-KO mice showed hyperactivity of CDC42 and reduced complexity of dendritic arborization (Rosário et al., 2012).

TRIO: TRIO (trio Rho guanine nucleotide exchange factor) is a conserved Rho GTPase regulator that is highly expressed during brain development (Debant et al., 1996; Pengelly et al., 2016). It contains two functional GEF domains: GEFD1, which regulates RAC1 and RHOG activity, and GEFD2, which regulates RHOA activity. It is involved in actin remodeling and it is necessary for cell migration and growth. TRIO controls, through RAC1 activation, cytokinesis, axon outgrowth, and guidance and modulates excitatory synaptic transmission (Ba et al., 2013; Schmidt & Debant, 2014). In the developing hippocampal neurons, it limits dendrite formation without affecting the establishment of axon polarity. While Trio-KO has been shown to be embryonically lethal (O'Brien et al., 2000), hippocampus- and corte x-specific Trio-KO and heterozygous mice show progressive defects in learning ability, sociability, and motor coordination (Katrancha et al., 2019; Pengelly et al., 2016). Whole-exome sequencing studies identified TRIO de novo mutations in several patients affected by NDDs in which ID appears as a prominent phenotype (Ba et al., 2016).

ARHGEF6 and ARHGEF7: ARHGEF6 and ARHGEF7 (Rho guanine nucleotide exchange factor 7, also known as βPIX) are GEFs of the Rho GTPases. ARHGEF6 has been shown to be specific for RAC1, activating and targeting it to membrane ruffles and focal adhesions (ten Klooster et al., 2006). On the other hand, Arhgef6-KO mice showed a significant reduction in the activity of both RAC1 and CDC42, but only at the hippocampal level (Ramakers et al., 2012). Both proteins share an SH3 domain, a prerequisite for the binding with PAK1, PAK2, and PAK3 (Manser et al., 1994; Santiago-Medina et al., 2013) stressed the importance of the subtle regulation exerted on adhesion dynamics and membrane protrusions by PAK–ARHGEF6 and PAK–ARHGEF7 interactions during neurite outgrowth, as the partial inhibition of the interaction robustly stimulates neurite outgrowth and growth cone point contacts' turnover, whereas the complete inhibition freezes it

stabilizing adhesions. Both ARHGEF6 and ARHGEF7 present the Dbl homology and pleckstrin domains, which possess RhoGEF activity. Moreover, an ARHGEF7 transcriptional isoform presents a PDZ target at the C-terminal, functional to the binding with PDZ protein, e.g., SHANKs (SH3 and multiple ankyrin repeat domains), at the excitatory synaptic sites (Park et al., 2003). Mutation screening of 119 patients with nonspecific ID revealed a T > C variant in the first intron of ARHGEF6 (c.166-11T > C) (Kutsche et al., 2000; Yntema et al., 1998), although the pathogenicity of this specific variant was then questioned [190]. In addition, a male patient with severe ID, carrying a molecularly unbalanced translocation (X;21) disrupting ARHGEF6, was then identified (Kutsche et al., 2000). *Arhgef6*-KO mice showed an increased dendritic length of hippocampal pyramidal neurons, reduced spine synapses, an overall reduction in early-phase LTP, and an increase in LTD, together with impaired spatial and complex learning and less behavioral control in mildly stressful situations, resembling the human ID phenotype, thus validating Arhgef6- KO mice as a proper ID animal model (Ramakers et al., 2012). For what concerns ARHGEF7, the case of two siblings presenting generalized epilepsy and ID was reported, consequently to the 13q34 deletion. This genomic locus contains two protein-coding genes, SOX1 (SRY-box transcription factor 1) and ARHGEF7, thereby supporting the possible contribution of ARHGEF7 haploinsufficiency to the pathogenic phenotype (Piton et al., 2013). *Arhgef7*-KO mice showed embryonic lethality at E9.5; for this reason, the in vivo role of ARHGEF7 was investigated through heterozygous or cortex-specific KO mice . These models demonstrated that ARHGEF7 is essential in both neuritogenesis and synaptogenesis during cortical and hippocampal development, since its loss results in extensive loss of axons and reduced dendritic complexity, as well as in a decrease of synaptic density. Furthermore, Arhgef7 heterozygous mice exhibited impaired social interactions (Kwon et al., 2019).

ARHGEF9: ARHGEF9 is a brain-specific GEF that specifically activates CDC42 [194]. It regulates, through the recruitment and activation of CDC42, the clustering of GPHN (gephyrin) at postsynaptic sites (Tyagarajan et al., 2011). GPHN clusters, in turn, promote postsynaptic clustering of glycine receptors and GABAA receptors (Pizzarelli et al., 2020). Arhgef9-KO mice showed reduced GABAA receptor clusters at dendritic spines, enhanced LTP, increased levels of anxiety, and impaired spatial learning (Papadopoulos et al., 2007). In humans, ARHGEF9 mutations cause a XLID syndrome associated with seizures and facial dysmorphism (Alber et al., 2017; J.-Y. Wang et al., 2018; R. Yao et al., 2020).

TIAM1: TIAM1 (TIAM Rac1 associated GEF 1) is a GEF protein highly expressed in the developing nervous system that activates RAC1 and, to a lesser extent, CDC42 and RHOA (Ehler et al., 1997; Michiels et al., 1995). RAC1 activation by TIAM1 is required for neurite outgrowth induced by NGF/NTRK1, BDNG/NTRK2, and Ephrin/Eph signaling (Leeuwen et al., 1997; Miyamoto et al., 2006). Moreover, suppression of TIAM1 activity leads to defects in axonogenesis and radial migration (Kawauchi, 2015; Kunda et al., 2001). TIAM1 is also required for spine formation and morphogenesis in response to various extracellular signals. In particular, Eprin-B1/EphB2 signaling promotes spine development by activating RAC1 through TIAM1, while NMDA-mediated calcium influx at glutamatergic synapses activates a CAMK2 (calcium/calmodulin-dependent protein kinase II)-TIAM1 complex that persistently activates RAC1, leading to LTP and spine enlargement (Saneyoshi et al., 2019; Tolias et al., 2007); interestingly, knock-in mice harboring a mutation that inhibits the formation of the CAMK2– TIAM1 complex showed reduced RAC1 activity and memory deficits (Kojima et al., 2019). TIAM1 activity seems to be exquisitely relevant for granule neurons of the dentate gyrus, as TIAM1 knock-down (KD) in these cells led to fewer glutamatergic synapses expressing AMPA receptor and to an increased spine length, while no effect was observed upon TIAM1 KD in CA1 neurons (Rao et al., 2019). Consistent with this finding, Tiam1-KO mice showed defective maintenance of the dendritic arborization and impaired stabilization of dendritic spines in the granule neurons (Cheng et al., 2021). Strikingly, these mice showed enhanced contextual learning and memory (Cheng et al., 2021). For this reason, and considering that TIAM1 is overexpressed in DS patients, the authors of this study speculated that elevated levels of TIAM1 contribute to the learning and memory deficits associated with DS.

1.2.3 Actin binding proteins

The effects of RAC1, CDC42, and RHOA on actin dynamics are mediated by actin-binding proteins (ABPs), which are classified according to their activity: actin depolymerization, such as ADF/cofilin, branching, such as ARP2/3, severing, such as GSN (gelsolin), bundling, such as fascin family proteins, and nucleotide exchanging, such as profilin family proteins (Winder & Ayscough, 2005).

ADF/cofilin: LIMK1 inhibits ADF/cofilin proteins by phosphorylation at the Ser3 residue (Arber et al., 1998; Lappalainen & Drubin, 1997). This protein family is composed of three isoforms: DSTN (destrin, actin depolymerizing factor, also known as ADF), CFL1 (cofilin 1), which is the most expressed in the central nervous system, and CFL2, which is specifically expressed in muscle tissue (Agnew

et al., 1995; Maciver & Hussey, 2002). Since most studies addressing the roles of ADF/cofilin do not specify the isoform and most antibodies do not differentiate between these isoforms, this protein family is referred to simply as ADF/cofilin. ADF/cofilin binds to ADP-actin, increasing the depolymerization rate of the pointed end and causing the severing of actin filaments (Sumi et al., 1999; Svitkina & Borisy, 1999). This leads to an increase in G-actin availability and the number of barbed ends, resulting, at physiological ATP-actin concentrations, in actin reorganization and promoting axon elongation. Importantly, not only the balance but also the cycling between the active and inactive forms of ADF/cofilin plays a role in modulating actin dynamics (Bravo-Cordero et al., 2013; Garvalov et al., 2007; Meberg & Bamburg, 2000). SSH: Proteins of the Slingshot family (SSH1-3 in mammals) dephosphorylate ADF/cofilin at Ser3 (Niwa et al., 2002), thereby controlling actin dynamics and reorganization. SSH proteins mediate NGF-induced neurite extension. SSH1 and SSH2 KD suppress neurite extension by increasing the concentration of the non-phosphorylated form of ADF/cofilin (Endo et al., 2007).

YWHAZ: YWHAZ (tyrosine 3-monooxygenase/tryptophan 5-monooxygenase activation protein zeta, also known as 14-3-3 ζ) is an adaptor protein that affects actin dynamics via the stabilization of phospho-ADF/cofilin (Gohla & Bokoch, 2002) and the regulation of SSH and Int. J. Mol. Sci. 2021, 22, 6167 13 of 43 LIMK1 (Soosairajah et al., 2005). Additionally, it has been shown that 14-3-3 ζ inhibits the ubiquitin-mediated degradation of δ-catenin (Toyo-oka et al., 2014), a component of the cadherin–catenin cell adhesion complex, which in turn inhibits RHOA and activates CDC42 and RAC1 (Anastasiadis et al., 2000; Noren et al., 2000; Taniuchi et al., 2005). 14-3-3 ζ-KO mice present reduced spine density, stressing the importance of this protein in the regulation of the actin cytoskeleton (Xu et al., 2015).

ARP2/3: The ARP2/3 complex is a heptameric complex formed by ACTR2 (actin-related protein 2, also known as ARP2), ACTR3 (also known as ARP3), and ARPC1-5 (actin-related protein complex 1–5) (Rotty et al., 2013). It binds existing actin filaments and initiates the formation of new filaments that branch off the existing filaments at an angle of about 70◦ (Pollard, 2007). The axon guidance molecules VEGF and SEMA3A affect actin dynamics at the growth cone by increasing and decreasing ARP2/3 activity, respectively (Brown & Bridgman, 2009; Schlau et al., 2018). Thus, ARP2/3 is essential for neuronal migration (Yoshihara et al., 2009b) but also for spine formation, maturation, and maintenance (Chou & Wang, 2016; I. H. Kim et al., 2013). The postnatal loss of ARPC3 in forebrain excitatory neurons leads to progressive spine loss and defective LTP-

induced spine volume expansion (I. H. Kim et al., 2013). Moreover, ARP2/3 activity is required for the maturation of filopodia into spines and for the recruitment at the postsynaptic membrane of AMPA receptors, a process that is essential for the functional maturation of excitatory synapses (Spence et al., 2016). The activity of ARP2/3 is also controlled by PAK1, which can phosphorylate ARPC1 promoting F-actin polymerization and branching (Vadlamudi et al., 2004).

NPFs: The activity of nucleation-promoting factors (NPFs) is required to activate the nucleation and branching activity of the ARP2/3 complex. These factors include WASP (Wiskott–Aldrich syndrome protein), N-WASP (neural WASP), the WAVE regulatory complex (WRC) formed by WASF1 (WASP family member 1), CYFIP1 (cytoplasmic FMR1 interacting protein 1), ABI2 (abl interactor 2), NCKAP1 (NCK associated protein 1), and BRIK (BRICK1 subunit of SCAR/WAVE actin nucleating complex), or paralogues of these, and the WASH complex, formed by WASHC1-5 (WASH complex subunit 1–5) (Z. Chen et al., 2010; Rotty et al., 2013). The activity of NPFs is controlled by Rho GTPases; in particular, active RAC1 and CDC42 activate N-WASP and WASP, respectively, by binding to their CRIB region (A. S. Kim et al., 2000; Tomasevic et al., 2007). Active RAC1 has also been shown to activate WRC (Eden et al., 2002). Notably, dominant-negative WASF1 abolishes the formation of RAC1-dependent lamellipodia and RAC1-dependent neurite extension (Miki et al., 1998). Strong genetic evidence indicates that alterations in the NPFs-ARP2/3 signaling module may lead to ID: copy number variants of the chromosomal region 15q11-q13, encompassing CYFIP1, were identified in patients with ASD and ID (Bardoni & Abekhoukh, 2014), with several studies indicating a pathogenic role for both increased and decreased CYPFI1 dosage (Bozdagi et al., 2012; Davenport et al., 2019; Oguro-Ando et al., 2015); 21 de novo missense CYPFI2 variants, most of which were shown to impact on WRCmediated actin remodeling, have been reported in 37 ID patients (Begemann et al., 2021; Schaks et al., 2020); WASHC4 has been identified as an autosomal recessive ID gene (Assoum et al., 2020; Ropers et al., 2011); NCKAP1 variants predicted to be deleterious for protein function have been associated with ID (H. Guo et al., 2020, p. 202); ABI2 is a candidate autosomal recessive ID gene (Harripaul et al., 2018); de novo splice site mutations of WASHC5 were shown to cause Ritscher–Schinzel/3C syndrome, a disorder characterized by several phenotypes, among which ID (Elliott et al., 2013).

GSN: GSN (gelsolin) acts by severing actin filaments and capping free barbed ends (Feldt et al., 2018). Its depletion in hippocampal neurons increases the number of filopodia by reducing their retraction (Lu et al., 1997). GSN is recruited to

dendritic spines following LTD (Hlushchenko & Hotulainen, 2019), presumably by the increase in calcium concentration (Khaitlina & Hinssen, 2002), suggesting its involvement in synaptic plasticity.

FMN2: FMN2 (formin 2) is an ABP that belongs to the family of formin homology (FH) domain proteins. Since it is involved in the maturation of tip adhesion, it is essential for the generation of traction forces by filopodia and the stabilization of the growth cone (Sahasrabudhe et al., 2016). By binding to the actin cytoskeleton, it functions as a clutch with the extracellular matrix at adhesion sites. FMN2 was found localized to ventral actin stress fibers in fibroblasts (Sahasrabudhe et al., 2016) and punctae along dendrites in neurons (Law et al., 2014). Notably, FMN2 truncating mutations in two consanguineous families lead to decreased spine density and non-syndromic autosomal-recessive ID (Law et al., 2014).

Profilins: Profilin family proteins (PFN1-4) promote the conversion of ADP-actin into ATP-actin, thus providing the actin monomers necessary to sustain barbed end elongation (Pollard, 2016). In striking contrast, low levels of profilin can also inhibit actin polymerization by sequestering actin monomers (Carlsson et al., 1977; Pollard & Cooper, 1984; Tobacman & Korn, 1982). Profilins may have a role in the stabilization of spine morphology (Borovac et al., 2018), and it is involved in the regulation of actin polymerization in growing neurites, as both overexpression and expression of dominant-negative profilin lead to impaired neurite outgrowth (Lambrechts et al., 2006).

SHTN1: PAK1 phosphorylates SHTN1 (shootin 1), promoting its interaction with F-actin (Toriyama et al., 2013). SHTN1 physically interacts with L1-CAM and F-actin, thus allowing the force generated by actin retrograde flow to be transmitted to the extracellular matrix and coupling actin polymerization with neurite elongation (C.-H. Lin & Forscher, 1995; Shimada et al., 2008). Interestingly, SHTN1 mRNA was found to be consistently down-regulated in blood samples of ID patients harboring mutations in the transcription factors CCNT2, CDK9, and TAF2 (InanlooRahatloo et al., 2019).

1.3 Forebrain GABAergic INs generation maturation

The generation of GABAergic interneurons (INs) in the cortex and hippocampus is a complex process involving the interplay of spatial and temporal genetic programming, influenced by both intrinsic and extrinsic cues. These INs

originate from progenitor zones in the subpallium, the ventral aspect of the embryonic telencephalon. Three main progenitor zones in the subpallium give rise to cortical and hippocampal INs: the medial ganglionic eminence (MGE), the caudal ganglionic eminence (CGE), and the preoptic area (POA) (Anderson et al., 1997; de Carlos et al., 1996; DeDiego et al., 1994; Gelman et al., 2012; Silva et al., 2019; Tamamaki et al., 1997). The MGE is the largest contributor, generating about 60% of cortical INs, and primarily producing parvalbumin (PVALB) and somatostatin (STT) expressing INs. The CGE contributes approximately 30% of cortical INs, and is the main source of vasoactive intestinal peptide (VIP) and reelin (RLN) expressing INs. The POA, the smallest contributor, generates about 10% of cortical INs, with a mixed population of subtypes (Kessaris et al., 2014; Sultan et al., 2013). The MGE produces hippocampal INs that will migrate to the hippocampus CA regions and avoid the dentate gyrus (Pleasure et al., 2000; Polleux et al., 2002; Wichterle et al., 2001), while the CGE generates INs that migrate to both the CA and the dentate gyrus regions (Nery et al., 2002). In mice expressing the Green Fluorescent Protein (GFP) under the control of the GAD65 promoter, GFP-positive cells arise from the three GE but are mainly generated in the CGE at late stages of embryonic development ((López-Bendito et al., 2004)). Within each progenitor zone, further spatial patterning refines IN subtype specification. For example, the MGE is subdivided into dorsal, intermediate, and ventral domains, each with a distinct potential for generating specific subtypes (Lim et al., 2018). The dorsal MGE (dMGE) is the exclusive source of STT-expressing INs, including those that express calretinin (CR). Temporal patterning also plays a crucial role in IN subtype generation. Different cohorts of INs arise at different stages of development, even from the same progenitor domain. This suggests a progressive restriction of progenitor potential over time. A complex network of transcription factors orchestrates IN subtype specification and differentiation. DLX1 and DLX2 are essential for the development of all cortical INs. NKX2.1 defines the MGE neuroepithelium and activates a cascade of genes, including LHX6, SOX6, and SATB1, crucial for MGE-derived IN development. NKX6.2 and GLI1 are enriched in the dMGE and contribute to its unique identity. PROX1 and SP8 are expressed in CGE-derived INs (Kessaris et al., 2014; Lim et al., 2018). Extrinsic cues, including neuronal activity and neurotrophic factors, also influence IN development, migration, and integration. BDNF signaling promotes the migration and maturation of MGE-derived INs (Williams & Riedemann, 2021; Yamada et al., 2002). Neuronal activity is essential for the development of specific IN subtypes and influences their laminar distribution (De Marco García et al., 2011; Williams & Riedemann, 2021).

After exiting the cell cycle, immature INs initiate tangential migration to reach the cortical and hippocampal primordia, following stereotyped routes (Kelsom & Lu, 2013; D. H. Tanaka et al., 2011). During this tangential migration, Rho GTPases and their regulatory network have been implicated in linking extracellular signals to directional control (de Curtis, 2014; Tivodar et al., 2015). Once in the appropriate areas, INs reorient their trajectory by approximately 90 degrees, transitioning from tangential to radial migration to reach their final positions (J. Guo & Anton, 2014; Hatanaka et al., 2016). Factors controlling the migration of INs remain poorly understood, with only a few identified thus far, including neuregulins, sonic hedgehog, and thalamocortical projections (Alfonso et al., 2015; Bartolini et al., 2017; Baudoin et al., 2012; Flames et al., 2004; Zechel et al., 2016).

1.3.1 Defective INs maturation and developmental disorders

In the mouse cortex, projection neurons constitute the majority of neuronal population, while INs comprise approximately 20-30% (DeFelipe, 1993; Markram et al., 2004). Projection neurons target diverse cortical and extracortical regions, whereas cortical INs primarily form local circuits. The balance between excitatory and inhibitory input within these circuits is crucial for maintaining cortical function (Fishell & Rudy, 2011; Froemke, 2015; Isaacson & Scanziani, 2011). A growing body of evidence suggests that abnormalities in IN development can lead to IN dysfunction and disrupted inhibitory circuits in the cortex, which are strongly implicated in the etiology and progression of neurodevelopmental disorders, including autism spectrum disorders (ASDs), intellectual disability (ID), schizophrenia, and epilepsy (Marín, 2012; Powell et al., 2003). This dysfunction can manifest as either a decrease or increase in inhibitory activity, leading to an imbalance in neural circuits. While decreased inhibition thus pathological hyperexcitability are often linked to the emergence of epilepsy (Galanopoulou, 2010; Poduri & Lowenstein, 2011), evidence from other neurological conditions, such as Down syndrome and neurofibromatosis type 1, suggests that excessive inhibition within critical neural circuits may also contribute to the onset of pathological processes. (Belichenko et al., 2009; R. M. Costa et al., 2002; Kleschevnikov et al., 2004). The timing of genetic or environmental insults during IN development can significantly impact the severity and manifestation of NDDs. Early disruptions might affect IN migration and number, leading to more severe phenotypes like epilepsy, while later disruptions might primarily affect connectivity and contribute to milder phenotypes like behavioral abnormalities. Other specific examples of IN dysfunction in different NDDs include:

Schizophrenia:

- Reduced expression of GAD67 in PVALB+ INs in the dorsolateral prefrontal cortex, potentially impairing their inhibitory function and contributing to cognitive deficits (Akbarian et al., 1995; Hashimoto et al., 2003).
- Defective inhibitory transmission from INs to pyramidal cells, possibly due to a reduced number of inhibitory synapses (T. U. Woo et al., 1998).
- Deficient excitation of PVALB+ INs, leading to reduced inhibitory output (Belforte et al., 2010; Carlén et al., 2012, p. 20; Korotkova et al., 2010).

Autism spectrum disorders:

- Mutations in genes like MECP2, NLGN3, SHANK3, and CNTNAP2 are implicated in autism and can affect the development and function of GABAergic circuits (Chadman et al., 2008; Chao et al., 2010; R. Z. Chen et al., 2001; Guy et al., 2001; Peça et al., 2011; Peñagarikano et al., 2011; Radyushkin et al., 2009).
- Deletion of MECP2 from forebrain GABAergic neurons in mice recapitulates several features of Rett's syndrome, highlighting the role of GABAergic dysfunction in autism-like symptoms (Adachi et al., 2009; Chao et al., 2010; Gemelli et al., 2006; Samaco et al., 2009).

Intellectual disabilities:

- In Angelman's syndrome, deletions or mutations in UBE3A and GABRB3 are implicated in defective inhibitory function (Homanics et al., 1997; Jiang et al., 2010).
- Fragile X syndrome, caused by mutations in FMR1, exhibits various alterations in GABAergic signaling, including reduced IN numbers, altered GABA receptor expression, and impaired GABA synthesis (Centonze et al., 2008; Curia et al., 2009; Gibson et al., 2008; Olmos-Serrano et al., 2010; Penagarikano et al., 2007; Selby et al., 2007).

Understanding the generation and development of cortical and hippocampal GABAergic INs is critical for unraveling the complexity of brain development and function. Continued research in this field will provide valuable insights into the pathogenesis of NDDs and potentially lead to the development of novel therapeutic strategies.

Chapter 2
The role of ARHGAP15 in cortical INs maturation

2.1 Abstract

GTPases of the Rho family are components of signaling pathways linking extracellular signals to the control of cytoskeleton dynamics. Among these, RAC1 plays key roles during brain development, ranging from neuronal migration to neuritogenesis, synaptogenesis, and plasticity. RAC1 activity is positively and negatively controlled by guanine nucleotide exchange factors (GEFs), guanosine nucleotide dissociation inhibitors (GDIs), and GTPase-activating proteins (GAPs), but the specific role of each regulator in vivo is poorly known. ARHGAP15 is a RAC1-specific GAP expressed during development in a fraction of migrating cortical INs (CINs) and in the majority of adult CINs. During development, loss of ARHGAP15 causes altered directionality of the leading process of tangentially migrating CINs, along with altered morphology in vitro. Likewise, time-lapse imaging of embryonic CINs revealed a poorly coordinated directional control during radial migration, possibly due to hyper-exploratory behavior. In the adult cortex, the observed defects lead to subtle alteration in the distribution of CALB2-, SST-, and VIP-positive INs. Adult *Arhgap15*-knock-out mice also show reduced CINs intrinsic excitability, spontaneous subclinical seizures, and increased susceptibility to the pro-epileptic drug pilocarpine. These results indicate that ARHGAP15 imposes a fine negative regulation on RAC1 that is required for morphological maturation and directional control during CIN migration, with consequences on their laminar distribution and inhibitory function.

2.2 Introduction

Neuronal networks within the adult cerebral cortex are progressively established during development and postnatal life via extensive neuronal migration, neuritogenesis, and synaptogenesis in a highly temporally and spatially coordinated fashion. These cellular processes share common cellular mechanisms regulating the continuous and dynamic reorganization of the growth cone, a highly polarized structure at the tip of the leading process, which is essential to sense guidance cues, establish a trajectory, and orient the cell body (Murakoshi et al., 2011; Vitriol & Zheng, 2012). These dynamic processes are driven by extensive polymerization/depolymerization, branching, and severing of the actin filaments (Cooper, 2008, 2013; Nadarajah et al., 2001). The Rho family of small GTPases controls the spatial and dynamic changes in neuronal actin cytoskeleton organization (Gonzalez-Billault et al., 2012; Govek et al., 2011; Heasman & Ridley, 2008; Marín, 2013; Tcherkezian & Lamarche-Vane, 2007). Rho GTPases regulate protrusion, retraction, and adhesion at the growth cone of immature neurons through the control of microtubule stability and actin filament polymerization/depolymerization, actomyosin contractility, and engagement of intracellular adhesion and anchoring mechanisms (Gomez & Letourneau, 2014). Rho GTPases link extracellular cues to motility responses, as shown, for instance, in migrating cerebellar granule cells, in which the conditional inactivation of RAC1 phenocopies the defects observed in *Sema6A* and *Plxna2* knock-out (KO) mice (Renaud & Chédotal, 2014; Tahirovic et al., 2010). Broadly speaking, the activity of RAC1/RAC3 and CDC42 is associated with attractive growth cone turning, whereas the activity of RHOA is associated with responsiveness to repulsive cues (Luo, 2000). RAC1 is expressed in the embryonic and adult brain; embryonic RAC1 is mainly localized at the growth cone of migrating neurons (Hall & Lalli, 2010) and is essential for neuronal migration (L. Chen et al., 2007; Govek et al., 2011; Heasman & Ridley, 2008; Kawauchi, 2015; T. Yang et al., 2012) and maturation (Gomez & Letourneau, 2014), both *in vitro* and *in vivo*. In mice, the *Rac1 whole-body KO* is embryonically lethal (L. Chen et al., 2007; Y. Chen et al., 2009), while the *Syn1*-cre-mediated conditional deletion of Rac1 (named Rac-N) in neurons leads to migration, differentiation, and connectivity defects (Corbetta et al., 2008, 2009; Pennucci et al., 2011; Vaghi et al., 2012, p. 201). Mice with both Rac-N and Rac3 null mutations show defective migration and maturation of cortical and hippocampal inhibitory neurons, severe neurological and cognitive deficits, and spontaneous epilepsy, while the single disruption of Rac3 does not cause evident defects (Corbetta et al., 2008, 2009; Pennucci et al., 2011; Vaghi et al., 2012).

GTPases cycle between an inactive GDP-bound and an active GTP-bound state, a binary switch that is tightly regulated by multiple guanine nucleotide exchange factors (GEFs), GTPase-activating proteins (GAPs), and guanine nucleotide dissociation inhibitors (GDIs) (Peck et al., 2002; Watabe-Uchida et al., 2006). The GAP protein ARHGAP15 is a RAC1-specific negative regulator whose overexpression results in an increased actin stress fibers formation and cell contraction (C. Costa et al., 2011; Seoh et al., 2003). The GAP domain of ARHGAP15 binds the C-terminal half of RAC1 in a nucleotide-independent manner, promoting the RAC1 GDP-bound state and the consequent switch-off of the downstream pathway. A novel biochemical mechanism of RAC1 inactivation by ARHGAP15 may involve the interaction and mutual antagonism with PAK1, a well-known RAC1 effector (Radu et al., 2013). Animal models revealed specific functions of RAC1 GTPase in the development of inhibitory networks (Corbetta et al., 2008, 2009; Pennucci et al., 2011; Vaghi et al., 2012). The principal inhibitory neurons in the cortex are the GABAergic cortical INs (CINs) derived from progenitors that reside in the ventral telencephalon of the embryonic brain, namely the ganglionic eminences, and in the preoptic area (POA) (Gelman et al., 2012). The ganglionic eminences appear around E11 and can be subdivided into the medial ganglionic eminence (MGE), the caudal ganglionic eminence (CGE), and the lateral ganglionic eminence (LGE) (Anderson et al., 1997, p. 1997; de Carlos et al., 1996; DeDiego et al., 1994; Tamamaki et al., 1997). CINs that colonize the cortex derive mainly from NKX2.1-positive progenitors in the MGE and POA, while the LGE mostly contributes to striatal and olfactory bulb INs. After exiting the cell cycle, immature CINs begin to migrate tangentially to reach the cortex and the hippocampus primordia following stereotyped routes (Kelsom & Lu, 2013; D. H. Tanaka et al., 2011). During this tangential migration, Rho GTPases and their regulatory network have been shown to link extracellular signals to directional control (de Curtis, 2014; Tivodar et al., 2015). Mice lacking RAC1 in MGEderived cells exhibit a 50% reduction in the number of GABAergic CINs in the postnatal cortex (Vidaki et al., 2012). Once in the appropriate cortical areas, CINs reorient their trajectory by approximately 90°, leaving the tangential path and proceeding with radial migration to reach their final position (J. Guo & Anton, 2014; Hatanaka et al., 2016). Factors that control the migration of CINs into the cortical plate are poorly known, as only a few of them have been identified (*e.g.*, neuregulins, sonic hedgehog, and the thalamocortical projections) (Alfonso et al., 2015; Bartolini et al., 2017; Baudoin et al., 2012; Flames et al., 2004; Zechel et al., 2016). Here, we provide evidence for the requirement of the RAC1-specific negative regulator ARHGAP15 in the control of CIN migration, morphology, and functionality.

Specifically, *Arhgap15-KO* CINs show a disoriented leading process during both tangential and radial migration and do not undergo proper cortical lamination. Moreover, *Arhgap15-KO* mice show increased susceptibility to sporadic spontaneous and induced seizures, probably due to reduced CINs intrinsic excitability.

2.3 Results

Here, I provide evidence for the requirement of the RAC1-specific negative regulator ARHGAP15 in the control of CIN migration, morphology, and functionality. Specifically, *Arhgap15*-KO CINs show a disoriented leading process during both tangential and radial migration and do not undergo proper cortical lamination. Moreover, *Arhgap15*-KO mice show increased susceptibility to sporadic spontaneous and induced seizures, probably due to reduced CINs intrinsic excitability.

2.3.1 Expression of Arhgap15 in embryonic and adult CINs

We previously reported ARHGAP15 expression in the cortex, hippocampus, and olfactory bulbs of early postnatal and adult mice (Zamboni et al., 2016; Zamboni, Jones, et al., 2018). To evaluate the expression of ARHGAP15 in embryonic and adult CINs, we examined the expression of the LacZ knock-in reporter in brain sections of *Arhgap15*$^{LacZ/+}$*;GAD67-eGFP* animals by immunostaining for β-GAL. LacZ expression was not detected in E11.5 and E12.5 brains (**Figure 1A**). In sections of E14.5 brains, LacZ expression was detected in 26 ± 0.9%, 23 ± 1.7%, and 18 ± 2% of CINs in the marginal zone (MZ), cortical plate (CP), and intermediate zone (IZ)/subventricular zone (SVZ), respectively (**Figures 1B,E**). No LacZ expression was detected in the ganglionic eminences, indicating that embryonic CINs start expressing ARHGAP15 only after they start migrating and enter the neocortex (NCX). In sections of early postanal (P2) and adult (P45) brains, LacZ expression was detected in 35 ± 1.3% and 56 ± 2.6% of CINs, respectively (**Figures 1C,F,G**). To determine the expression of ARHGAP15 in the major CIN subtypes, we carried out double immunostainings for β−GAL and either PVALB, CALB2, SST, or VIP on sections of P45 *Arhgap15*$^{LacZ/+}$ brains. The results show that *Arhgap15* is expressed by 57 ± 3%, 53 ± 4%, 53 ± 1%, and 52 ± 1% of PVALB-, CALB2-, SST, and VIP-positive neurons, respectively (**Figures 2A–E**). These results indicate that *Arhgap15* starts to be expressed in migrating CINs between the embryonic stages E13.5 and E14.5, and it is expressed by most (about 60%) of adult CINs, not being specific for any of the major CIN subtypes.

2.3.2 Altered morphology of *Arhgap15*$^{LacZ/LacZ}$ CINs in vitro

RAC1 is critical for neuritogenesis during development (Sayyad et al., 2016). To determine whether loss of ARHGAP15, hence hyperactive RAC1, affects CINs morphology (*i.e.*, neurite elongation and complexity), we examined cultures of

dissociated neurons from cortices of E15.5 *GAD67-eGFP* and *Arhgap15$^{LacZ/LacZ}$;GAD67-eGFP* embryos at 3 and 10 DIV. We selected eGFP-positive neurons and examined their neurites length and complexity (**Figures 3A,B**). At 3 DIV, *Arhgap15$^{LacZ/LacZ}$* eGFP-positive neurons displayed a reduced number of branches (**Figure 3C**). At 3 DIV, but not at 10 DIV, *Arhgap15$^{LacZ/LacZ}$* eGFP-positive neurons also showed a reduced length of the longest neurite compared to the *GAD67-eGFP* (**Figures 3D,E**). At both 3 and 10 DIV, *Arhgap15$^{LacZ/LacZ}$ eGFP*-positive neurons showed a reduced number of primary neurites (**Figures 3F,G**). Moreover, at 10 DIV, but not at 3 DIV, a reduction in soma diameter was also observed in *Arhgap15$^{LacZ/LacZ}$* eGFP-positive neurons (**Figures 3H,I**). Sholl analysis revealed that, at 3 DIV, *Arhgap15$^{LacZ/LacZ}$* eGFP-positive neurons showed a lower number of intersections at various distances from the cell body (**Figure 3J**), indicating a reduced efficiency in neuritogenesis and branching, whereas at 10 DIV they showed a lower number of intersections in the region more proximal to the soma, but a higher number of distal intersections (**Figure 3K**). These results suggest that *Arhgap15$^{LacZ/LacZ}$* CINs fail to undergo an efficient neuritogenesis and branching in the first maturation steps in vitro, but they later develop an increased number and/or branching of secondary neurites, possibly to compensate for their defective number of primary neurites.

To confirm that cultured eGFP-positive neurons express ARHGAP15, we performed immunostainings for β−GAL on primary cultures derived from *Arhgap15$^{LacZ/+}$;GAD67-eGFP* embryos at 3, 10, and 18 DIV. This analysis showed that about half of eGFP-positive neurons express ARHGAP15 also in culture (**Supplementary figure 1**).

2.3.3 Defective orientation of tangentially migrating *Arhgap15$^{LacZ/LacZ}$* CINs

Neuronal migration requires extensive cytoskeletal reorganization at the growth cone, a process in which small Rho GTPases play a critical role (Liaci et al., 2021). Since INs cover a longer and more complex migratory path as compared to other neurons (Cooper, 2013) and were shown to express ARHGAP15 during their migration from the GE to the NCX (**Figure 1B**), we looked at their cortical migration. We determined the number and position of tangentially migrating CINs in the cortices of *GAD67-eGFP* and *Arhgap15$^{LacZ/LacZ}$;GAD67-eGFP* embryos by analyzing coronal sections of E14.5 brains (**Figure 4A**). No significant changes in the number of tangentially migrating CINs were detected between the two genotypes (**Figure 4B**). We examined the orientation of eGFP-positive neurons by

determining the angle between their leading process and the canonical direction of their tangential migration (*i.e.*, parallel to the pial and ventricular surfaces). In the *Arhgap15$^{LacZ/LacZ}$;GAD67-eGFP* embryonic cortex, the leading process of migrating CINs displayed a mean angle relative to the tangential trajectory significantly wider than that of GAD67-eGFP control neurons (**Figure 4C**), indicating that *Arhgap15$^{LacZ/LacZ}$* CINs tend to deviate from the canonical tangential direction of migration. No differences were observed comparing the length of the leading processes of GAD67-eGFP and *Arhgap15$^{LacZ/LacZ}$;GAD67-eGFP* tangentially migrating CINs (**Figure 4D**). Thus, the absence of ARHGAP15 alters the control of leading process directionality during tangential migration.

2.3.4 Defective orientation of radially migrating *Arhgap15$^{LacZ/LacZ}$* CINs

After E15.5, eGFP-positive tangentially migrating neurons present in the MZ and the IZ/SVZ routes have colonized all the cortical areas (Martini et al., 2009). Subsequently, they activate a different migration mode, namely the radial migration, perpendicular to the cortical and ventricular surfaces. Specifically, neurons in the MZ and IZ/SVZ migrate deeply to occupy the CP. Only a small fraction of CINs migrate through the subplate (Marín, 2013; D. H. Tanaka & Nakajima, 2012). We looked at CINs trajectory during their radial migration in coronal sections of E17.5 *GAD67-eGFP* and *Arhgap15$^{LacZ/LacZ}$;GAD67-eGFP* brains. The magnifications of CPs suggested that radially migrating CINs may have altered trajectories with respect to the canonical radial direction (**Figure 5A**). To precisely determine CINs trajectory in the cortical primordium, we monitored single eGFP- positive CINs by time-lapse video imaging in 300 μm thick slices of E17.5 *GAD67- GFP* and *Arhgap15$^{LacZ/LacZ}$;GAD67-eGFP* cortices maintained in organotypic cultures. We examined the trajectory of *GAD67-eGFP* and *Arhgap15$^{LacZ/LacZ}$;GAD67-eGFP* CINs after their tangential-to-radial switch and tracked their leading process movements for at least 100 min. Most of them were stationary after 65 min. The criteria used for identifying radially migrating neurons are graphically illustrated in **Figure 5B** (Martini et al., 2009). We calculated the ratio between the path length and linear distance between the initial and final positions of the leading process of each neuron (**Figure 5C**). We observed that *Arhgap15$^{LacZ/LacZ}$;GAD67-eGFP* neurons deviate from the physiological radial direction of migration significantly more often than *GAD67-eGFP* (**Figure 5D**). This result suggests a loss of directional control (or a gain of directional flexibility) in *Arhgap15*-KO CINs, in accordance with data shown in Figure 4.

2.3.5 Altered distribution of CALB2-, SST-, and VIP-positive neurons across the *Arhgap15$^{LacZ/LacZ}$* adult cortical layers

Given the alterations in CIN migration described above, we examined the laminar distribution of CINs in WT and *Arhgap15$^{LacZ/LacZ}$* adult (P45) cortices. We examined the laminar organization of the most common CIN subtypes in the somatosensory cortical area of WT and *Arhgap15$^{LacZ/LacZ}$* cortices, by immunostaining coronal sections for PVALB, CALB2, SST, and VIP. We observed a significant increase in the number of CALB2-positive neurons in bins 5, 6, and 7 of *Arhgap15$^{LacZ/LacZ}$* mice (**Figures 6A,C**). Subtle changes were observed in the distribution of SST- and VIP-positive neurons in bins 10 and 6, respectively (**Figures 6A,D,E**). No significant alterations were observed in the distribution of PVALB-positive neurons in the absence of ARHGAP15 (**Figures 6A,B**). We found a slight increase in the total number of CALB2-positive CIN in *Arhgap15$^{LacZ/LacZ}$* mice, which, however, does not reach statistical
significance. The total number of PVALB-positive, SST-positive, and VIP-positive CINs is unaltered in the *Arhgap15$^{LacZ/LacZ}$* mice. These results show that the stratification of adult CALB2-positive CINs in the forebrain cortex is altered in the absence of ARHGAP15, along with milder alteration in the layering of SST- and VIP-positive cells, probably due to the migratory defects observed.

2.3.6 Spontaneous subclinical epileptic spikes in *Arhgap15$^{LacZ/LacZ}$* mice

We previously observed an altered density of excitatory and inhibitory synapses on the soma of *Arhgap15$^{LacZ/LacZ}$* cortical pyramidal neurons, and also noticed significant differences between the electroencephalography (EEG) of sleeping WT and *Arhgap15$^{LacZ/LacZ}$* animals (Zamboni, Jones, et al., 2018).We noted that, occasionally, following moderate stress, *Arhgap15$^{LacZ/LacZ}$* mice (5 out of 150) manifested stiffening, leg extension, and absence of movements lasting less than 5 s, which were never seen in WT mice (n > 200), probably manifestations of tonic-clonic convulsions (*i.e.*, spontaneous epileptic seizures). For this reason, we monitored and quantified the cortex-derived electrical activity of free-moving WT and *Arhgap15$^{LacZ/LacZ}$* adult (P120) mice. The majority of mutant mice showed an abnormal EEG with epileptiform discharges, usually associated with tonicclonic convulsions, and/or a series of single spikes, associated with less severe myoclonus (**Figure 7A**) (Erbayat-Altay et al., 2008). The mean number of spikes per hour was significantly greater in *Arhgap15$^{LacZ/LacZ}$*, as compared to WT mice (**Figure 7B**)

(Purtell et al., 2018). A significantly higher fraction of *Arhgap15*$^{LacZ/LacZ}$ mice exhibited spikes and slow waves activity and/or trains of spikes, as compared to WT mice (spikes and slow waves: 1 out of 10 WT mice, 5 out of 8 KO mice; trains of spikes: 1 out of 10 WT mice, 3 out of 8 KO mice) (**Figure 7C**). These results indicate that *Arhgap15*$^{LacZ/LacZ}$ mice show a subclinical epileptic-like phenotype characterized by spike activity.

2.3.7 Increased susceptibility to pilocarpine-induced epilepsy in *Arhgap15*$^{LacZ/LacZ}$ mice

We tested the susceptibility of *Arhgap15*$^{LacZ/LacZ}$ mice to acute treatment with pilocarpine, a widely used inducer of epilepsy (Curia et al., 2008). Mice were administered with a single dose of atropine to prevent the peripheral side effects and, after 30 min, with a single dose of pilocarpine (**Figure 7D**). The epileptogenic activity of the drug was assessed by scoring 7 progressive epilepsy stages, according to the modified Racine scale (Racine, 1972) (**Figure 7D**). *Arhgap15*$^{LacZ/LacZ}$ mice exhibited a higher likelihood to enter stages 2, 4, 5, and 6, as compared to control animals (**Figure 7E**). Moreover, they showed a significantly higher mortality rate at 90 min (stage 7; **Figure 7E**). This data confirms that the loss of ARHGAP15 increases susceptibility to drug-induced epilepsy.

2.3.8 Reduced intrinsic excitability of *Arhgap15*$^{LacZ/LacZ}$ CINs

To determine the impact of ARHGAP15 depletion on CINs electrophysiological properties, we performed whole-cell patch-clamp recordings in acute slices obtained from adult *GAD67-eGFP* and *Arhgap15*$^{LacZ/LacZ}$*;GAD67-eGFP* mice. INs showed similar input resistance (R_{in}) and resting membrane voltage (V_{rest}) (**Figures 8A–C**), whereas the membrane capacitance of *Arhgap15*$^{LacZ/LacZ}$*;GAD67-eGFP* was significantly higher (**Figure 8D**). We observed a reduced firing rate of *Arhgap15*-KO CINs in response to the injection of current pulses of increasing amplitude (from 0 to 200 pA) till 130 pA of amplitude (**Figures 8E,F**). We also found that the rheobase was significantly higher in *Arhgap15-KO* INs, thus highlighting their low intrinsic excitability (**Figure 8G**). No differences were found in the single action potential (AP) properties (*i.e.*, AP peak amplitude, AP half-width, AP max rising slope, and AP max repolarizing slope) (**Figures 8H−L**).

To confirm the altered phenotype in vitro, we examined the firing properties of CINs in dissociated primary cultures derived from E15.5 *GAD67-eGFP* and

Arhgap15$^{LacZ/LacZ}$*;GAD67-eGFP* embryos at 17 DIV. Consistent with previous results, we did not observe any differences in Rin and Vrest (**Supplementary figures 2A–C**). We found a decrease in the response of *Arhgap15*-KO INs to current injections from 20 to 180 pA (**Supplementary figures 2D,E**), therefore confirming the functional defect also *in vitro*.

2.4 Discussion

Loss of ARHGAP15 has been reported in one case of severe intellectual disability and a rare variant of Mowat–Wilson syndrome, a disease characterized by epilepsy (Mulatinho et al., 2012; Smigiel et al., 2010). Also, exome sequencing in sporadic autism spectrum disorders patients identified a synonymous de novo mutation in this gene (O'Roak et al., 2011). Here, we provide evidence that, in the absence of ARHGAP15, the leading process of tangentially and radially migrating CINs shows an increased tendency to deviate from the physiological trajectory. This result suggests that hyperactive RAC1 causes an abnormally fast and uncontrolled reorganization of the leading process in new directions. Strikingly, neutrophils from *Arhgap15*$^{LacZ/LacZ}$ mice also miscontrol their directionality when following a gradient of chemoattractant cytokines (C. Costa et al., 2011). Our results show that the RAC1 negative regulator ARHGAP15 plays a similar function in migrating neurons and is required for the control of the orientation of these cells. We propose that ARHGAP15 is required to restrict the directional plasticity of the leading process and limit the rapid reorganization of the actin cytoskeleton. A similar function may be exerted by closely related RAC1 GAPs in other cell types. Hyperactive RAC1 may result in a relative instability and hyperdynamicity of the actin cytoskeleton at the tip of the leading process, resulting in an increased tendency to extend and retract the leading process, which may be interpreted as an over-physiological exploration of the environment for directional cues.

The involvement of Rho GTPases and their activating/inactivating regulators in this process is supported by the fact that RHOA, CDC42, and RAC1 participate in most intracellular events that link extracellular signaling with cytoskeletal reorganization (Hall & Lalli, 2010). Actin cytoskeleton remodeling is essential for cell migration and neurite elongation, two cellular processes that share ultrastructural features and molecular regulations (Burridge & Wennerberg, 2004; Govek et al., 2011; Hall & Nobes, 2000; Hua et al., 2005). During migration, neurons form F-Actin-rich filopodial and lamellipodial membrane protrusions at the peripheral region of the growth cone toward the direction of movement (Cooper, 2013). At the growth cone, RAC1 controls actin filaments dynamics, severing, and branching, necessary for axon elongation and turning. Consistently, in the presence of hyperactive RAC1, we previously observed defects in migration trajectory, neurite complexity, and axon guidance of other neural cell types (Zamboni, Armentano, et al., 2018; Zamboni et al., 2016). Although we cannot exclude RAC1-independent mechanisms, the altered migratory behavior observed in the cortex of *Arhgap15*$^{LacZ/LacZ}$ mice likely results from the hyperactivity of the RAC1-PAK1-

LIMK1 transduction pathway, leading to ADF/cofilin hyperphosphorylation (hence inactivation) and aberrant actin dynamics (Liaci et al., 2021), phenomena observed in cultured *Arhgap15*$^{LacZ/LacZ}$ neurons (Zamboni, Armentano, et al., 2018; Zamboni et al., 2016).

The activity of other kinases downstream RAC1 has been implicated in CIN migration and neuritogenesis (*i.e.*, PAK3 and PAK6). Although PAK3 expression is almost undetectable in newborn and migrating precursor INs, in the post-migratory MGE-derived CINs its expression increases robustly and promotes neurites outgrowth and branching after reaching the cortex (Cobos et al., 2005). Similar functions and expression dynamics have been described for PAK6 in POA-derived cells. PAK6-expressing neurons represent the post-migratory neurons derived from the POA in the late stage of maturation (Pensold et al., 2017). Interestingly, PAK3 and PAK6 are repressed during migration by DLX1/2 and DNMT1, respectively, to avoid premature differentiation of MGE-derived and POA-derived INs (Cobos et al., 2007, p. 200; Pensold et al., 2017).

At the extracellular level, IN migration is controlled by a complex combination of long-range attractive and repulsive signals, short-range instructive molecules, cell-adhesion dynamics, and intrinsic motogenic factors (Métin et al., 2006). Only a few of the signals and transduction mechanisms involved have been identified, some of which belong to the family of EGF-related neuregulins (Alfonso et al., 2015; Bartolini et al., 2017; Flames et al., 2004; Zechel et al., 2016). Focusing on CIN migration in the developing cortex, RAC1 is a key hub for interpreting local cues, as it integrates and transduces several input signals into a small set of biochemical responses. RAC1 response to signals consists of an initial activation followed by a rapid return to the basal level, a process known as adaptation. Notably, *Arhgap15*$^{LacZ/LacZ}$ neutrophils show altered RAC1 activation and adaptation in response to cytokine stimulation, resulting in an altered mobilization (Campa et al., 2016), indicating that ARHGAP15 normally contributes to determining the magnitude and timescale of RAC1 activity in response to signals. Our results in neurons further support this, as *Arhgap15*$^{LacZ/LacZ}$ CINs show altered directionality and imprecise decision-making in a context of unchanged cues.

The control of CIN migration during embryonic development is critical for the establishment of their correct laminar architecture and connectivity in early postnatal life (Clowry, 2015; Le Magueresse & Monyer, 2013; Tamamaki et al., 1997). During development, CINs also contribute indirectly to key aspects of forebrain organization and maturation (Le Magueresse & Monyer, 2013). As a

consequence of defective control of directionality, we observed a significant alteration of the CIN laminar organization in the adult cortex (*i.e.*, abnormal distribution of CALB2-positive CINs and subtle alterations in SST- and VIP-positive CINs lamination). Moreover, as we previously observed for hippocampal (Zamboni et al., 2016) and pyramidal cortical (Zamboni, Armentano, et al., 2018) *Arhgap15*$^{LacZ/LacZ}$ neurons, here we show that *Arhgap15*$^{LacZ/LacZ}$ CINs present an altered morphology in vitro. These defects, along with the observed alterations in the CINs electrophysiological properties (*i.e.*, reduced intrinsic excitability), are associated with pyramidal neuron hyperexcitability (Zamboni, Armentano, et al., 2018; Zamboni et al., 2016) and increased susceptibility to sporadic spontaneous and induced seizures. Notably, changes in the morphology and/or function of INs have been linked to neurological disorders (Juarez & Martínez Cerdeño, 2022). Altered CIN development, activity, and lamination have been shown to result in an altered balance between excitation and inhibition, thereby contributing to neurological and cognitive disorders (*e.g.*, epilepsy, autism spectrum disorders, Down syndrome, Rett syndrome, and schizophrenia) (Levitt, 2005; Levitt et al., 2004; Penzes et al., 2013; Rossignol, 2011; Sanacora et al., 2000). Epilepsy has been causally linked to GABAergic system impairments (Tan et al., 2007). Specifically, altered CIN migration, altered inhibitory control in the postnatal brain, as well as deprivation of the neurotrophic role of GABA in early development, may result in epilepsy (Ben-Ari, 2002; Galanopoulou, 2010; Kato, 2015; D. H. Tanaka & Nakajima, 2012).

In previous work, we demonstrated that, although pyramidal cortical neurons are hyperexcitable in absence of ARHGAP15, their electrical intrinsic properties (*i.e.*, input resistance and minimum current intensity for action potential) are not altered (Zamboni, et al., 2018), strongly suggesting that the defect could be about the inhibitory network. Here, we provide evidence for the reduced excitability of INs in the absence of ARHGAP15; this defect, together with the previously observed reduction in the number of VGAT punctae may be the cause of the excitatory/inhibitory imbalance observed in the EEG and MEA analysis previously conducted (Zamboni et al., 2016), and of the subsequently increased susceptibility to seizure (Cheng et al., 2021; Shao et al., 2019; Tai et al., 2014).

Considering that ARHGAP15 is not expressed by all CINs and it is expressed by other cells in the cortex, such as pyramidal neurons (Zamboni et al., 2018), it is expected that the overall disease phenotype entails non-cell-autonomous effects. Further experiments are needed to demonstrate this possible contribution. Several studies have previously shown that a specific subpopulation of CINs, the fast-

spiking PVALB-positive CINs, play a central role in epilepsy (Cammarota et al., 2013; Sessolo et al., 2015); nevertheless, our present data and other studies have also shown that alterations in the SST-positive, CALB2-, and VIP- bpositive populations of CINs may also contribute to epileptic activity (Cobos et al., 2005). It has been shown that damage in the dendritic tree of CALB2-positive neurons may result in impaired synchronization of the entire IN network responsible for dendritic inhibition, resulting in an asynchronous, thus less effective, inhibition of principal cells, which may be involved in epilepsy onset (Tóth & Maglóczky, 2014). For what concerns the SST-positive neurons, studies on human and mouse models, both in vivo and in vitro, have provided evidence for a correlation between epilepsy and the loss of this CIN population (Tallent & Siggins, 1999; Vezzani et al., 1991). Also, VIP-positive neurons have been implicated in seizure susceptibility, as VIP neuropeptide is released during sustained high-frequency activity (5–40 Hz) occurring during epileptiform activity (Clynen et al., 2014). Overall, the relative contribution of each CIN subtype on the epileptic-like phenotype observed in our model remains to be fully evaluated.

2.5 Figures

Figure 1

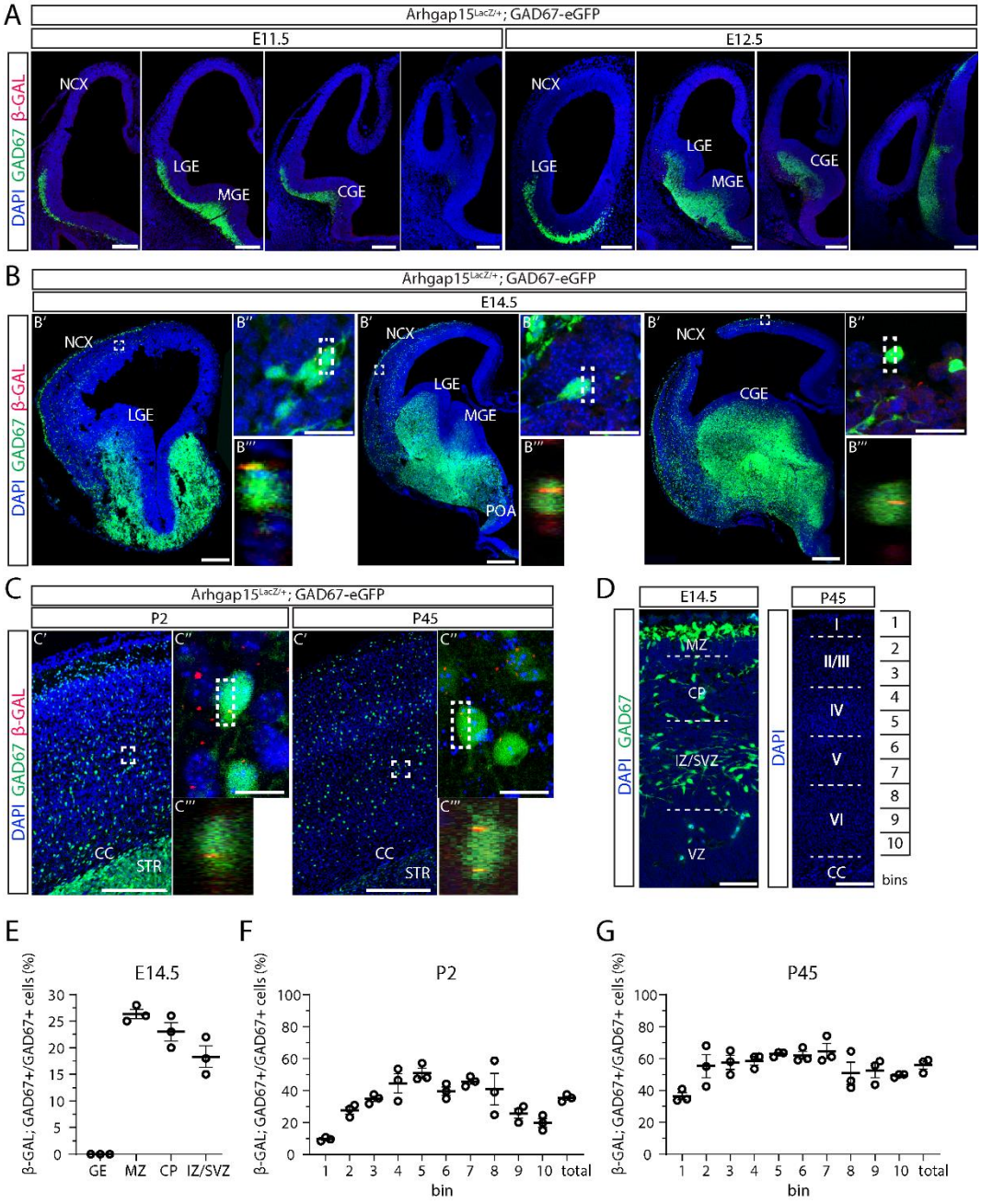

Figure 2

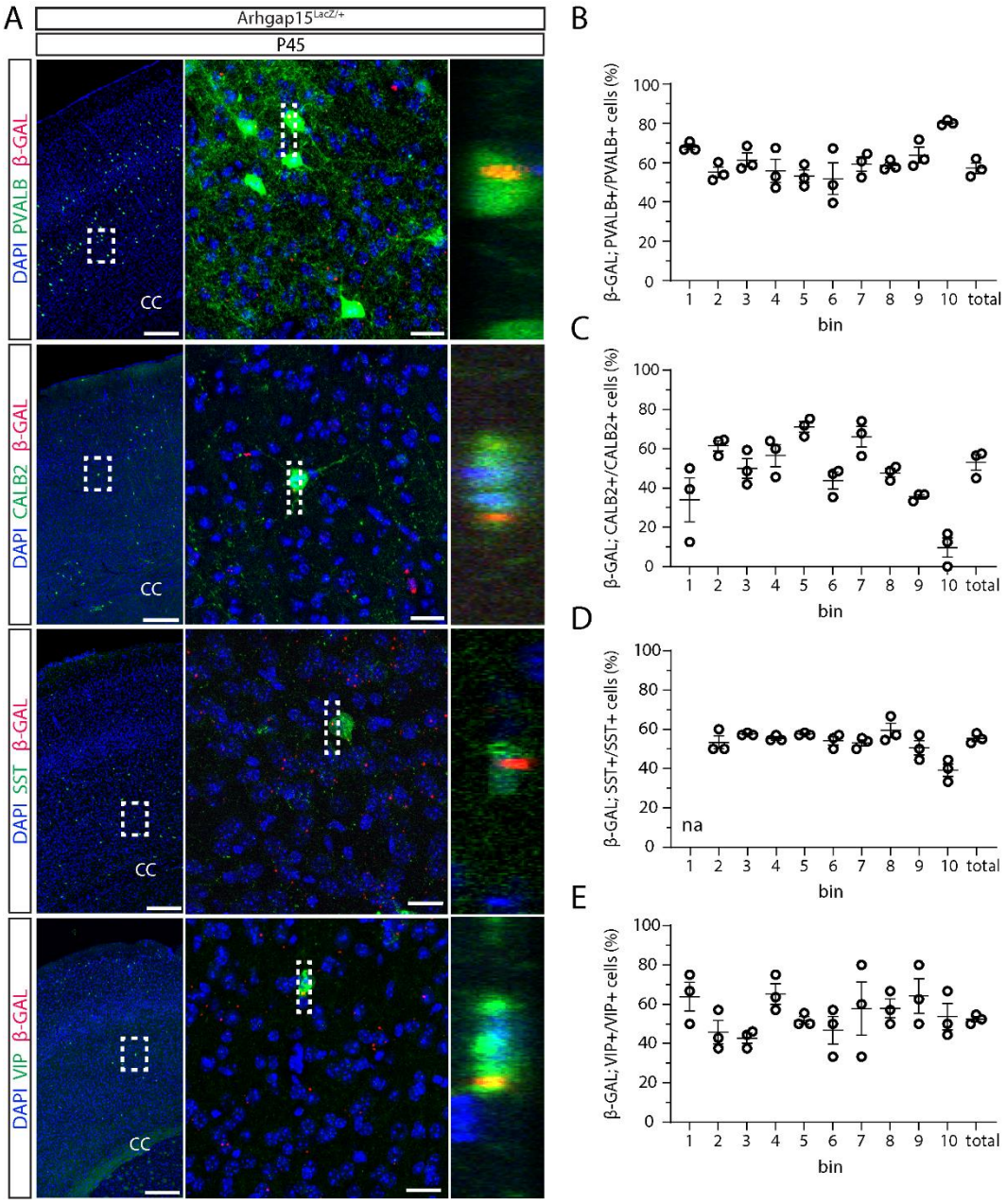
A
Arhgap15LacZ/+
P45
DAPI PVALB β-GAL
DAPI CALB2 β-GAL
DAPI SST β-GAL
DAPI VIP β-GAL
CC
B
β-GAL; PVALB+/PVALB+ cells (%)
C
β-GAL; CALB2+/CALB2+ cells (%)
D
β-GAL; SST+/SST+ cells (%)
na
E
β-GAL; VIP+/VIP+ cells (%)
bin
1 2 3 4 5 6 7 8 9 10 total
0 20 40 60 80 100

Figure 3

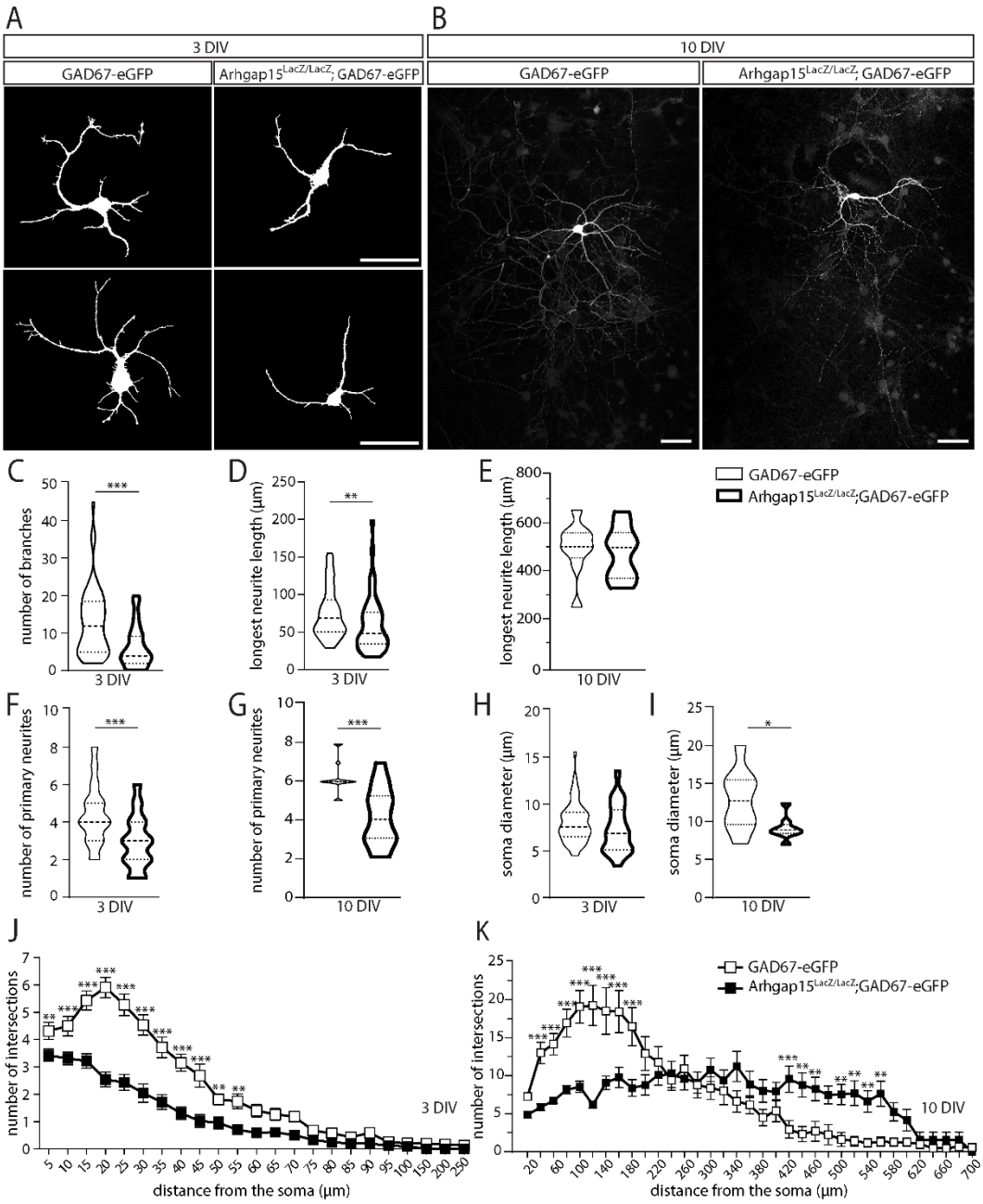
A
B
3 DIV
10 DIV
GAD67-eGFP
Arhgap15LacZ/LacZ; GAD67-eGFP
C
number of branches
3 DIV
D
longest neurite length (µm)
3 DIV
E
longest neurite length (µm)
10 DIV
GAD67-eGFP
Arhgap15LacZ/LacZ;GAD67-eGFP
F
number of primary neurites
3 DIV
G
number of primary neurites
10 DIV
H
soma diameter (µm)
3 DIV
I
soma diameter (µm)
10 DIV
J
number of intersections
3 DIV
distance from the soma (µm)
K
number of intersections
10 DIV
distance from the soma (µm)

Figure 4

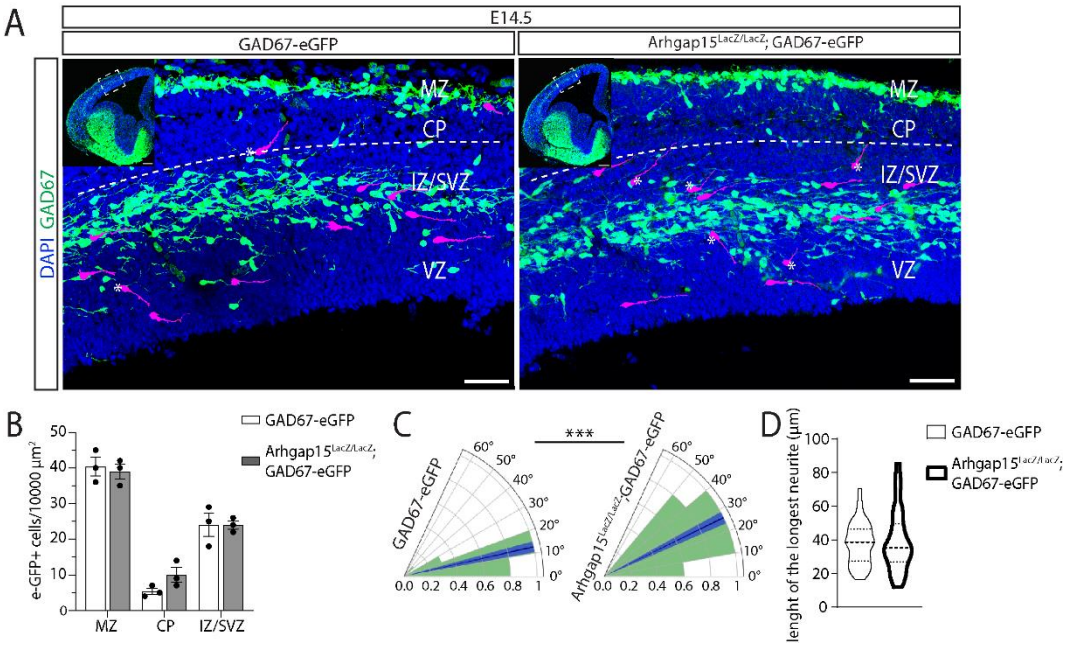
A
E14.5
GAD67-eGFP
Arhgap15LacZ/LacZ; GAD67-eGFP
DAPI GAD67
MZ
CP
IZ/SVZ
VZ
B
GAD67-eGFP
Arhgap15LacZ/LacZ; GAD67-eGFP
e-GFP+ cells/10000 µm2
MZ
CP
IZ/SVZ
C
***
GAD67-eGFP
Arhgap15LacZ/LacZ;GAD67-eGFP
D
GAD67-eGFP
Arhgap15LacZ/LacZ; GAD67-eGFP
lenght of the longest neurite (µm)

Figure 5

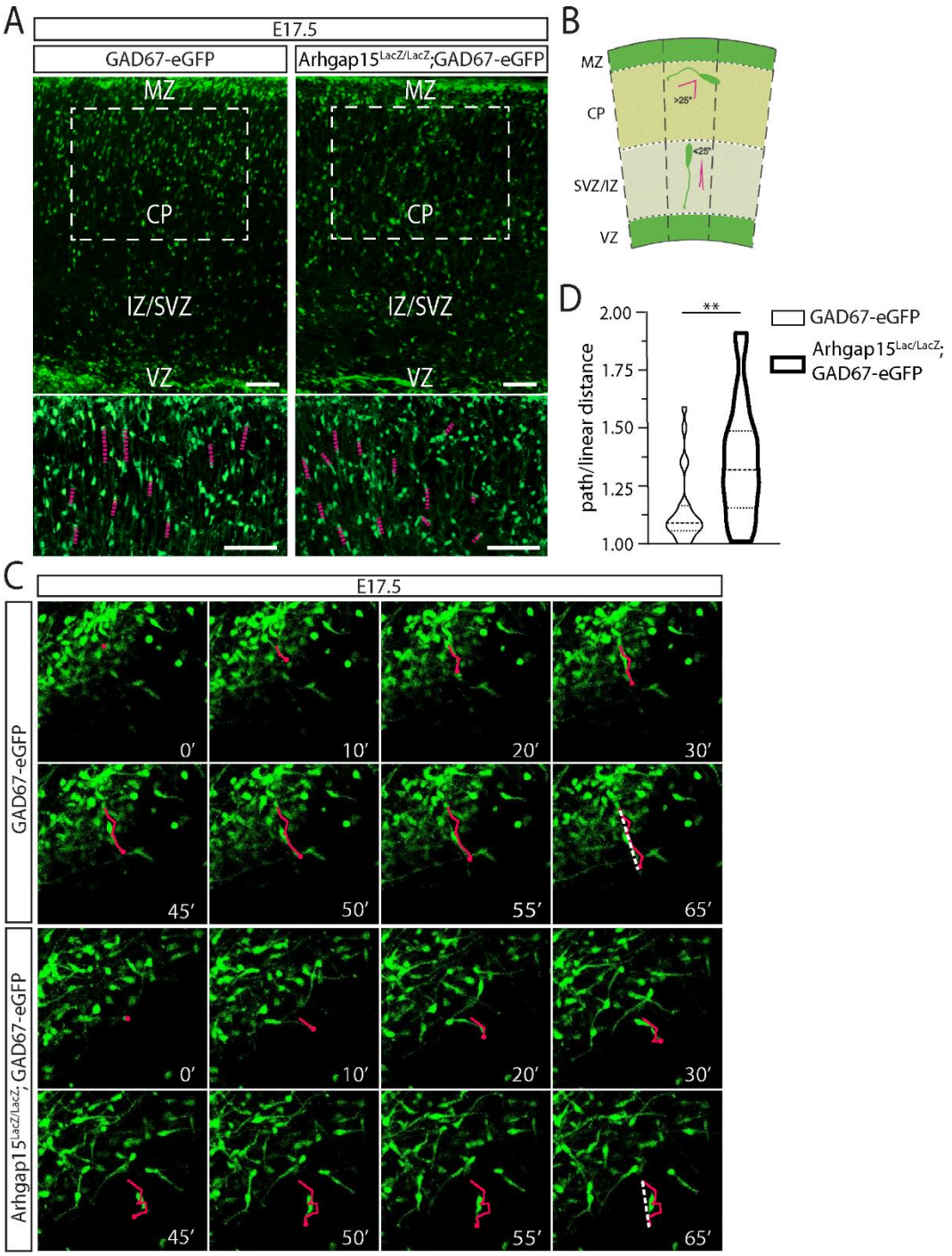
A
E17.5
GAD67-eGFP
Arhgap15LacZ/LacZ;GAD67-eGFP
MZ
CP
IZ/SVZ
VZ
B
MZ
CP
SVZ/IZ
VZ
>25°
<25°
D
**
path/linear distance
2.00
1.75
1.50
1.25
1.00
GAD67-eGFP
Arhgap15Lac/LacZ;
GAD67-eGFP
C
E17.5
GAD67-eGFP
Arhgap15LacZ/LacZ; GAD67-eGFP
0′
10′
20′
30′
45′
50′
55′
65′

Figure 6

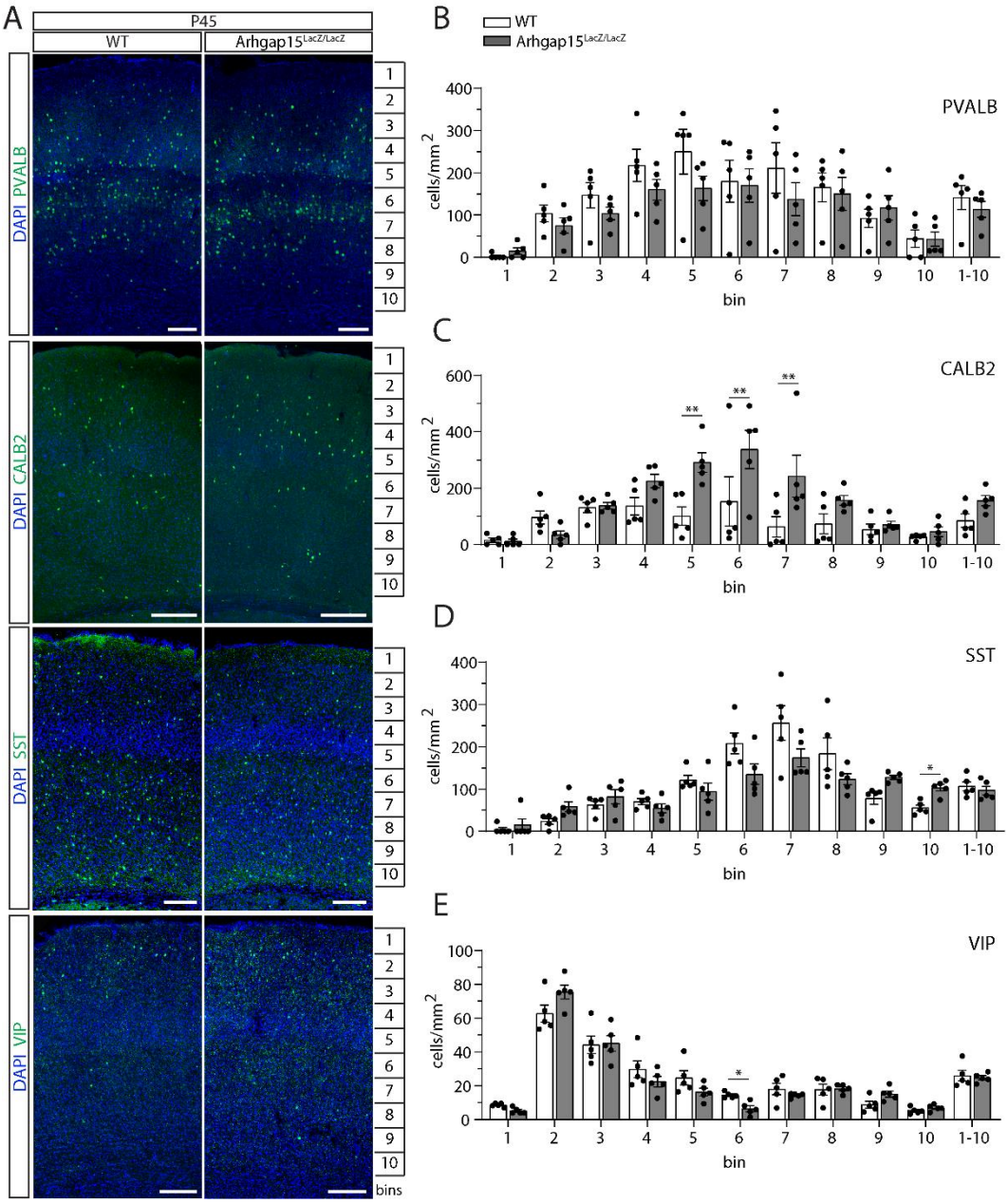
A
P45
WT
Arhgap15LacZ/LacZ
DAPI PVALB
DAPI CALB2
DAPI SST
DAPI VIP
1
2
3
4
5
6
7
8
9
10
bins
B
WT
Arhgap15LacZ/LacZ
PVALB
cells/mm2
bin
1-10
C
CALB2
**
D
SST
*
E
VIP

Figure 7

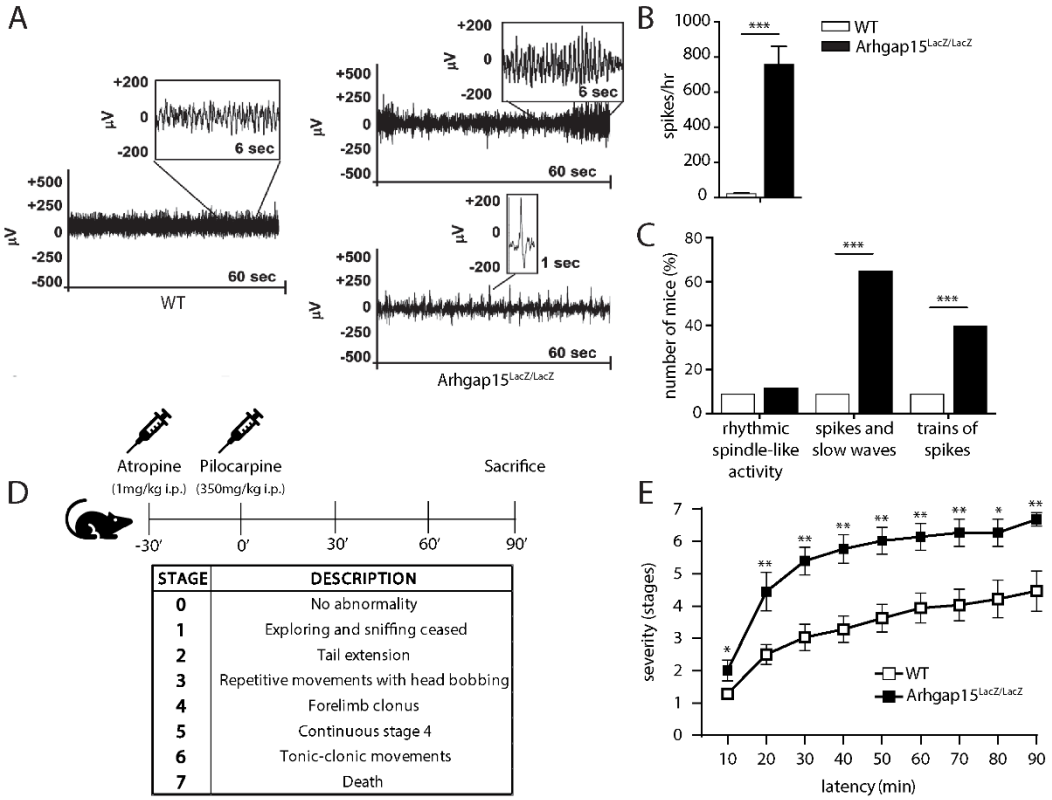

STAGE	DESCRIPTION
0	No abnormality
1	Exploring and sniffing ceased
2	Tail extension
3	Repetitive movements with head bobbing
4	Forelimb clonus
5	Continuous stage 4
6	Tonic-clonic movements
7	Death

Figure 8

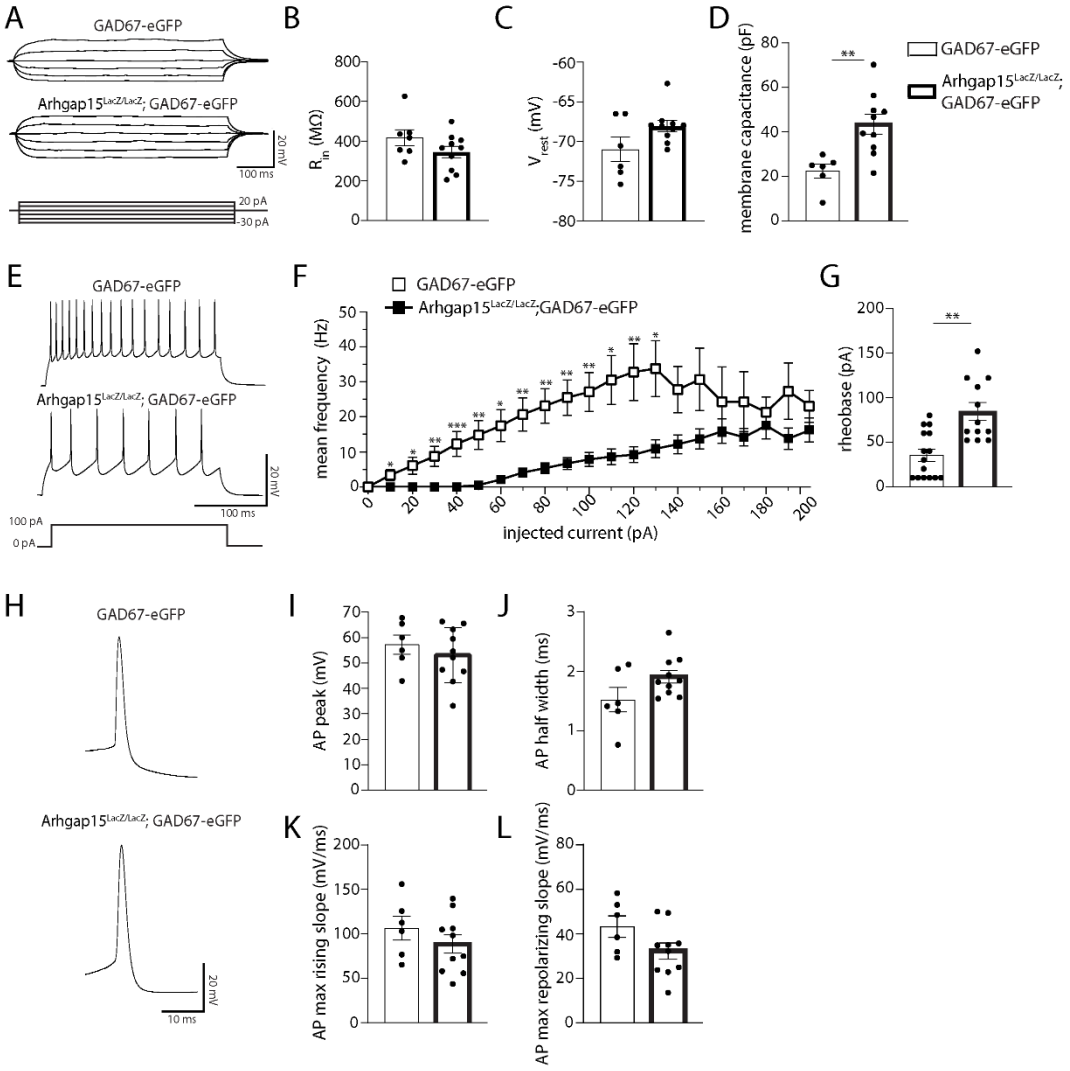
A
GAD67-eGFP
Arhgap15LacZ/LacZ; GAD67-eGFP
20 mV
100 ms
20 pA
-30 pA
B
Rin (MΩ)
C
Vrest (mV)
D
membrane capacitance (pF)
**
GAD67-eGFP
Arhgap15LacZ/LacZ; GAD67-eGFP
E
GAD67-eGFP
Arhgap15LacZ/LacZ; GAD67-eGFP
20 mV
100 ms
100 pA
0 pA
F
GAD67-eGFP
Arhgap15LacZ/LacZ;GAD67-eGFP
mean frequency (Hz)
injected current (pA)
G
rheobase (pA)
**
H
GAD67-eGFP
Arhgap15LacZ/LacZ; GAD67-eGFP
20 mV
10 ms
I
AP peak (mV)
J
AP half width (ms)
K
AP max rising slope (mV/ms)
L
AP max repolarizing slope (mV/ms)

Supplementary figure 1

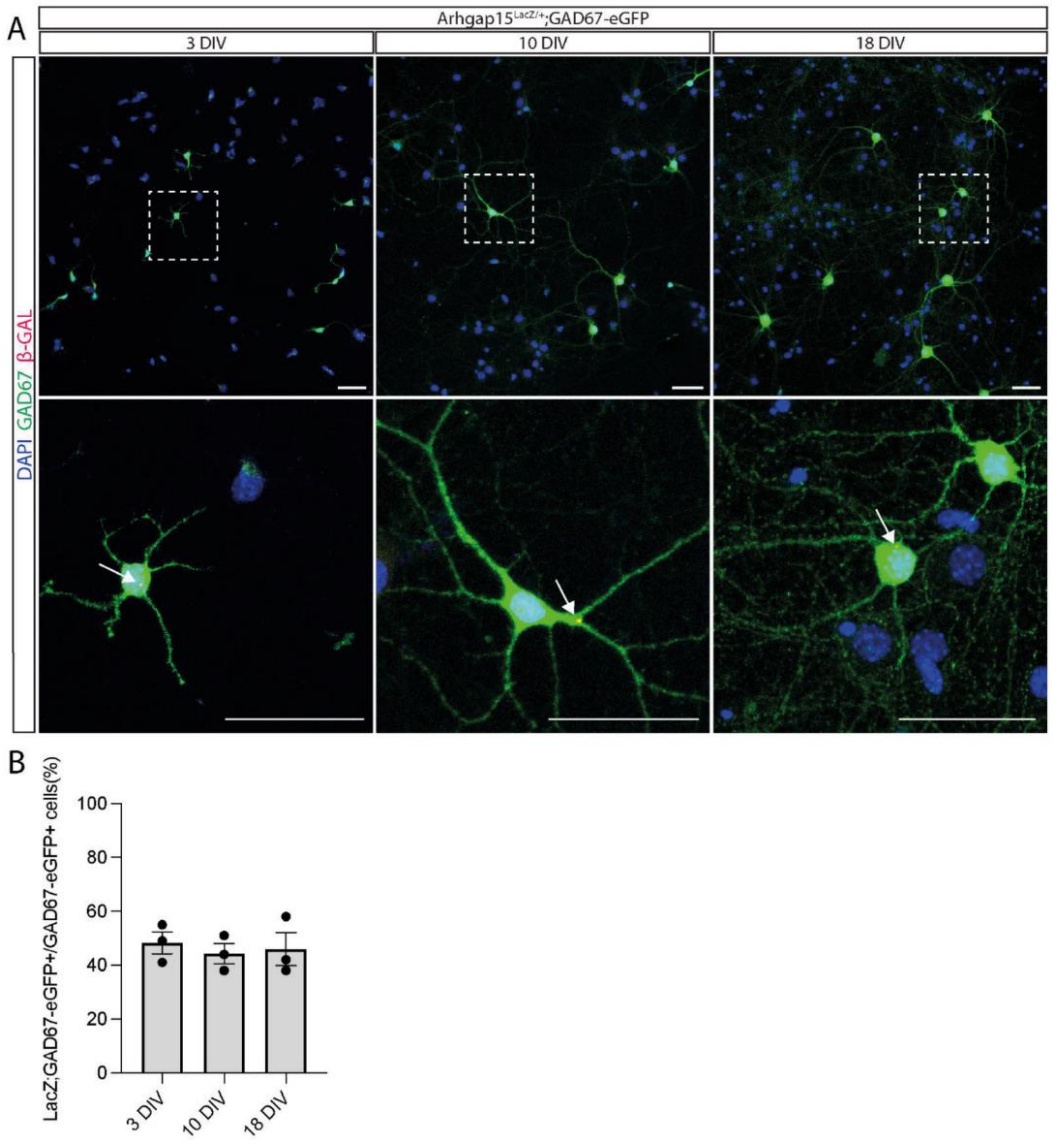

Supplementary figure 2

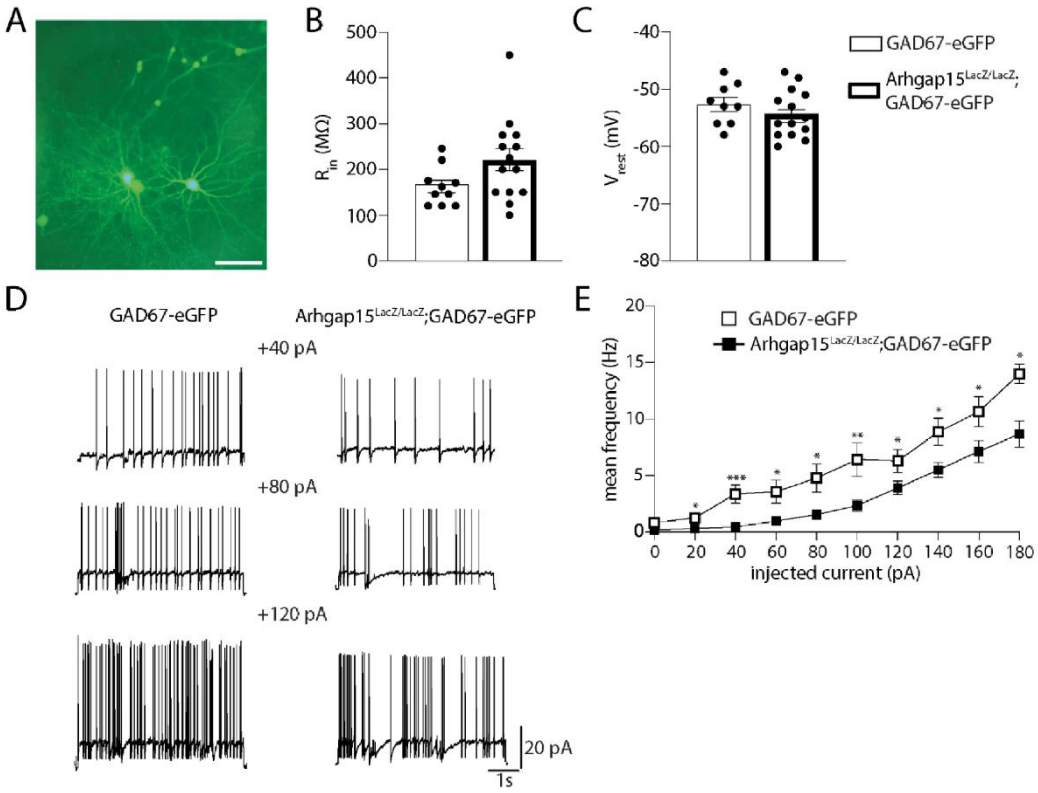

Figure legends

Figure 1. Expression of ARHGAP15 in embryonic and adult CINs. (**A**) Maximum intensity projections of z-stack images (5 serial image planes; z step size = 2 µm) of coronal sections of E11.5 and E12.5 *Arhgap15*$^{LacZ/+}$*;GAD67-eGFP* brains immunostained for β-GAL. The left-right order of the images recapitulates the rostral-caudal axis. Scale bars: 200 µm. (**B**) Coronal sections of E14.5 *Arhgap15*$^{LacZ/+}$*;GAD67-eGFP* brains. (B′) Confocal optical sections of E14.5 *Arhgap15*$^{LacZ/+}$*;GAD67-eGFP* brains immunostained for β-GAL; (B″) Maximum intensity projections of z-stack images (20 serial image planes; z step size = 0.5 µm) of the regions inside the dashed boxes in B′; (B‴) Orthogonal projections of the regions inside the dashed boxes in B″ showing the co-localization of the GAD67 and β-GAL signals. Scale bars: 200 µm in B′ and 20 µm in B″. (**C**) Coronal sections of P2 and P45 *Arhgap15*$^{LacZ/+}$*;GAD67-eGFP* brains; (C′) Maximum intensity projections of z-stack images (5 serial image planes; z step size = 2 µm) of the somatosensory cortex of P2 and P45 *Arhgap15*$^{LacZ/+}$*;GAD67-eGFP* brains immunostained for β-GAL; (C″) Maximum intensity projections of z-stack images (20 serial image planes; z step size = 0.5 µm) of the regions inside the dashed boxes in C′; (C‴) Orthogonal projections of the regions inside the dashed boxes in C″ showing the co-localization of the GAD67 and β-GAL signals. Scale bars: 200 µm in C′ and 20 µm in C″. (**D**) Representation of the different subregions of the E14.5 neocortex (left) and the correspondence between bins and cortical layers in the adult (P45) cortex (right). Scale bars: 50 µm (left) and 200 µm (right). (**E–G**) Percentage of β-GAL/GAD67 double-positive cells over the total of GAD67-positive cells across the E14.5 neocortex subregions (E), early postanal (P2) (F), and adult (P45) cortical bins (G). n = 3 E14.5 embryos, 3 P2 and 3 P45 mice. At least 100 cells were evaluated for β-GAL expression in each subregion of each brain. Data are presented as mean ± SEM. NCX, neocortex; LGE, lateral ganglionic eminence; MGE, medial ganglionic eminence; CGE, caudal ganglionic eminence; POA, preoptic area; CC, corpus callosum; STR, striatum; MZ, marginal zone; CP, cortical plate; IZ, intermediate zone; SVZ, subventricular zone; VZ, ventricular zone; GE, ganglionic eminence.

Figure 2. Expression of ARHGAP15 across the major CIN subtypes. (**A**) In the left column, maximum intensity projections of z-stack images (10 serial image planes; z step size = 2 µm) of the somatosensory cortex of P45 *Arhgap15*$^{LacZ/+}$*;GAD67-eGFP* brains immunostained for β-GAL and PVALB, CALB2, SST, or VIP. In the central column, maximum intensity projections of z-stack images (10 serial image planes; z step size = 0.5 µm) of the regions inside the

dashed boxes on the left. In the right column, orthogonal projections of the regions inside the dashed boxes in the middle showing the co-localization of the PVALB, CALB2, SST, or VIP and the β-GAL signals. Scale bars: 200 μm (left), 20 μm (middle). (**B–E**) Percentage of β-GAL/PVALB (B), β-GAL/CALB2 (C), β-GAL/SST (D), and β-GAL/VIP (E) double-positive cells over the total of PVALB, CALB2, SST, and VIP-positive cells, respectively. n = 3 mice; about 120 cells were evaluated for β-GAL expression for each bin in each brain. Data are presented as mean ± SEM.

Figure 3. Morphological analysis of primary CINs. (**A,B**) Representative fluorescence micrographs of eGFP-positive primary CINs from *GAD67-eGFP* (control) and *Arhgap15*$^{LacZ/LacZ}$*;GAD67-eGFP* mice after 3 (A) and 10 (B) DIV. Scale bars: 20 μm. (**C**) Number of branches in GAD67-eGFP and *Arhgap15*$^{LacZ/LacZ}$*;GAD67-eGFP* primary CINs after 3 DIV ($p = 8 \times 10^{-6}$). (**D,E**) Length of the longest neurite in *GAD67-eGFP* and *Arhgap15*$^{LacZ/LacZ}$*;GAD67-eGFP* primary CINs after 3 (D; $p = 7 \times 10^{-3}$) and 10 (E; p = 0.75) DIV. (**F,G**) Number of primary neurites in *GAD67-eGFP* and *Arhgap15*$^{LacZ/LacZ}$*;GAD67-eGFP* primary CINs after 3 (F; $p = 3 \times 10^{-6}$) and 10 (G; $p = 4 \times 10^{-4}$) DIV. (**H,I**) Average diameter of the soma of *GAD67-eGFP* and *Arhgap15*$^{LacZ/LacZ}$*;GAD67-eGFP* primary CINs after 3 (H; p = 0.08) and 10 (I; p = 0.04) DIV. (**J,K**) Sholl analysis showing the overall complexity of arborization in *GAD67-eGFP* and *Arhgap15*$^{LacZ/LacZ}$*;GAD67-eGFP* primary CINs after 3 DIV (J; p (from 5 to 250 μm) = 0.03, 6×10^{-3}, 2×10^{-6}, 1×10^{-6}, 1×10^{-6}, 3×10^{-6}, 3×10^{-5}, 5×10^{-6}, 6×10^{-4}, 5×10^{-3}, 2×10^{-3}, 7×10^{-3}, 0.02, 7×10^{-3}, 0.05, 0.04, 0.06, 0.01, 0.17, 0.30, 0.03, 0.10, 0.10) and 10 DIV (K; p (from 10 to 700 μm) = 0.23, 2×10^{-4}, 2×10^{-4}, 1×10^{-5}, 1×10^{-6}, 2×10^{-6}, 1×10^{-5}, 5 × 0−5, 0.04, 0.39, 0.70, 0.51, 0.88, 0.23, 0.49, 0.20, 0.18, 0.07,0.20, 9×10^{-4}, 0.20, 1×10^{-3}, 5×10^{-3}, 8×10^{-3}, 3×10^{-3}, 2×10^{-3}, 6×10^{-3}, 1×10^{-3}, 0.04, 0.14, 0.80, 0.59, 0.59, 0.64, 0.79). At least 70 (3 DIV) and 35 (10 DIV) neurons from 3 independent primary cultures were analyzed for each genotype. Data are presented as mean ± SEM. p-values were calculated using unpaired Mann–Whitney test (C–I) and unpaired multiple t-test corrected for False Discovery Rate (<1%) (J,K).*= p <0.05, ** = p <0.01, *** = p <0.001. DIV, days *in vitro*.

Figure 4. CIN tangential migration in the embryonic cortex. (**A**) Maximum intensity projections of z-stack images (10 serial image planes; z step size = 1 μm) of the neocortex of E14.5 *GAD67-eGFP* (control) and *Arhgap15*$^{LacZ/LacZ}$*;GAD67-eGFP* brains. Inserts show the analyzed cortical region. some eGFP-positive neurons are highlighted in magenta to improve visualization. The dashed line

represents the canonical CINs tangential migratory route, parallel to the pia. * indicates tangentially migrating CINs deviating from the canonical trajectory. Scale bars: 50 μm (main panels) and 200 μm (inserts). (**B**) Average density of eGFP-positive neurons in the MZ, CP, and IZ/SVZ of E14.5 *GAD67-eGFP* and *Arhgap15*$^{LacZ/LacZ}$*;GAD67-eGFP* embryos (p (from MZ to IZ/SVZ) = 0.8, 0.2, 0.99). (**C**) Polar plots showing the distribution (expressed as normalized frequency) of angles measured between tangentially migrating CIN leading processes and the line parallel to the pia in E14.5 *GAD67-eGFP* and *Arhgap15*$^{LacZ/LacZ}$*;GAD67-eGFP* brains. The dark blue line represents the average angle, the light blue area represents SEM ($p = 2.9 \times 10^{-4}$). (**D**) Average length of the longest neurite in E14.5 *GAD67-eGFP* and *Arhgap15*$^{LacZ/LacZ}$*;GAD67-eGFP* migrating CINs (p = 0.16). At least 50 neurons from 3 different embryos were analyzed for each genotype. p-values were calculated using unpaired Mann–Whitney test. *** = p< 0.001. MZ, marginal zone; CP, cortical plate; IZ, intermediate zone; SVZ, subventricular zone; VZ, ventricular zone.

Figure 5. CIN radial migration in the embryonic cortex. (**A**) Maximum intensity projections of z-stack images (5 serial image planes; z step size = 1 μm) of E17.5 *GAD67-eGFP* and *Arhgap15*$^{LacZ/LacZ}$*;GAD67-eGFP* mouse cortices. Scale bars: 100 μm. The bottom panels show a higher magnification of the region in the dashed box. Scale bars: 100 μm. (**B**) Schematic representation of the criteria used to discriminate between tangential and radial migrating CINs. The dashed lines indicate perpendicular lines to both the pia and ventricle. Leading processes forming an angle higher than 25° with the dashed line are classified as tangentially migrating CINs, while the ones forming an angle lower than (or equal to) 25° are classified as radially migrating CINs. (**C**) Frames of representative time-lapse videos of E17.5 *GAD67-eGFP* and *Arhgap15*$^{LacZ/LacZ}$*;GAD67-eGFP* mouse cortices at different time points (from 0 to 65 min). In each frame, the tip of the leading edge of representative neurons was marked to reconstruct the migratory path. In the last frame (65 min), the dashed line shows the linear distance covered by the leading edge. (**D**) Average ratio between the path and the linear distance covered by *GAD67-eGFP* and *Arhgap15*$^{LacZ/LacZ}$*;GAD67-eGFP* radially migrating neurons in the time window of the time-lapse video. At least 50 neurons from 3 different mice were analyzed for each genotype. p = 0.007. Data are presented as mean ± SEM. p-value was calculated using unpaired Mann–Whitney test. ** = p< 0.01. MZ, marginal zone; CP, cortical plate; IZ, intermediate zone; SVZ, subventricular zone, VZ, ventricular zone.

Figure 6. CIN distribution across layers in the adult cortex. (**A**) Maximum intensity projections of z-stack images (10 serial image planes; z step size = 2 μm) of coronal sections of WT and *Arhgap15LacZ/LacZ* P45 somatosensory cortices immunostained for PVALB, CALB2, SST, and VIP. (**B–E**) Average density of PVALB- (B), CALB2- (C), SST- (D), and VIP- (E) positive neurons in each bin of P45 WT and *Arhgap15*$^{LacZ/LacZ}$ somatosensory cortices. At least 4 sections from 5 different mice were analyzed for each genotype. p (PVALB) >0.99 for all bins; p (CALB2, from bin 1 to 1-10) = 0.99, 0.71, 0.99, 0.47, 0.003, 0.004, 0.005, 0.52, 0.99, 0.99, 0.65; p (SST, from bin 1 to 1-10) = 0.78, 0.32, 0.78, 0.78, 0.78, 0.44, 0.60, 0.72, 0.18, 0.02, 0.78; p (VIP, from bin 1 to 1-10) = 0.07, 0.51, 0.99, 0.76, 0.59, 0.03, 0.77, 0.99, 0.33, 0.72, 0.98. Data are presented as mean ± SEM. p-values were calculated using unpaired multiple t-test corrected for multiple comparisons using the Holm-Sidak method. * = p <0.05; ** = p <0.01.

Figure 7. Electroencephalography and pilocarpine treatment. (**A**) Representative electroencephalograms of 1 WT and 2 Arhgap15LacZ/LacZ mice. For *Arhgap15*$^{LacZ/LacZ}$ mice, both trains of spikes (top) and a series of single spikes (bottom) are shown. (**B**) Average number of spikes per hour in WT and *Arhgap15*$^{LacZ/LacZ}$ mice traces. p <0.0001. (**C**) Percentage of mice showing rhythmic spindle-like activity (left; p = 0.8), spikes and slow waves (center; p = 0.008), and trains of spikes (right; p = 0.002). n = 10 WT and 8 *Arhgap15*$^{LacZ/LacZ}$ mice. (**D**) Schematic representation of the experimental timeline (top) and a table indicating the stage classification criteria according to the modified Racine scale (bottom). (**E**) Time course of pilocarpine induced seizure manifestation (scored as stage 1–7) of WT and *Arhgap15*$^{LacZ/LacZ}$ mice. p (from 10 to 90 min) = 0.03, 0.008, 0.004, 0.005, 0.004, 0.006, 0.008, 0.03, 0.005. n = 8 (5 females and 3 males) P90 mice for each genotype. Data are presented as mean ± SEM. p-values were calculated using unpaired two-tailed Student's t-test (B), chi-square test (C), and unpaired Mann-Whitney test (E).* = p <0.05, ** = p <0.01, *** = p <0.001.

Figure 8. Whole-cell patch-clamp in acute slices. (**A**) Representative whole-cell current-clamp recordings of eGFP-positive CINs in acute slices prepared from adult *GAD67-eGFP* and *Arhgap15LacZ/LacZ;GAD67-eGFP* mice. Traces were obtained by injecting six current steps (from -30 to 20 pA, with 10 pA steps) lasting 500. ms. (**B–D**) Input resistance (R_{in}) (B; p = 0.16), resting membrane potential (V_{rest}) (C; p = 0.26), and membrane capacitance (D; p = 4×10^{-3}) of *GAD67-eGFP* and *Arhgap15*$^{LacZ/LacZ}$*;GAD67-eGFP* CINs. n = 6 cells from 4 *GAD67-eGFP* mice and 10 cells from 4 *Arhgap15*$^{LacZ/LacZ}$*;GAD67-eGFP* mice. (**E**) Representative whole-cell current clamp recordings of action potentials (APs) evoked by 100 pA

step current (bottom) for *GAD67-eGFP* (top) and *Arhgap15$^{LacZ/LacZ}$;GAD67-eGFP* (middle) CINs. (**F**) Average firing frequency vs. current relationships recorded in *GAD67-eGFP* and *Arhgap15$^{LacZ/LacZ}$;GAD67-eGFP* CINs in response to a set of injected current steps (from 0 to 200 pA, with 10 pA steps). p (from 0 to 200 pA) = 0.99, 0.02, 0.01, 0.005, 6×10^{-4}, 0.006, 0.01, 0.003, 0.003, 0.002, 0.005, 0.01, 0.007, 0.01, 0.06, 0.09, 0.35, 0.27, 0.47, 0.12, 0.38. (**G**) Average rheobase (minimum amount of current required to trigger an AP) in *GAD67-eGFP* and *Arhgap15$^{LacZ/LacZ}$;GAD67-eGFP* CINs. $p = 2 \times 10^{-3}$. n = 15 cells from 4 GAD67-eGFP mice and 12 cells from 4 *Arhgap15$^{LacZ/LacZ}$;GAD67-eGFP* mice. (**H**) Representative APs recorded from GAD67-eGFP (top) and *Arhgap15$^{LacZ/LacZ}$;GAD67-eGFP* (bottom) CINs. (**I–L**) Average AP peak (I; p = 0.45), half-width (J; p = 0.08), maximum rising slope (K; p = 0.31), and maximum repolarizing slope (L; p = 0.88) of evoked APs in *GAD67-eGFP* and *Arhgap15$^{LacZ/LacZ}$;GAD67-eGFP* CINs. n = 6 cells from 4 *GAD67-eGFP* mice and 10 cells from 4 *Arhgap15$^{LacZ/LacZ}$;GAD67-eGFP* mice. p-values were calculated using unpaired twotailed Student's t-test (B,D,I−L) and unpaired Mann–Whitney test (C,F,G). Data are presented as mean ± SEM. * = p <0.05, ** = p <0.01, *** = p <0.001.

Supplementary figure 1. β-Galactosidase expression in *Arhgap15$^{LacZ/+}$;GAD67-eGFP* cortical primary cultures. (**A**) Fluorescence micrographs of cortical primary cultures derived from *Arhgap15$^{LacZ/+}$;GAD67-eGFP* embryos after 3 (left),10 (middle), and 18 (right) DIV, immunostained for β-GAL. Images on the bottom are zoomed images of the regions inside the dashed boxes. Scale bars: 20 µm. (**B**) Percentage of β-GAL/GAD67 double-positive cells over the total of GAD67-positive cells in cortical primary cultures after 3, 10, and 18 DIV. n = 3 independent primary cultures; at least 40 (3 DIV), 30 (10 DIV), and 20 (18 DIV) neurons were analyzed for each culture. Data are presented as mean ± SEM.

Supplementary figure 2. *In vitro* current clamp analysis of *GAD67-eGFP* and *Arhgap15$^{LacZ/LacZ}$;GAD67-eGFP* primary CINs. (**A**) Epifluorescence image of eGFP-positive primary neurons at 17 DIV. Scale bar: 20 µm. (**B,C**) Input resistance (R_{in}) (B; p=0.12) and resting membrane potential (V_{rest}) (C; p=0.34) of *GAD67-eGFP* (control) and *Arhgap15$^{LacZ/LacZ}$;GAD67-eGFP* primary CINs. (**D**) Representative traces of *GAD67-eGFP* (left) and *Arhgap15$^{LacZ/LacZ}$;GAD67-eGFP* (right) primary neurons at +40 pA, +80 pA, and +120 pA pulse steps. (E) Average firing frequency vs. current relationships recorded in *GAD67-eGFP* and *Arhgap15$^{LacZ/LacZ}$;GAD67-eGFP* cultured CINs in response to a set of injected

current steps (from 0 pA to 180 pA, with 20 pA steps). p (from 0 to 180 pA) = 0.29, 0.02, 4×10^{-4}, 0.01, 0.01, 0.008, 0.04, 0.02, 0.04, 0.03; n=9 *GAD67-eGFP* and 14 *Arhgap15*$^{LacZ/LacZ}$*;GAD67-eGFP* cells. Data are represented as mean ± SEM. p values were calculated using unpaired Mann-Whitney test. * = p <0.001.

2.6 Material and methods

2.6.1 Mouse strains

All animal procedures were approved by the local Animal Ethics Committee and the Ministry of Health. Animals were maintained according to institutional animal welfare guidelines and legislation, under veterinarian surveillance. The *Arhgap15*$^{LacZ/LacZ}$ mouse strain has been previously described (C. Costa et al., 2011; Zamboni et al., 2016). Heterozygous and homozygous mutant mice are born at normal Mendelian frequency, appear overall normal, are viable and fertile, mate at regular rates, and do not show evident neurological or motor impairments. Animals were maintained in a mixed c57/bl6 genetic background. The *GAD67-eGFP* reporter mouse strain was generated by homologous recombination, introducing the enhanced-GFP (eGFP) cDNA cassette into the murine GAD1 locus, coding for GAD67 (glutamic aciddecarboxylase-67), which is expressed by GABAergic neurons starting from early developmental stages (DeDiego et al., 1994; Sakai & Miyazaki, 1997; Tamamaki et al., 2003). Heterozygous progeny was obtained from chimeric males and backcrossed to the C57BL/6 background. The loxP-flanked PGK-neo cassette, used as a selection marker for screening the recombinant embryonic stem cells, was successfully excised by mating *GAD67-eGFP* mice with CAG-cre transgenic mice (Tamamaki et al., 2003).

2.6.2 Brain preparation for histological analysis

For the collection of postnatal brains, mice were anesthetized with Avertin (30 µl of pure Avertin in 400 µl of PBS) and transcardially perfused with 10 ml of PBS (pH 7.4) and 10 ml of 4% (w/v) PFA in PBS (pH 7.4, adjusted with NaOH). Brains were removed, post-fixed overnight at 4°C in 4% PFA, placed overnight at 4°C in 30% (w/v) sucrose in PBS for cryoprotection, embedded in OCT blocks, and stored at −80° C until analysis. OCT blocks were cut into 30 µm-thick coronal sections using a cryotome (Leica CM 1950). Free-floating sections were collected in PBS in multiwell plates and stored at −20°C in a cryoprotectant solution (30% (v/v) glycerol and 30% (v/v) ethylene glycol in 0.2 M phosphate buffer, pH 7.4) until processed. The range of sections used for analysis corresponds to coronal sections 44–54 of the reference Allen Brain Atlas (Allen Reference Atlas–Mouse Brain [brain atlas]; available from atlas.brainmap.org). For the analysis, we selected neurons in the somatosensory cortical region. For the collection of embryonic brains, embryos were obtained through cesarean section at E11.5, 12.5, E14.5, or E17.5 (considering the day of the vaginal plug as E0.5) from anesthetized pregnant

dams and transferred in PBS. Embryonic brains used for immunohistochemistry were dissected and fixed overnight at 4°C in 4% PFA, then placed overnight at 4°C in 30% (w/v) sucrose in PBS for cryoprotection, embedded in OCT blocks, and stored at -80°C until analysis. OCT blocks were cut into 15 µm-thick coronal sections and collected on super-adhesive glass slides.

2.6.3 Primary cultures of cortical neurons

Round glass slides were incubated with 80% nitric acid overnight, washed with deionized water several times, sterilized by autoclaving, coated with 1 mg/ml poly-L-lysine (Sigma) in borate buffer (pH 8.5) in a 12-well plate, and washed again with deionized water. One day before establishing the culture, glass slides were rinsed in a MEM (Gibco) solution with 1% (v/v) pyruvate 100X (Gibco), 7% (w/v) glucose, 1% (v/v) Penicillin-Streptomycin, and 10% (v/v) horse serum (Gibco). *GAD67-eGFP* and *Arhgap15*$^{LacZ/LacZ}$*; GAD67-eGFP* E15.5 embryos were used to establish primary cultures of cortical neurons. Embryonic heads were dissected in sterile conditions in a cold solution of 1% (v/v) HEPES in HBSS with calcium and magnesium (Gibco). Cortices were dissected free of the rest of the brain, deprived of the meninges, washed with a cold solution containing 1% Penicillin-Streptomycin and 1% HEPES in HBSS with calcium and magnesium (Gibco), and incubated in 500 µl of Trypsine 0.05% (Gibco). Cortices were washed 5 times in HBSS at room temperature and disaggregated in a solution containing DNAase (used 1:1,000; Promega) by pipetting. Cells were counted and 80.000 cells were plated on each glass slide in a 12- well plate containing Neurobasal medium (Gibco) additioned with 1% Penicillin-Streptomycin, 2% (v/v) B27 (Gibco), and 0.25% (v/v) GlutaMAX (Gibco). Neurons were incubated at 37°C in a 5% CO2 saturation atmosphere.

2.6.4 Immunostaining and image analysis

Brain sections were washed three times in PBS, incubated for 1 h at room temperature with a blocking solution (10% goat or donkey serum and 0.2% Triton X-100 in PBS), and incubated overnight at 4°C with the primary antibodies diluted in a solution composed of 0.5% Triton X-100 and 5% goat or donkey serum. Then, sections were incubated for 2 h at room temperature with fluorophore-conjugated secondary antibodies diluted in a solution composed of 0.2% Triton X-100 and 3% goat or donkey serum and washed three times in PBS. Finally, sections were counterstained with DAPI and mounted with Mowiol onto super-adhesive glass slides. Double-immunostainings performed using two antibodies from the same

host species were performed using the Tyramide SuperBoost™ kit with AlexaFluor™ Tyramides (Invitrogen). Primary cortical cultures were fixed at 3, 10, and 18 days *in vitro* (DIV) with 4% PFA in PBS for 20 min at room temperature. Neurons were incubated for 1 h at room temperature with a blocking solution containing 5% goat serum and 0.1% Triton X-100 in PBS. The primary antibody was diluted in a solution containing 3% goat serum and 0.1% Triton X-100 in PBS and incubated overnight at 4°C. Secondary antibodies were incubated for 1 h at room temperature. Coverslips were mounted with Mowiol onto glass slides. Primary antibodies: rabbit anti-CALB2 (Calretinin; used 1:500; Swant, 7,697), rabbit anti-PVALB (Parvalbumin; used 1:1,000; Swant, PVALB27), goat anti-SST (Somatostatin; used 1:500; SantaCruz, sc-7819s), rabbit anti-β-GAL (β-Galactosidase; used 1:1,000; MP Biomedicals, SKU:085597-CF), and rabbit anti-VIP (Vasoactive intestinal peptide; used 1:500; Invitrogen, PA5- 78224). Secondary antibodies: Alexa Fluor 488 donkey antirabbit IgG and AlexaFluor 568 goat anti-mouse IgG (used 1:500; Invitrogen). Slides were examined with a Leica SP8 confocal microscope. Raw images were digitally processed to normalize the background and optimize the contrast, rotated, and sized with ImageJ (NIH, Bethesda, Maryland; http://imagej.nih.gov/ij/). For expression and layering analysis, cortices were divided into 10 horizontal bins of equal thickness (bin one is the outermost and closest to the pia, bin 10 is the innermost and closest to the ventricle). For tangential migration analysis, polar plots were generated by using matplotlib Python library (https://matplotlib. org/stable/#). Morphological analysis on primary cultures was performed using ImageJ (NIH, Bethesda, Maryland; http://imagej.nih.gov/ij/); arborization of each neuron was quantified by performing Sholl analysis (Sholl, 1953) by ImageJ plugin Sholl Analysis Plugin (v1.0), Ghosh Lab Software (http://ghoshlab.org/ software/index.html).

2.6.5 Live imaging of radially migrating neurons in organotypic slice cultures

300 μm-thick brain slices were prepared by vibratome sectioning from E17.5 *GAD67-eGFP* and *Arhgap15*$^{LacZ/LacZ}$*; GAD67-eGFP* embryos. Slices were kept in cold PBS for 20 min, then transferred in Neurobasal medium (Gibco) additioned with 1% Penicillin-Streptomycin, 2% B27 (Gibco), and 0.25% GlutaMAX (Gibco) and maintained in culture for 6 h at 37°C and 5% CO2. The organotypic slice cultures were imaged, while kept at 37°C and 5% CO2, by time-lapse video imaging for about 5 h with a frame interval of 5 min using a ×20 objective. The acquired movies were used to determine the migration trajectory of individual CINs. Videos were analyzed using the Manual Tracking plugin of ImageJ (NIH, Bethesda,

Maryland; http://imagej.nih.gov/ij/) and Photoshop (Adobe). A virtual grid with lines perpendicular to the SVZ and the pial surfaces was superimposed in each frame. Neurons were considered to be in radial orientation if their leading process (the longest and widest forward branch) formed an angle between 0° and 25° with the perpendicular lines of the grid, as previously done (Martini et al., 2009). The paths were measured by tracking the movements of the leading process of each neuron throughout the entire timelapse.

2.6.6 EEG recording of awake animals

Mice were anesthetized with isoflurane (2% (v/v) in 1 L/min O2). Four screw electrodes (Bilaney Consultants GMBH) were inserted bilaterally through the skull (anteroposterior +2.0–3.0 mm, mediolateral 2.0 mm from bregma). A grounding electrode was placed into the nasal bone. The five electrodes were connected to a pedestal and fixed with acrylic cement (Palavit), as previously described (Manfredi et al., 2009). EEGs were recorded from eighteen (ten wild-type and eight *Arhgap15*$^{LacZ/LacZ}$) freely moving awake animals in a Faraday chamber, using a Power-Lab digital acquisition system (AD Instruments) with a sampling rate of 100 Hz and a resolution of 0.2 Hz. The basal cerebral activity was recorded continuously for 6 h. EEG tracings were analyzed and scored for the presence of rhythmic 4–6 Hz sharp waves of rhythmic spindle-like events (Erbayat-Altay et al., 2008), spikes and solitary spikes followed by slow waves activity, and trains of spikes. Spikes were recognized as having a duration <200 ms with a baseline amplitude set to 4.5 times the standard deviation of the EEG signal (determined during interspike activity periods). Repetitive spiking activity (trains of spikes) was defined by the presence of at least five consecutive spikes in less than 5 s (Berretta et al., 2022). The classification “trains of spikes” was attributed to mice showing at least four events. Spike activity was quantified using LabChart 8 (AD Instruments). Segments with movement artifacts or electrical noise were excluded from statistical analysis.

2.6.7 Chemical induction of epilepsy

Eight (five females and three males) P90 mice for each genotype were transferred to individual cages in a quiet room. Atropine (1 mg/kg; Sigma) was administered by intraperitoneal injection to limit the peripheral side effects of pilocarpine. After 30 min, pilocarpine hydrochloride (350 mg/kg; Sigma) was administered by intraperitoneal injection. Animals were monitored every 10 min for 90 min after pilocarpine administration. We used a seizure staging system adapted from the established rodent seizure Racine’s scale (Racine, 1972): stage 0,

no abnormality; stage 1, exploring, sniffing and grooming ceased, becoming motionless; stage 2, forelimb and/or tail extension, appearance of rigid posture; stage 3, myoclonic jerks of the head and neck, with brief twitching or repetitive movements with head bobbing; stage 4, forelimb clonus and partial or occasional rearing and falling; stage 5, forelimb clonus, continuous rearing and falling; stage 6, tonic-clonic movements with loss of posture tone; stage 7, death.

2.6.8 Whole-cell patch-clamp recording

For acute slices, 4 *GAD67-eGFP* and 4 *Arhgap15*$^{LacZ/LacZ}$*; GAD67-eGFP* P150 mice were killed by cervical dislocation. Brains were removed and placed at 4°C in oxygenated (95% O2–5%CO2) adapted artificial cerebrospinal fluid (ACSF), containing 120 mM choline chloride, 3.5 mM KCl, 0.5 mM $CaCl_2$, 6 mM $MgSO_4$, 1.25 mM NaH_2PO_4, 25 mM D-glucose and 25 mM $NaHCO_3$. somatosensory cortex coronal slices (300 μm) were cut in ice-cold ACSF using a vibratome (Microm HM 650 V, Thermo Scientific) and subsequently placed for 30 min in ACSF containing 120 mM NaCl, 3.5 mM KCl, 25 mM, $NaHCO_3$, 25 mM D-glucose, 2.5 mM $CaCl_2$, 1.3 mM $MgSO_4$, and 1.25 mM NaH_2PO_4, at 32 °C. Slices were kept at room temperature for at least 1 h before recording. Patch electrodes of borosilicate glasses (Hilgenberg, Mansfield, Germany) were pulled to a final resistance of 5–9 MΩ. For current-clamp recordings in both brain slice and primary cultured neurons, the internal solution contained: 135 mM gluconic acid (potassium salt: K-gluconate), 5 mM NaCl, 2 mM $MgCl_2$, 10 mM HEPES, 0.5 mM EGTA, 2 mM ATP Tris, and 0.4 mM Tris-GTP. Patch-clamp recordings from CINs (somatosensory cortex, layer IV-VI) were performed in whole-cell configuration using an EPC-10 amplifier (HEKA Elektronic, Lambrecht, Germany). Traces were sampled at 10 kHz and filtered using a low-pass Bessel filter set at 2 kHz. All the experiments were performed at room temperature (22–24°C). Resting membrane potential (V_{rest}) and membrane capacitance (C_m) were routinely acquired when the whole-cell patch-clamp configuration was established. The membrane time constant (t_m) was calculated by Clampfit software following a step current injection of −30 pA. The membrane capacitance (C_m) was calculated by applying the formula $C_m = \tau_m/R_{in}$. The action potential (AP) parameters were obtained by analyzing a series of spikes recorded during tonic firing of 1–2 min duration. Tonic firing was elicited by depolarizing membranes with a minimum amount of current corresponding to the rheobase value (Marcantoni et al., 2014). After reaching steady-state condition during tonic firing, at least five APs were selected and averaged for each cell, then the measures of AP peak amplitude, half-width, maximum rising slope, and maximum repolarizing slope were performed with Clampfit software (Axon

Instruments). The peak amplitude of AP was measured from the threshold to the AP peak and the halfwidth was calculated at half-maximal AP height. To analyze the relationship between firing frequency and injected current, the membrane potential was adjusted to −70 mV and then 20 pulses of increasing intensity (from -30–160 pA, 500 ms duration) were injected. The mean firing frequency of each current step was calculated as the number of spikes per second. The rheobase was determined as the minimum amount of current required to trigger one spike. Input resistance (Rin) was calculated in a linear region of the membrane voltage injected current curve centered at the holding potential (−70 mV), through the injection of hyperpolarizing and depolarizing current steps (from −30 to 30 pA; 10 pA steps). For primary neuronal cultures, the extracellular solution for current recordings (Tyrode's solution) contained: 2 mM $CaCl_2$, 10 mM HEPES, 130 mM NaCl, 4 mM KCl, 2 mM $MgCl_2$, and 10 mM D-glucose (Tomagra et al., 2019). Patch-clamp recordings were performed using an EPC-9 amplifier (HEKA Elektronic, Lambrecht, Germany) and pClamp software (Molecular Devices, Silicon Valley, CA, United States). Analysis of firing activity was performed with Clampfit software (Axon Instruments).

2.6.9 Statistical analysis

For the statistical comparisons, GraphPad Prism software (GraphPad Software Inc.) was used. For each experiment, the statistical test used is reported in the figure legends. Shapiro-Wilk and Kolmogorov-Smirnov tests were used to test for normality, F test was used to test for equality of variance, and results were evaluated to choose the appropriate statistical test. The results are shown as mean ± Standard Error of Mean (SEM). The threshold for statistical significance was set at $p < 0.05$.

Chapter 3
The role of ARHGEF6 in INs maturation

3.1 Abstract

Mutations in the ARHGEF6 gene are associated with non-syndromic X-linked intellectual disability (ID) MRX46 (Kutsche et al., 2000; Yntema et al., 1998). The gene encodes aPIX/Cool-2, a guanine nucleotide exchange factor for the Rho GTPases RAC1. Deficiencies in this gene can result in altered activation of Rho GTPases, which underlie changes in brain microstructure, learning and memory deficits, and altered synaptic plasticity (Ramakers et al., 2012).

We observed that *Arhgef6* expression in mice starts in the ganglionic eminences around embryonic day (E) 14.5. In adulthood, *Arhgef6* is primarily expressed in the CA3 region of the hippocampus, particularly in PVALB-positive INs (INs). The absence of Arhgef6 leads to defects in hippocampal IN maturation and number in *Arhgef6-knockout* (*KO*) mice. Electrophysiological recordings in acute brain slices revealed that the loss of ARHGEF6 results in intrinsic hypoexcitability of INs. These findings suggest that ARHGEF6 is essential for the morphological and electrical maturation of INs during murine hippocampal development, supporting a link between altered inhibition and ID pathophysiology.

To investigate the role of ARHGEF6 in the human context, we generated mutant human induced pluripotent stem cell (iPSC)-derived models that recapitulate neurodevelopmental processes associated with ARHGEF6 loss-of-function mutations in patients. Forebrain dorsal and ventral organoids were derived

from mutant cells and isogenic controls. Both types of organoids exhibited substantial morphometric alterations in terms of size and shape in the absence of ARHGEF6. A more detailed study of ventral organoids revealed impaired proliferation, neurogenesis, cell survival, and differentiation. Dorsal and ventral forebrain organoids were fused together to study IN migration dynamics. The model demonstrated alterations in saltatory behavior and an overall decreased efficiency during migration. Overall, this study uncovers early neurodevelopmental underpinnings of MRX46 neuropathological defects, with a focus on the development of the inhibitory circuit at the forebrain level.

3.2 Introduction

ARHGEF6, a guanine nucleotide exchange factor (GEF), is crucial for the proper functioning and development of the brain, primarily by activating RAC1 and CDC42, which are members of the Rho GTPase family. These GTPases are central players in controlling actin cytoskeleton dynamics, a process essential for cellular structure, particularly within neurons. *ARHGEF6* mutations are indeed directly linked to X-linked intellectual disability (ID) MRX46 in humans, underscoring the significance of its normal function in brain development and cognitive processes.

Studies in mice reveal that ARHGEF6 deficiency has profound effects on forebrain neurons, specifically increasing dendritic length and spine density but leading to a reduction in functional synapses and synaptic plasticity. These structural anomalies are paralleled by cognitive impairments, including difficulties in spatial and complex learning. Specifically, ARHGEF6-deficient mice exhibit a reduction in early-phase long-term potentiation (LTP) and an increase in long-term depression (LTD) in the hippocampus's CA1 region. This impaired plasticity correlates with reduced activation of RAC1 and CDC42, indicating that the abnormalities seen in these mice likely arise from dysregulated activity of these Rho GTPases in hippocampal cells (Ramakers et al., 2012).

ARHGEF6 is particularly abundant in the hippocampus, localizing within dendritic spines and possibly acting as a component of postsynaptic density (PSD) complexes. This localization hints at a role for ARHGEF6 in spine morphogenesis, which it appears to accomplish in part through the activation of PAK3, a downstream kinase that affects actin organization within spines. Knockdown of ARHGEF6 produces notable changes in spine morphology, a phenotype also observed with PAK3 knockdown, suggesting a shared pathway. Importantly, introducing a constitutively active form of PAK3 rescues the spine abnormalities caused by ARHGEF6 deficiency, indicating a functional synergy between ARHGEF6 and PAK3 in maintaining spine structure (Nodé-Langlois et al., 2006).

RAC1, a critical factor in neuritogenesis during neuronal development, relies on GEF proteins like ARHGEF6 for its proper activation. This connection is especially relevant for forming actin-rich structures in neurons, including dendrites, spines, and growth cones. Additionally, ARHGEF7, another Rac GEF a close homolog of ARHGEF6, is involved in recruiting RAC1 in response to CDC42 to promote the formation of protrusions, such as lamellipodia, in fibroblasts (Mamula

et al., 2021). This interaction exemplifies the broader role of ARHGEF proteins in controlling actin dynamics and morphology across multiple cell types.

ARHGEF6 also plays a role in dendritic Golgi translocation in hippocampal neurons, a process influenced by reelin signaling. Reelin not only promotes dendritic Golgi translocation but enhances the effects of ARHGEF6 on this process. This effect is highly specific: Reelin tends to promote Golgi translocation into the dendrite closest to its source, which may influence apical dendrite selection and positioning during brain development (Meseke et al., 2013). This spatial aspect of reelin signaling, combined with ARHGEF6 function, further supports the precise mechanisms underlying dendritic formation and organization in neurons.

Mutations in genes involved in RAC1 regulation, such as ARHGAP15 and TRIO, have been associated with defects in IN migration and morphology. Specifically, TRIO, another Rho GEF and high-risk gene for autism spectrum disorders (ASD, ID, and epilepsy, functions in parallel with ARHGEF6 in brain development. It is abundantly expressed in both excitatory and inhibitory neurons during key developmental stages (Sun et al., 2021). TRIO deficiencies lead to disrupted neurite formation and alter glutamatergic signaling in excitatory neurons. Moreover, TRIO's hypofunction alters the proportion of IN migration and subtypes in the forebrain, reducing the overall number of INs. These effects underscore the importance of TRIO in both neurite development and in maintaining a balance between excitatory and inhibitory neuron populations (Sun et al., 2021).

Inspired by recent discoveries regarding ARHGAP15, TRIO and their influence on IN development, we sought to investigate the role of ARHGEF6, particularly within subpallial embryonic structures and in the context of GABAergic IN migration and maturation.

3.3 Results

3.3.1 *Arhgef6* expression is enriched in the hippocampal CA3 region and in GABAergic INs

Previous studies have reported *Arhgef6* expression in the adult mouse brain, particularly within the neuropil regions of the hippocampus (Ramakers et al., 2012). To precisely evaluate the expression of *Arhgef6* in adult mice (P60), we examined the localization of its mRNA by means of spatial transcriptomic. We analyzed the results of spatially resolved transcriptomics performed using the 10X Genomics Visium platform on adult wild-type (WT) mice. This method allows for simultaneous quantification of gene expression and retention of spatial information within the analyzed tissue. Coronal sections corresponding to slice 79 of the Allen Brain Reference Atlas were analyzed across a total of 8 slides (https://brain-map.org/). To validate the spatial distribution of *Arhgef6* expression, we further examined the expression patterns of established regional markers. This included *Grik4* (cornu Ammonis 3, CA3), *Prox1* (dentate gyrus, DG), and *Spink8* (CA1, CA2). While *Arhgef6* expression was detected throughout the brain, a clear enrichment was observed within the CA3 region of the hippocampus (**Figure 1A**). The overall increased expression in the hippocampus was further confirmed by western blot analysis on lysates derived from adult mouse cortex, hippocampus, and cerebellum (**Figure 1B**). As a negative control, we utilized lysates from a previously characterized *Arhgef6 knockout* (*KO*) mouse line (Ramakers et al., 2012).

To identify the specific cell types expressing *Arhgef6*, we performed a meta-analysis of a publicly available Allen Brain Atlas scRNAseq dataset (https://brain-map.org/) **(**10X Genomics) on the whole cortex and hippocampus (Z. Yao et al., 2021). While *Arhgef6* expression was relatively low overall, enrichment was observed in specific cell clusters. These clusters included various subtypes of GABAergic INs (INs), particularly somatostatin-positive (STT) and Parvalbumin-positive (PVALB) cells, as well as hippocampal INs expressing Lamp5, Lhx6, and Ntng1. Notably, CA3 glutamatergic neurons and Mossy cells displayed higher expression levels compared to other clusters (**Figure 1C**).

Contextually, in situ hybridization (ISH) assays using a previously validated Arhgef6 probe (Lein et al., 2007) revealed that the earliest regions to exhibit *Arhgef6* expression during murine telencephalon development are the lateral,

medial, and caudal ganglionic eminences, approximately at embryonic day (E) 14.5. These regions are the primary sources of INs (INs) for pallial structures.

3.3.2 Loss of ARHGEF6 reduces the number of GABAergic INs the adult hippocampus

To investigate the specific role of ARHGEF6 in INs, we crossed *Arhgef6-KO* mice with the *GAD67-eGFP* reporter strain (Tamamaki et al., 2003). Subsequently, we examined coronal sections of the hippocampus and cortex from adult P45 *Arhgef6-KO;GAD67-eGFP* mice and compared them to sections from *GAD67-eGFP* control mice. The brains of *Arhgef6-KO;GAD67-eGFP* mice exhibited a significant reduction in the density of eGFP-positive cells throughout the hippocampus, particularly within the CA2 and CA3 regions (**Figure 1E-F**).

3.3.3 *Arhgef6-KO* primary hippocampal INs exhibit an altered morphology

Given the well-established role of RAC1 GTPase in neurite outgrowth, we aimed to determine whether the hypoactivation of the RAC1 pathway, resulting from the loss of ARHGEF6 (Ramakers et al., 2012), might affect the morphology of hippocampal GABAergic INs. To address this, we prepared primary cultures of dissociated neurons from the hippocampi of *GAD67-eGFP* and *Arhgef6-KO;GAD67-eGFP* pups at postnatal day (P) 0 and maintained the cultures for 10 days *in vitro* (DIV). eGFP-positive neurons were readily visible, but immunofluorescent staining against GFP was performed to enhance resolution (**Figure 2A**). The neurons were then analyzed for neurite length and overall complexity (**Figures 2B-E**). Sholl analysis was employed to assess neurite arborization. At 10 DIV, *Arhgef6-KO* eGFP-positive neurons displayed a decreasing number of intersections in the distance range of 60 to 200 µm from the soma. In contrast, the number of intersections for eGFP-positive cells derived from *GAD67-eGFP* hippocampi increased with distance from the soma, up to 200 µm. Overall, *Arhgef6-KO eGFP*-positive neurons exhibited a significant lower number of intersections compared to GAD67-eGFP neurons in the distance range of 80 to 200 µm (**Figure 2B**). These findings suggest that *Arhgef6-KO* neurons may have impaired branching ability during later stages of *in vitro* maturation. No significant differences were observed in the number of primary neurites, length of the longest neurite, or soma diameter between the two groups (**Figures 2C-E**).

3.3.4 Loss of ARHGEF6 results in INs hypoexcitability

Previous studies have demonstrated that the absence of ARHGEF6 in hippocampal pyramidal neurons leads to alterations in long-term potentiation (LTP) and long-term depression (LTD) within the Schaffer collateral-CA1 circuitry (Ramakers et al., 2012). To determine the impact of ARHGEF6 depletion on INs electrophysiological properties, we performed whole-cell patch-clamp recordings in acute slices obtained from adult *GAD67-eGFP* and *Arhgef6-KO;GAD67-eGFP* mice (**Figures 2F-S**). Representative traces of evoked action potentials (APs) revealed differences in the baseline and frequency between *WT* and *Arhgef6-KO* mice (**Figure 2G**). We observed a reduced firing rate of *Arhgef6-KO* INs in response to the injection of current pulses of increasing amplitude (from 0 to 300 pA), starting from 70 pA of amplitude (**Figures 2H**). We measured the instantaneous firing frequency at the onset (f_o) and steady-state (f_{ss}) of the spike train (**Figures 2I, J**). By plotting f_o and f_{ss} against injected current, we assessed the spike frequency adaptation of these neurons. A significant reduction in both f_o and f_{ss} was observed at 120, 180, and 280 pA of injected current, with the exception of f_o at 280 pA (**Figures 2I,J**).Despite this, INs exhibited similar input resistance (R_{in}), resting membrane voltage (V_{rest}), membrane capacitance, and rheobase (**Figures 2K-N**). No differences were found in the single action potential (AP) properties (*i.e.*, AP peak amplitude, AP half-width, AP max rising slope, and AP max repolarizing slope) (**Figures 2O-S**).

3.3.5 *ARHGEF6-KO* hiPSCs-derived NPCs display altered cytoskeletal organization and a reduced expression of telencephalic markers

To investigate the role of ARHGEF6 during human telencephalon development, with a specific focus on subpallial (ventral) development, we generated an *ARHGEF6-KO* line of human induced pluripotent stem cells (hiPSCs) using CRISPR-Cas9 technology. A commercially available male hiPSC line was targeted, and a CRISPR guide RNA (crRNA) was designed to target the first common exon to all isoforms, specifically the third exon. The resulting mutation in the selected clone is a frameshift mutation caused by a 1-base pair deletion (**Figure 3A**). The line was sequenced to confirm the absence of mutations in the top three off-target sites predicted by IDT (**Supplementary figure 1**). The control line, termed the ribonucleoprotein (RNP) negative control, was obtained by electroporating the cells with a crRNA computationally designed to not have

homology to genomic targets in human. The mutated cell line was successfully maintained as a pluripotent stem cell line (OCT4 and SOX2-positive) and differentiated into neural progenitor cells (NPCs; NESTIN and SOX2-positive), radial-glia like cells (RGCs; PAX6 and FABP7-positive), neurons, and embryoid bodies (EBs) with tissues derived from the three germinal layers (ectoderm TUJ1-positive, mesoderm ACTA2-positive, and endoderm GATA4-positive) (**Figures 3B-F**).

To assess the impact of the RAC1 pathway on cytoskeletal dynamics, phalloidin-FITC staining was performed on NPCs to visualize F-actin filaments and evaluate cytoskeletal organization (**Figure 3F**). The anisotropy index, a measure of F-actin fiber orientation distribution, was calculated. Cells exhibiting a higher number of fibers aligned in the same direction were considered more anisotropic. *ARHGEF6-KO* cells displayed a significantly higher anisotropy index (**Figure 3G**), suggesting a shared preference for fiber orientation angles with control cells (Figure 3H). The cellular content of polymerized actin was determined by quantifying the fluorescent phalloidin signal, normalized to background fluorescence, and calculating the corrected total cell fluorescence (CTCF). *ARHGEF6-KO* cells exhibited a significant reduction in F-actin content compared to controls (**Figure 3I**), despite no significant difference in the number of F-actin punctae (**Figure 3J**) or average cell surface area (**Figure 3K**). The same NPC cell cultures exhibited decreased expression of the telencephalic markers PAX6 and EMX2, as well as the radial glia marker FABP7.

3.3.6 *ARHGEF6-KO* organoids exhibit altered shape, density and reduced size

To assess the impact of ARHGEF6 ablation on the morphology and polarity of RGC, we employed a standardized single-neural rosette protocol (Birtele et al., 2023; Knight et al., 2018), enabling high-throughput generation and analysis of rosette formation. We observed homogeneous expression of the cortical progenitor marker SOX2, accompanied by radially organized acetylated tubulin networks, in rosettes derived from the *ARHGEF6-KO* cell line. (not shown) However, these structures exhibited reduced organization in *ARHGEF6-KO* tissues, and their formation rate was elevated compared to the RNP negative control (**Figure 4A**).

To address the limitations inherent to the study of human forebrain development in 2D cell cultures, we utilized 3D forebrain organoids. These organoids can be induced to differentiate into specific brain regions through the

application of morphogens, signaling molecules capable of specifying cell fates in a concentration-dependent manner. To selectively enhance the consistency and yield of ventral forebrain regions within a specific organoid cohort, we incorporated a drug treatment regimen that augments SHH signaling while concurrently inhibiting WNT signaling, as previously described (Bagley et al., 2017; Birey et al., 2017, 2022). At 24 days, a time point corresponding to the conclusion of the patterning phase of the differentiation protocol, all organoids exhibited multiple germinal areas (rosettes) upon brightfield microscopy analysis (not shown). At the two-month time point, both dorsal and ventral *ARHGEF6-KO* organoids exhibited a significant reduction in overall area and density, quantified as the product of the area and mean gray value within the organoid compared to the isogenic controls (**Figures 4D,F**). Furthermore, alterations were observed in morphological parameters. Both dorsal and ventral organoids displayed changes in aspect ratio and roundness (**Figures 4G,H).** However, only *ARHGEF6-KO* dorsal organoids demonstrated an increase in circularity and solidity indices, accompanied by a decrease in the overall number of inflection points (**Figures 4E,I,L**), which directly correlates with the number and size of ventricles (Chiaradia et al., 2023).

3.3.7 One-month-old *ARHGEF6-KO* ventral organoids exhibit impaired neuronal survival and ventral patterning

To elucidate the underlying cause of the reduced size observed in *ARHGEF6-KO* organoids compared to RNP negative controls, we conducted a detailed cellular analysis of survival, proliferation, and differentiation dynamics at both the one- and two-month (2M) time points. TUNEL staining performed on 1M ventral organoids revealed an elevated mortality rate in *ARHGEF6-KO* organoids compared to controls (**Figures 5A-B**). Specifically, TUNEL-positive punctae were distributed throughout the organoid, with a higher density observed in intergerminal areas, suggesting that the increased mortality may predominantly affect post-mitotic cells rather than proliferative progenitor cells within the rosettes. Consistent with this observation, both the number of neurons (NEUN-positive cells) and NPCs was decreased in *ARHGEF6-KO* organoids compared to RNP negative controls, with a more pronounced reduction in the number of neurons (**Figures 5C-E**). Notably, the ratio between the two cell types remained relatively unchanged between the two genotypes (**Figure 5G**). A slight, non-significant reduction ($p = 0.0652$) in the number of MKI67-positive cells was observed. The presence of NKX2.1 is a key indicator of successful ventral forebrain development, specifically the formation of medial ganglionic eminence (MGE)-like structures that are the major source of INs in humans (Hansen et al., 2013; Ma et al., 2013). Immunostaining for NKX2.1 in

both genotypes revealed successful ventral patterning. However, quantification of the NKX2.1/SOX2-positive cell ratio indicated a reduction in the number of NKX2.1-positive progenitor cells in *ARHGEF6-KO* organoids compared to controls (**Figures 5F,I**). Collectively, these findings suggest that the loss of ARHGEF6 during the early stages of ventral forebrain development may compromise cell survival, particularly of newly generated neurons, and lead to subtle defects in ventral patterning.

3.3.8 Two-month-old *ARHGEF6-KO* ventral organoids exhibit a delayed depletion of the progenitor pool

Given the significant structural reorganization of ventral organoids at 2M, marked by the absence of rosettes and a neuronal surge, we selected this time point for a comparative analysis similar to that conducted at 1M. TUNEL staining of 2M ventral organoids revealed a significantly higher mortality rate in *ARHGEF6-KO* organoids compared to controls (**Figures 6A-B**). While a slight, non-significant reduction in NEUN-positive cells was observed (p=0.1523), a substantial increase in SOX2-positive cells was noted (p=0.0007) (**Figures 6C-E**). This, coupled with a marked decrease in the overall NEUN/SOX2 ratio (**Figure 6F**), suggests a potential delay in developmental trajectory. The increased number of SOX2-positive cells in *ARHGEF6-KO* organoids, as compared to RNP-negative controls, is further supported by an increase in MKI67-positive cells (**Figures 6G,H**). Notably, the MKI67/DAPI ratio in 2M KO organoids more closely resembles that of 1M-old control organoids (**Figures 5H, 6H**).

3.3.9 *ARHGEF6-KO* INs exhibit impaired migration in dorsal-ventral assembloids

Defects in IN migration can disrupt the formation of cortical circuits and contribute to neurodevelopmental disorders. To investigate interregional interactions between the ventral and dorsal forebrain in the context of migrating GABAergic neurons, we infected ventral organoids with lentivirus LV-DLX1/2-eGFP to label INs. At 2 months, we fused these ventral organoids with dorsal organoids to create dorsal-ventral forebrain assembloids, following previously established protocols (Bagley et al., 2017; Birey et al., 2017, 2022) (**Figures 7A,B**). These dorsal-ventral assembloids recapitulate the migration of multiple MGE-derived IN subtypes (Bagley et al., 2017). They also recapitulate the INs peculiar saltatory migration observed in the developing fetal forebrain which is a type of

movement characterized by alternating phases of rapid movement ("saltations") and pauses (Birey et al., 2017).

To examine the behavior of migrating eGFP-positive cells, we performed time-lapse recordings of eGFP-positive cells in dorsal-ventral assembloids cultured for 1-2 weeks (**Figure 7C**). The eGFP-positive ventral region was readily distinguishable from the eGFP-negative dorsal region, allowing for clear visualization of the morphology of sparsely labeled eGFP-positive cells migrating into the dorsal region. *ARHGEF6-KO* eGFP-positive INs exhibited a distinct migration phenotype, characterized by decreased saltation frequency (**Figure 7E**), decreased saltation length (**Figure 7F**), and increased saltation duration (**Figurse 7H,I**). The overall average velocity of *ARHGEF6-KO* eGFP-positive INs was consistently reduced compared to RNP-negative controls (**Figure 7G**). To quantify the directness of migration, we calculated the ratio of the actual path length to the vectorial distance. A higher ratio indicates a more tortuous path. The index of *ARHGEF6-KO* eGFP-positive INs was significantly increased compared to RNP-negative control assembloids. While the percentage of cells migrating in the interphase direction (ventral to dorsal) was comparable between genotypes (**Figure 7M**), the number of eGFP-positive cells in the dorsal compartment was reduced in *ARHGEF6-KO* assembloids after 2 weeks post-fusion compared to RNP-negative controls (**Figures 7N,D**), normalizing the dorsal-to-ventral eGFP-positive cell density ratio. To investigate potential non-cell autonomous effects due to alterations in dorsal compartment cues, we employed a mixed and matched approach, creating chimeric assembloids with *ARHGEF6-KO* dorsal compartments fused with RNP-negative ventral compartments and vice versa. These experiments demonstrated that the number of cells in the dorsal compartment was primarily influenced by the genotype of the ventral compartment. A decrease in eGFP-positive cells was observed in RNP-negative dorsal-*ARHGEF6-KO*-ventral assembloids, but not in *ARHGEF6-KO* dorsal-RNP-negative ventral assembloids (**Figure 7N,D**).

3.4 Discussion

Alterations in GABAergic INs and GABA receptors have been implicated in ID and various NDDs that often include ID as a core feature (Marín, 2012). This suggests a critical role for INs in these disorders, although the precise pathoetiological mechanisms remain poorly understood. This work sheds light on the critical role of ARHGEF6, a gene associated with MRX46, in forebrain development, particularly in the maturation of GABAergic interneurons.

Our findings suggest that ARHGEF6 deficiency leads to a significant reduction in the total number of INs throughout the hippocampus, especially at the level of the CA2 and CA3 regions. Changes in IN density have been observed in different NDD patients and mouse models, although the specific IN subtypes affected can vary (Marín, 2012). Given the pivotal role of INs in modulating the delicate balance of excitation and inhibition in neural circuits, alterations in IN subtype ratios and distribution may contribute to network-level changes in excitability.

ARHGEF6 deficiency is known to alter long-term potentiation (LTP) and long-term depression (LTD) in the Schaffer collateral-CA1 pathway of hippocampal pyramidal neurons. Our preliminary electrophysiological analysis of hippocampal INs revealed a decrease in mean firing rate in response to current injection in ARHGEF6-deficient mice compared to controls. Further investigations are needed to fully understand the underlying mechanisms of reduced intrinsic excitability in these neurons. Furthermore, we have not yet determined the precise impact of GABAergic neuron hypoexcitability on overall network activity. The effect may vary depending on the specific subtype of interneuron most affected by the loss of ARHGEF6. Given the high expression of ARHGEF6 in hippocampal PVALB-positive interneurons of the CA3 region, these cells are likely to have a significant influence on the network excitation-inhibition balance.

Considering the established role of RAC1 GTPase in neurite outgrowth, we examined the impact of ARHGEF6 on INs morphology by culturing hippocampal neurons from *GAD67-eGFP* and *Arhgef6-KO;GAD67-eGFP* mice. Arhgef6-deficient INs exhibited altered morphological features *in vitro*, specifically decreased branching ability and reduced arborization complexity.

We extended our investigation to the human context by generating *ARHGEF6-KO* hiPSCs. Using these cells, we obtained 2D NPCs cultures and 3D organoids that recapitulate aspects of human forebrain development, including the

generation and migration of INs. NPCs reveal alterations in the cytoskeletal organization and reduced expression of telencephalic markers in *ARHGEF6-KO* organoids, whereas defects observed in forebrain ventral organoids revealed that the loss of ARHGEF6 collectively compromises cell survival of newly born neurons and the loss of depletion in the pool of progenitor cells at 2M, suggesting a potential developmental delay. We used a dorsal-ventral assembloid model to study IN migration dynamics. This sophisticated model combines dorsal and ventral forebrain organoids, allowing for the observation of interregional interactions between developing brain regions. The results show alterations in the saltatory behavior and a decrease in overall migration efficiency of INs in the *ARHGEF6-KO* assembloids.

Considering the results obtained *in vitro*, we hypothesize that the reduction in IN number may in part be due to impaired neuronal migration or maturation. GABAergic INs originate from progenitors in the ganglionic eminence and undergo a complex migratory journey to reach their final destinations. Their migration involves multiple and specific tangential and radial routes during telencephalic development, which are crucial for establishing the cellular complexity of various brain regions and neural circuits. The reduced number of INs in the brains of adult *Arhgef6-KO* mice may be attributed to impaired migration, leading to fewer INs exiting the ganglionic eminence.

While ARHGEF6 mutations have not been directly linked to microcephalic phenotypes in patients, the observed defects in progenitor cell proliferation and differentiation, along with the reduced organoid size, suggest a potential role in early neurodevelopmental processes. Interestingly, mutations in Rho GTPases and their regulators have been implicated in various NDDs; however, their involvement in neural progenitor cell (NPC) proliferation and developmental delay remains relatively unexplored. Confirmed microcephaly loci encode proteins that regulate the balance between cell cycle progression, apoptosis, and cytokinesis in neuroepithelial progenitors. Rho GTPases, including RAC1, influence the activity of cyclin-dependent kinases and the organization of the microtubule and actin cytoskeleton during mitosis (Jaffe & Hall, 2005). Although the specific role of RAC1 in mitosis is not fully understood, it may play a crucial role in the cytokinesis of neural progenitors. This hypothesis is supported by the identification of distinct missense variants in RAC1 (p.Cys18Tyr and p.Asn39Ser) in microcephalic patients, which result in dominant-negative alleles, reduced neuronal proliferation, and cerebellar abnormalities (Reijnders et al., 2017). Furthermore, RAC1 deficiency in rodent models leads to alterations in the radial glial cell pool and a

smaller forebrain (L. Chen et al., 2009). Also, considering the dual regulatory role of ARHGEF6 on both RAC1 and CDC42 (Ramakers et al., 2012), it will be essential to dissect the specific contributions of these GTPases to the observed cellular phenotypes, and to determine whether their dysregulation occurs independently or in concert

Overall, these findings provide compelling evidence for the crucial role of ARHGEF6 in forebrain development, particularly in the maturation and function of GABAergic interneurons. By demonstrating ARHGEF6's importance for the proper development and function of GABAergic interneurons, this work provides a potential cellular and molecular basis for the cognitive impairments associated with MRX46.

3.5 Figures

Figure 1

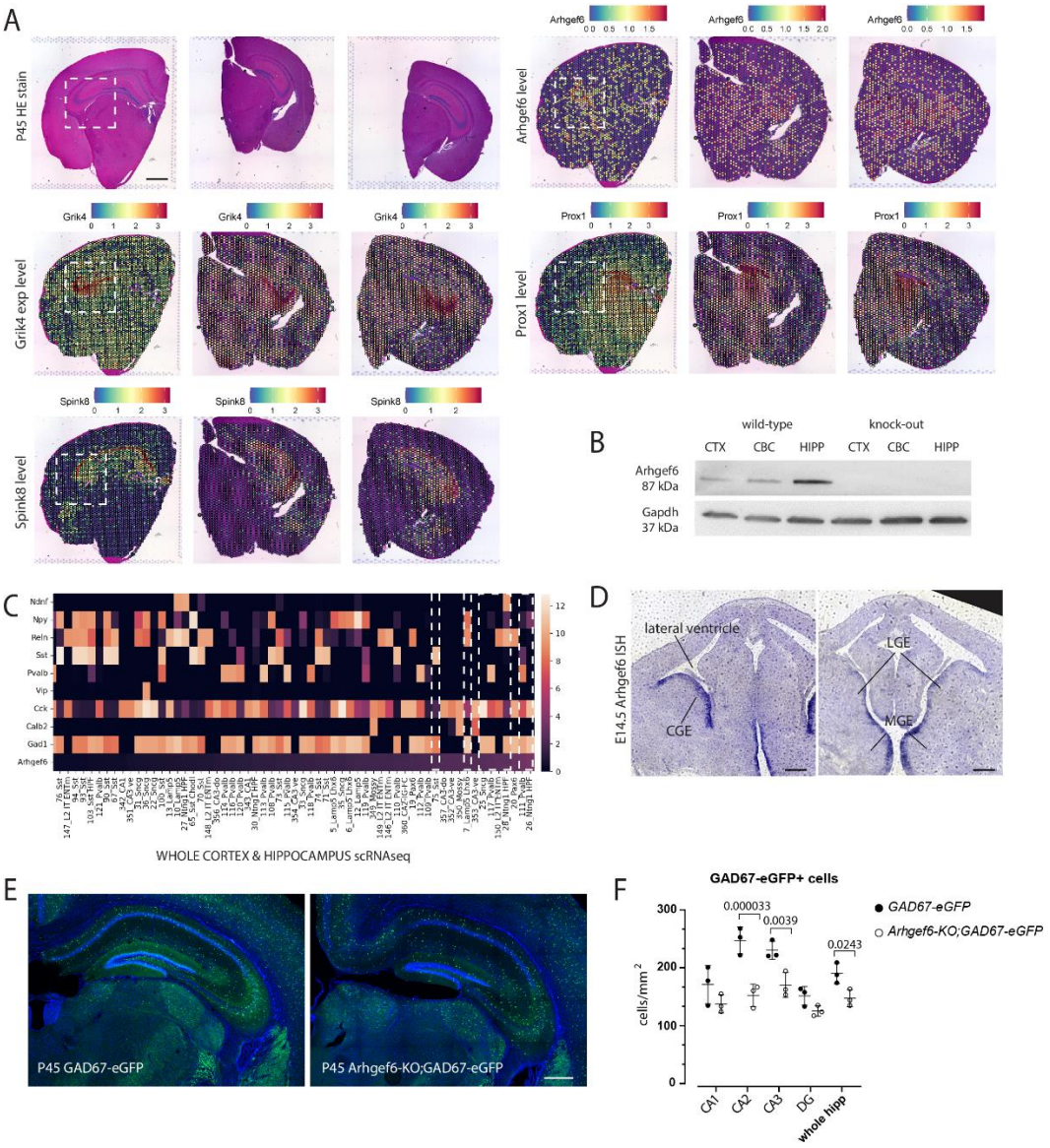

Figure 2

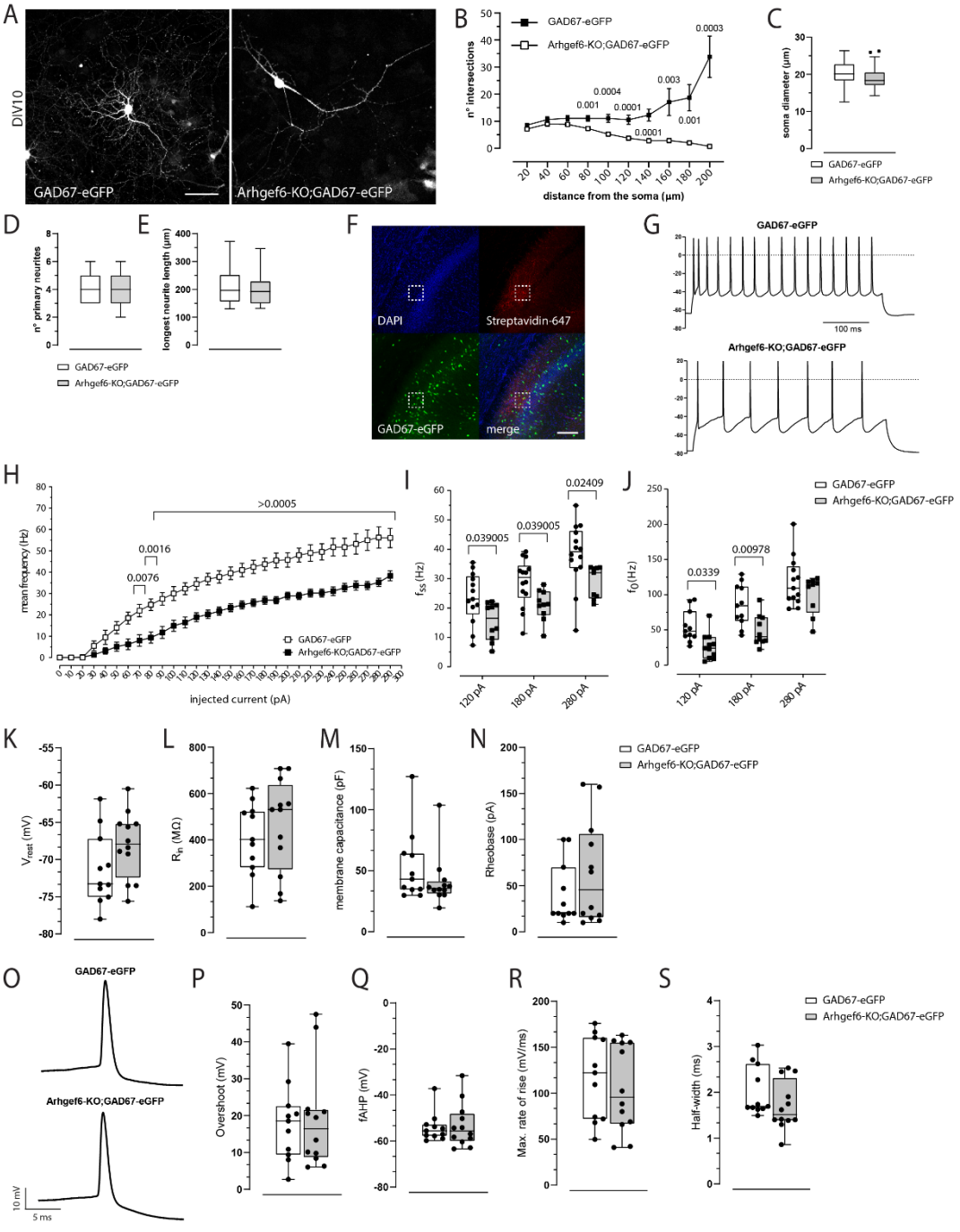
A
DIV10
GAD67-eGFP
Arhgef6-KO;GAD67-eGFP
B
GAD67-eGFP
Arhgef6-KO;GAD67-eGFP
n° intersections
distance from the soma (µm)
0.0003
0.003
0.0004
0.001
0.0001
0.001
0.0001
C
soma diameter (µm)
GAD67-eGFP
Arhgef6-KO;GAD67-eGFP
D
n° primary neurites
E
longest neurite length (µm)
F
DAPI
Streptavidin-647
GAD67-eGFP
merge
G
GAD67-eGFP
100 ms
Arhgef6-KO;GAD67-eGFP
H
mean frequency (Hz)
>0.0005
0.0016
0.0076
injected current (pA)
I
f_{SS} (Hz)
0.039005
0.039005
0.02409
120 pA
180 pA
280 pA
J
f_0 (Hz)
0.0339
0.00978
K
V_{rest} (mV)
L
R_{in} (MΩ)
M
membrane capacitance (pF)
N
Rheobase (pA)
O
GAD67-eGFP
Arhgef6-KO;GAD67-eGFP
10 mV
5 ms
P
Overshoot (mV)
Q
fAHP (mV)
R
Max. rate of rise (mV/ms)
S
Half-width (ms)

Figure 3

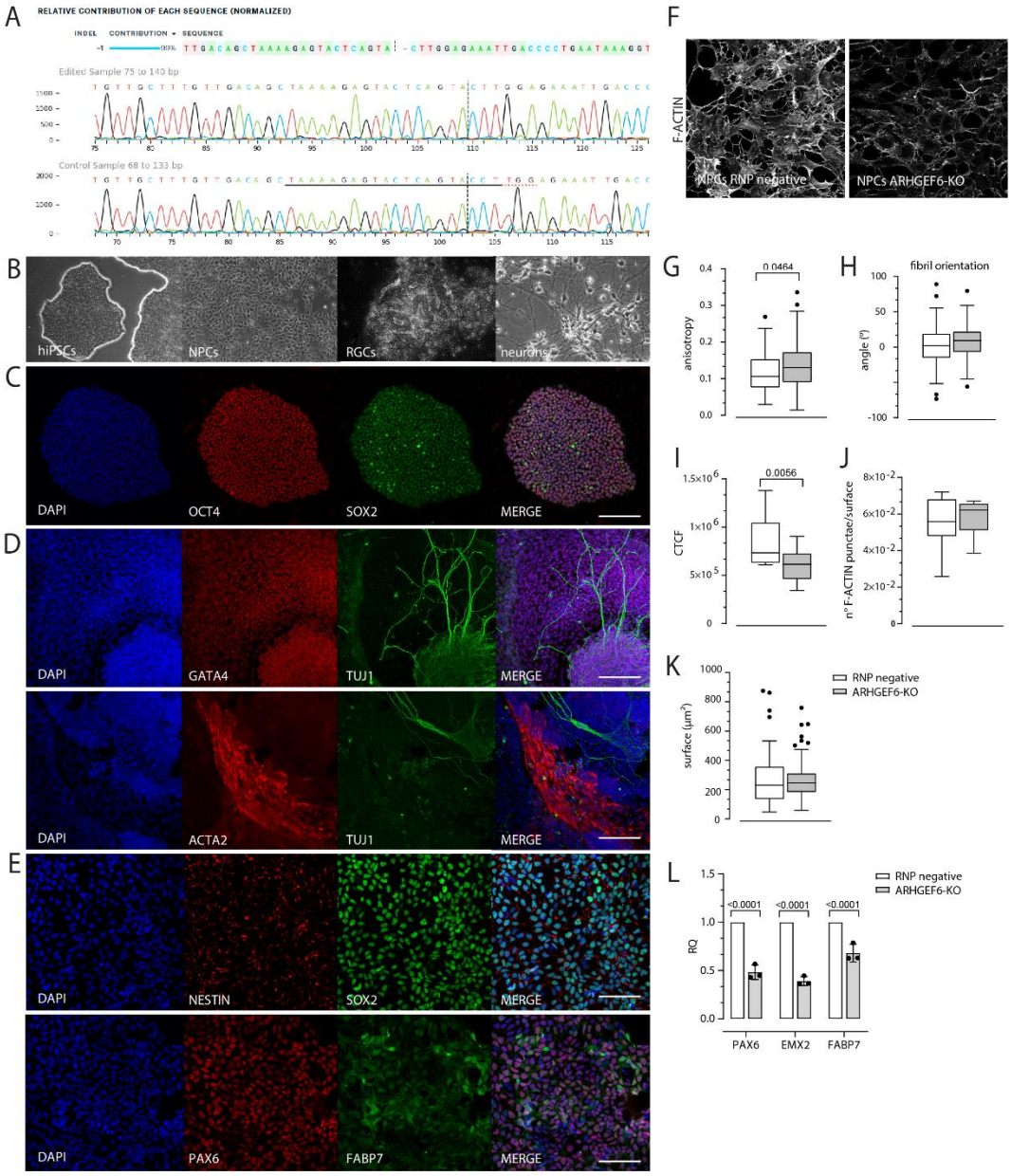
A
RELATIVE CONTRIBUTION OF EACH SEQUENCE (NORMALIZED)
INDEL CONTRIBUTION SEQUENCE
Edited Sample 75 to 140 bp
Control Sample 68 to 133 bp
B
hiPSCs
NPCs
RGCs
neurons
C
DAPI
OCT4
SOX2
MERGE
D
DAPI
GATA4
TUJ1
MERGE
DAPI
ACTA2
TUJ1
MERGE
E
DAPI
NESTIN
SOX2
MERGE
DAPI
PAX6
FABP7
MERGE
F
F-ACTIN
NPCs RNP negative
NPCs ARHGEF6-KO
G
0.0464
anisotropy
H
fibril orientation
angle (°)
I
0.0056
CTCF
J
n° F-ACTIN punctae/surface
K
RNP negative
ARHGEF6-KO
surface (µm²)
L
RNP negative
ARHGEF6-KO
<0.0001
<0.0001
<0.0001
RQ
PAX6
EMX2
FABP7

Figure 4

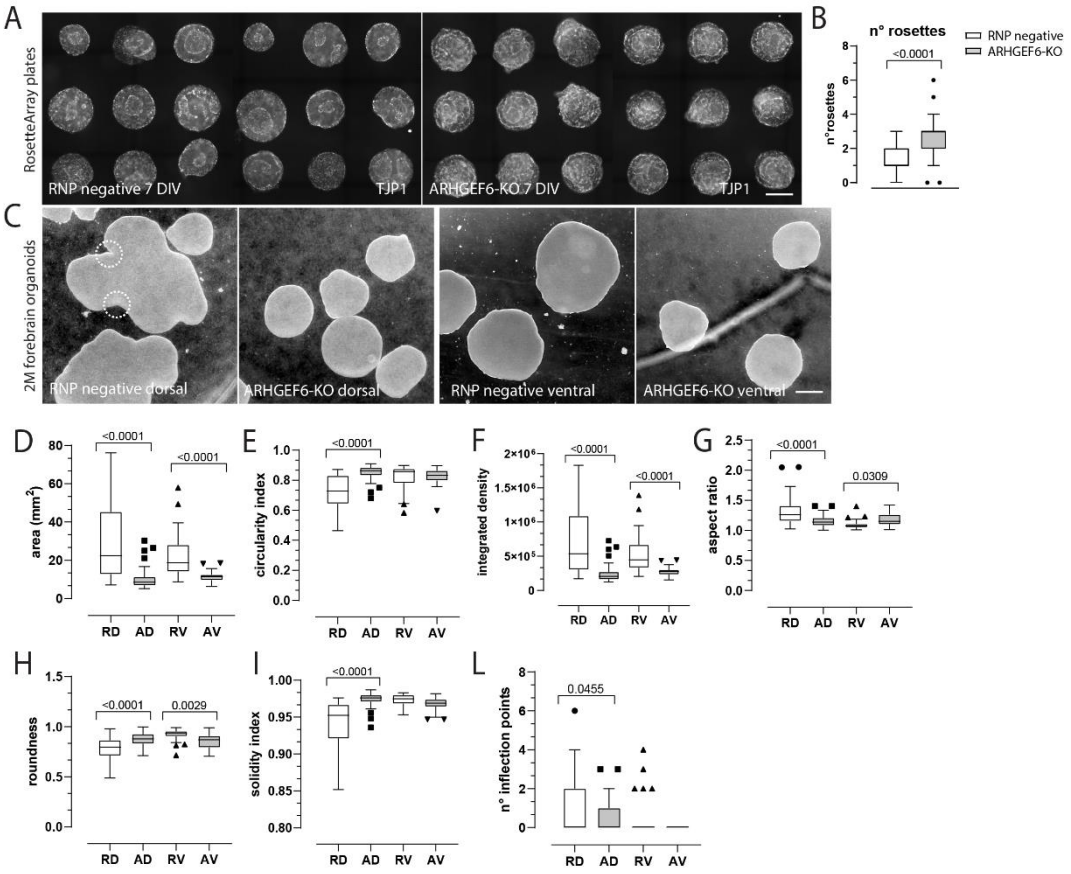
A
RosetteArray plates
RNP negative 7 DIV
TJP1
ARHGEF6-KO 7 DIV
TJP1
B
n° rosettes
RNP negative
ARHGEF6-KO
<0.0001
n°rosettes
C
2M forebrain organoids
RNP negative dorsal
ARHGEF6-KO dorsal
RNP negative ventral
ARHGEF6-KO ventral
D
area (mm²)
<0.0001
<0.0001
E
circularity index
<0.0001
F
integrated density
<0.0001
<0.0001
G
aspect ratio
<0.0001
0.0309
H
roundness
<0.0001
0.0029
I
solidity index
<0.0001
L
n° inflection points
0.0455
RD AD RV AV

Figure 5

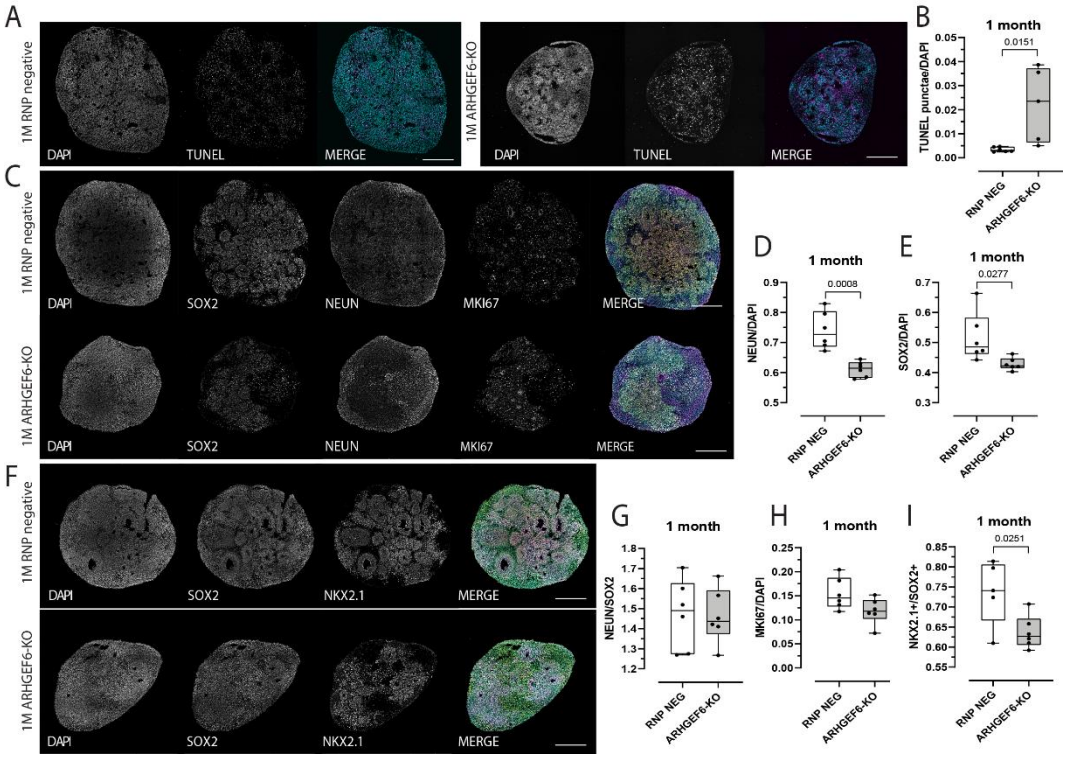
A
1M RNP negative
1M ARHGEF6-KO
DAPI
TUNEL
MERGE
B
1 month
0.0151
TUNEL punctae/DAPI
RNP NEG
ARHGEF6-KO
C
1M RNP negative
1M ARHGEF6-KO
DAPI
SOX2
NEUN
MKI67
MERGE
D
1 month
0.0008
NEUN/DAPI
E
1 month
0.0277
SOX2/DAPI
F
1M RNP negative
1M ARHGEF6-KO
DAPI
SOX2
NKX2.1
MERGE
G
1 month
NEUN/SOX2
H
1 month
MKI67/DAPI
I
1 month
0.0251
NKX2.1+/SOX2+

Figure 6

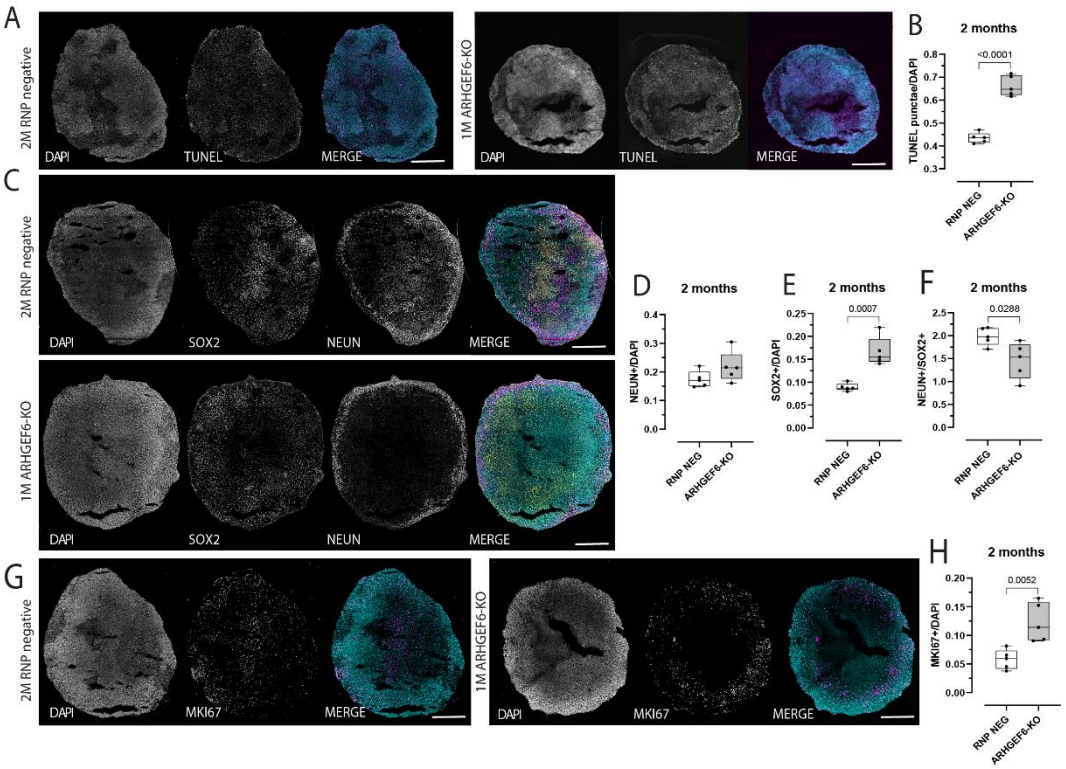
A
2M RNP negative
1M ARHGEF6-KO
DAPI
TUNEL
MERGE
B
2 months
<0.0001
TUNEL puncta/DAPI
RNP NEG
ARHGEF6-KO
C
2M RNP negative
1M ARHGEF6-KO
DAPI
SOX2
NEUN
MERGE
D
2 months
NEUN+/DAPI
E
2 months
0.0007
SOX2+/DAPI
F
2 months
0.0288
NEUN+/SOX2+
G
2M RNP negative
1M ARHGEF6-KO
DAPI
MKI67
MERGE
H
2 months
0.0052
MKI67+/DAPI

Figure 7

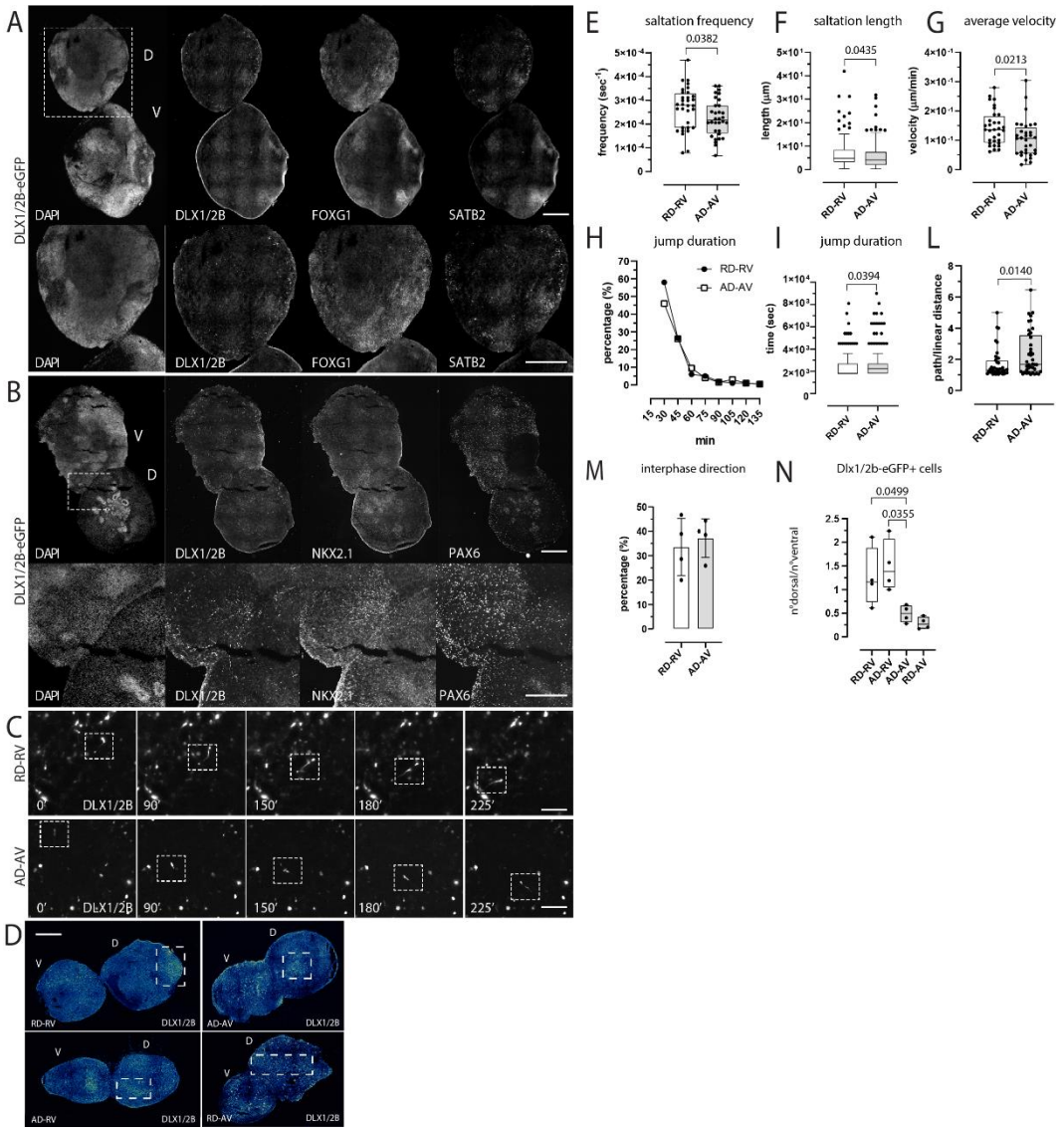
A
DLX1/2B-eGFP
D
V
DAPI
DLX1/2B
FOXG1
SATB2
B
NKX2.1
PAX6
C
RD-RV
AD-AV
0'
90'
150'
180'
225'
D
E
saltation frequency
0.0382
frequency (sec⁻¹)
F
saltation length
0.0435
length (µm)
G
average velocity
0.0213
velocity (µm/min)
RD-RV
AD-AV
H
jump duration
percentage (%)
min
I
jump duration
0.0394
time (sec)
L
0.0140
path/linear distance
M
interphase direction
percentage (%)
N
Dlx1/2b-eGFP+ cells
0.0499
0.0355
n°dorsal/n°ventral

Supplementary figure 1

A

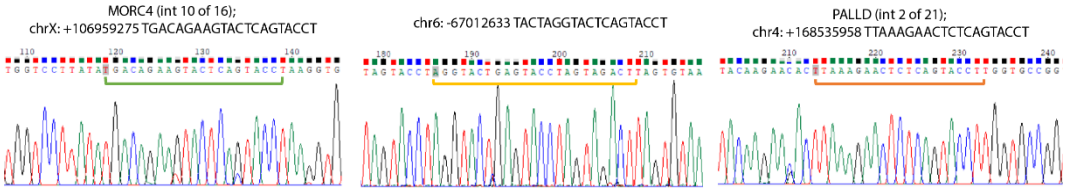

Figure legends

Figure 1. *Arhgef6* expression, localization, and GABAergic IN (IN) reduction in *Arhgef6-KO;GAD67-eGFP* mice. (**A**) Brightfield images of hematoxylin and eosin (HE) stained coronal brain slices from 3 postnatal 60 (P60) wild-type (WT) mice, followed by a heatmaps illustrating the expression levels (log2 fold change) of Arhgef6, Grik4, Prox1, and Spink8 within the same H&E-stained slices. Scale bars = µm. (**B**) Western blot analysis of ARHGEF6 and GAPDH expression in the cortex (CTX), cerebellum (CBC), and hippocampus (HIP) of WT and *Arhgef6-knock-out* (KO) adult mice. (**C**) Heatmap depicting Arhgef6 expression in the Allen Brain Atlas single cell-RNA sequencing (scRNAseq) database (https://brain-map.org/) alongside the expression of various neuronal markers. (**D**) *In situ* hybridization (ISH) for *Arhgef6* on coronal sections of embryonic day 14.5 (E14.5) mouse brains. Scale bars = µm. (**E**) Maximum intensity projections of z-stack images (z-step size = 2 µm) from coronal sections of the hippocampus in *GAD67-eGFP* and *Arhgef6-KO;GAD67-eGFP* mice. Scale bars = 600 µm. (**F**) Average density of eGFP-positive cells in the hippocampal cornu Ammonis 1 (CA1), CA2, CA3, dentate gyrus (DG), and whole hippocampus of P45 *GAD67-eGFP* and *Arhgef6-KO;GAD67-eGFP* mice.

Figure 2. Morphological analysis of primary INs (INs) and whole-cell patch-clamp in acute mouse brain slices. (**A**) Representative fluorescence micrographs of eGFP-positive primary INs from *GAD67-eGFP* (control) and *Arhgef6-KO;GAD67-eGFP* mice after 10 days *in vitro* (10 DIV). Scale bars: 20 µm. (**B**) Sholl analysis showing the overall complexity of arborization in *GAD67-eGFP* and *Arhgef6-KO;GAD67-eGFP* primary INs after 10 DIV (p (from 20 to 200 µm) = 0.068490, 0.177371, 0.050473, 0.001879, 0.000443, 0.000179, 0.000115, 0.001144, 0.000307). (**C**) Average diameter of the soma of *GAD67-eGFP* and *Arhgef6-KO;GAD67-eGFP* primary INs after 10 DIV (p = 0.1395). (**D**) Number of primary neurites in *GAD67-eGFP* and *Arhgef6-KO;GAD67-eGFP* primary INs after 10 DIV (p = 0.7599). (**E**) Length of the longest neurite in *GAD67-eGFP* and *Arhgef6-KO;GAD67-eGFP* primary INs after 10 DIV (p = 0.3855). At least 27 neurons were analyzed per genotype. Data are presented as box-and-whisker plots with Tukey's fences. p-values were calculated using unpaired multiple t-test corrected for False Discovery Rate (<1%) (B) and unpaired Mann–Whitney test (C-E). (**F**) Maximum intensity projections of z-stack images (z-step size = 2 µm) from sections of the hippocampus in *GAD67-eGFP and Arhgef6-KO;GAD67-eGFP* mice. The patched neuron was labeled by intracellular injection of biocytin followed by streptavidin-647 staining of fixed slices. (**G**) Representative whole-cell

current clamp recordings of action potentials (APs) evoked by 120 pA step current for adult *GAD67-eGFP* and *Arhgef6-KO;GAD67-eGFP* INs. (**H**) Average firing frequency vs. current relationships recorded in *GAD67-eGFP* and *Arhgef6-KO;GAD67-eGFP* INs in response to a set of injected current steps (from 0 to 300 pA, with 10 pA steps). p (from 0 to 300pA) = >0.999999, >0.999999, 0.952571, 0.265092, 0.087787, 0.017712, 0.001089, 0.000201, 0.000044, 0.000031, 0.000061, 0.000028, 0.000035, 0.000012, 0.000023, 0.000018, 0.000015, 0.000010, 0.000008, <0.000001, 0.000008, <0.000001, <0.000001, <0.000001, <0.000001, 0.000001, <0.000001, <0.000001, <0.000001, 0.000025. (**I, J**) Mean firing frequency vs. injected current for 120, 180, 280 pA frequencies (I, p (120, 180, 280 pA) = 0.039005, 0.039005, 0.024094; J, p (120, 180, 280 pA) = 0.033909, 0.009782, 0.127458). (**K**) Membrane capacitance (V_{rest}) (p = 0.1048), (**L**) input resistance (R_{in}) (p = 0.4637), (**M**) membrane capacitance (p = 0.2875), (**N**) rheobase (p = 0.2748), (**O**)) Representative APs recorded from *GAD67-eGFP* (top) and *Arhgef6-KO;GAD67-eGFP* (bottom) INs. (**P**) overshoot (p = 0.8295), (**Q**) fast afterhyperpolarization (fAHP) (p = 0.9279), (**R**) maximum rate of rise (p = 0.5535), (**S**) half-width (p = 0.1819) of *GAD67-eGFP* and *Arhgef6-KO;GAD67-eGFP* INs. n = 11 cells from 4 *GAD67-eGFP* mice and 12 cells from 4 *Arhgef6-KO;GAD67-eGFP* mice.

Figure 3. *ARHGEF6-KO* human induced pluripotent stem cells (hiPSCs)-derived embryoid bodied (EBs) and neural progenitor cells (NPCs). (**A**) Chromatogram of Sanger sequencing of hiPSCs ATCC-DYS0100: edited clone (top) and RNP negative isogenic control (bottom). The dashed line indicates the site of the CRISPR/Cas9 double-strand break. The mutation resulted in the deletion of a single cytosine, causing a frameshift mutation. Data were obtained from SYNTHEGO's ICE analysis (https://ice.synthego.com/). (**B**) Brightfield micrographs of human induced pluripotent stem cells (hiPSCs), neural progenitor cells (NPCs), radial glial cells (RGCs), and neurons. (**C**) Immunofluorescence staining showing the expression of iPSCs markers OCT4 (red) and SOX2 (green) in *ARHGEF6-KO* hiPSCs. Nuclei were stained with DAPI (blue). Scale bars: 20 µm. (**D**) Immunofluorescence staining of marker genes for all three germ layers in embryoid bodies (EBs) obtained from *ARHGEF6-KO* hiPSCs. GATA4 (red), TUJ1 (green), ACTA2 (red) and. Nuclei were stained with DAPI (blue). Scale bars: 20 µm. (**E**) Immunofluorescence staining of neuroepithelial marker genes Nestin (red), SOX2 (green), forebrain marker PAX6 (red), and RGCs marker FABP7 (green) in NPCs obtained from *ARHGEF6-KO* hiPSCs. Scale bars: 20 µm. (**F**) Phalloidin-FITC staining on RNP negative and *ARHGEF6-KO* NPCs. Scale bars: 20 µm. (**G**) anisotropy index (p = 0.0464), (**H**) mean angle of fibril orientation (p = 0.3221), (**I**)

corrected total cell fluorescence (CTCF) (p = 0.0056), (**J**) number of F-Actin punctae normalized to cell surface area (p = 0.3480), (**K**) cells surface area (p = 0.7601). Data are presented as box-and-whisker plots with Tukey's fences. p-values were calculated using unpaired t test. (**L**) Comparative quantitative real time-PCR analysis of dorsal forebrain markers PAX6, EMX2, and FABP7 in RNP negative and *ARHGEF6-KO* NPCs.

Figure 4. Morphometric analysis on single rosettes and forebrain organoids derived from RNP negative and *ARHGEF6-KO* hiPSC. (**A**) TJP1 immunostaining of single rosettes at 7 DIV obtained from RNP negative and *ARHGEF6-KO* hiPSCs. Scale bars: (**B**) Quantification of the number of rosettes generated by each genotype in a single rosette holder. (**C**) Brightfield images of forebrain dorsal and ventral organoids at 2 months (2M) obtained from RNP negative and *ARHGEF6-KO* hiPSCs. Inflection points are indicated by dashed circles. Scale bars: (**D**) Area (p (RD vs. AD) = <0.0001; p (RV vs. AV) = <0.0001), (**E**) circularity index (p (RD vs. AD) = <0.0001; p (RV vs. AV) = 0.9748), (**F**) integrated density (p (RD vs. AD) = <0.0001; p (RV vs. AV) = <0.0001), (**G**) aspect ratio (p (RD vs. AD) = <0.0001; p (RV vs. AV) = 0.0309), (**H**) roundness (p (RD vs. AD) = <0.0001; p (RV vs. AV) = 0.0029), (**I**) solidity index (p (RD vs. AD) = <0.0001; p (RV vs. AV) = 0.3385), and (**L**) number of inflection points (p (RD vs. AD) = 0.0455; p (RV vs. AV) = 0.4841) of RNP negative and *ARHGEF6-KO* 2M forebrain dorsal and ventral organoids. Data are presented as box-and-whisker plots with Tukey's fences. p-values were calculated using unpaired t test (B) and one-way ANOVA (D-L) corrected for False Discovery Rate (<1%). RD, RNP negative dorsal organoids; AD, *ARHGEF6-KO* dorsal organoids; RV, RNP negative ventral organoids; AV, *ARHGEF6-KO* ventral organoids.

Figure 5. Survival, proliferation, and differentiation analysis of 1-month-old (1M) ventral organoids derived from RNP-negative and *ARHGEF6-KO* hiPSCs. (**A, C, F**) Maximum intensity projections of z-stack images (5 serial images planes; z-step size = 1 µm) from sections of ventral RNP negative and *ARHGEF6-KO* 1M organoids stained for detecting (A) DNA fragmentation (terminal deoxynucleotidyl transferase dUTP nick end labeling, TUNEL staining), and expression of (C,F) SOX2, (C) NEUN, (C) MKI67, and (F) NKX2.1. Scale bars = µm. (**B**) Quantification of TUNEL punctae relative to DAPI-stained cells. (**D, E**) Quantification of (D) NEUN- and (E) SOX2-positive cells relative to DAPI-stained cells. (**G**) Ratio of NEUN-positive cells to SOX2-positive cells. (**H**) Quantification of MKI67-positive cells relative to DAPI-stained cells. (**I**) Ratio of NKX2.1-positive cells to SOX2-positive cells.

Figure 6. Survival, proliferation, and differentiation analysis of 2-month-old (2M) ventral organoids derived from RNP-negative and *ARHGEF6-KO* hiPSCs. (**A, C, G**) Maximum intensity projections of z-stack images (5 serial images planes; z-step size = 1 μm) from sections of ventral RNP negative and *ARHGEF6-KO* 2M organoids stained for detecting (A) DNA fragmentation (terminal deoxynucleotidyl transferase dUTP nick end labeling, TUNEL staining), and expression of (C) SOX2, (C) NEUN, and (G) MKI67. Scale bars = μm. (B) Quantification of TUNEL punctae relative to DAPI-stained cells. (**D, E**) Quantification of (D) NEUN- and (E) SOX2-positive cells relative to DAPI-stained cells. (**F**) Ratio of NEUN-positive cells to SOX2-positive cells. (**H**) Quantification of MKI67-positive cells relative to DAPI-stained cells.

Figure 7. Analysis of DLX1/2b-eGFP-positive cells migrating in fused dorsal-ventral assembloids. (**A, B**) Maximum intensity projections of z-stack images (5 serial images planes; z-step size = 1 μm) from sections of ventral RNP negative representative dorsal-ventral assembloids stained for dorsal markers (A) FOXG1 and SATB2, forebrain marker (B) PAX6, and ventral marker NKX2.1. Scale bars = μm. (**C**) Saltatory migration of DLX1/2b-eGFP-positive cells in fused dorsal-ventral assembloids. Representative time-lapse video frames of RNP-negative (RD-RV, control) and *ARHGEF6-KO* (AD-AV) assembloids at different time points (0, 90, 150, 180, and 225 min). The neuron being tracked is highlighted by a dashed square in each frame. (**D**) Royal scale (FIJI) visualization of DLX1/2b-eGFP-positive cell density across assembloids. Dashed squares highlight regions of elevated density within the dorsal compartment. Scale bars = μm. Quantification of saltation frequency (**E**) ($p = 0.0382$), saltation length (**F**) ($p = 0.0435$), average velocity (**G**) ($p = 0.0213$), jump duration (**H, I**) ($p = 0.0394$), and path/vector distance ratio (indirect measure of the directness) (**L**) ($p = 0.0140$), of individual DLX1/2b-eGFP-positive INs migrating in the RNP-negative (RD-RV, control) and *ARHGEF6-KO* (AD-AV) assembloids respectively. At least 30 neurons from 3 independent assembloids were analyzed per genotype. Data in F and I are presented as box-and-whisker plots with Tukey's fences. (**M**) Percentage of INs migrating in a ventral-to-dorsal direction across the interphase. ($p = 0.6238$). (**N**) Quantification of the total DLX1/2b-eGFP-positive INs in the dorsal compartment after 2 weeks of assembloids fusion. The number was first normalized to the surface area of the dorsal and ventral regions, and to the number of eGFP-positive cells in the ventral region to account for viral infection efficiency (p (RD-RV vs. AD-RV) = 0.8577; p (RD-RV vs. RD-AV) = 0.0339; p (RD-RV vs. AD-AV) = 0.1030; p (AD-RV vs. RD-AV) = 0.0085; p (AD-RV vs. AD-AV) = 0.0266; p (RD-AV vs. AD-AV) = 0.9135). RD, RNP negative dorsal organoids; D, dorsal; V, ventral; AD,

ARHGEF6-KO dorsal organoids; RV, RNP negative ventral organoids; AV, *ARHGEF6-KO* ventral organoids.

Supplementary figure 1. Analysis of crRNA off-targets. (**A**) Chromatogram of Sanger sequencing of hiPSCs ATCC-DYS0100: edited clone.

3.6 Material and methods

3.6.1 Mouse strains

All animal procedures were approved by the local Animal Ethics Committee and the Ministry of Health. Animals were maintained according to institutional animal welfare guidelines and legislation, under veterinarian surveillance. The *Arhgef-KO* mouse strain has been previously described (Ramakers et al., 2012). Heterozygous and homozygous mutant mice are born at normal Mendelian frequency, appear overall normal, are viable and fertile, mate at regular rates, and do not show evident neurological or motor impairments. Animals were maintained in a mixed c57/bl6 genetic background. The *GAD67-eGFP* reporter mouse strain has been previously described (DeDiego et al., 1994; Sakai & Miyazaki, 1997; Tamamaki et al., 2003). The progeny resulting from the cross between the reporter strain and the *Arhgef6-KO* strain were healthy and fertile.

3.6.2 Western blot

Brain's regions were collected from adult P45 mice ice, washed in cold PBS, and lysed with cold lysis buffer (1% Triton X-100, 50 mM Tris/HCl pH 7.4, 150 mM NaCl, 1mM EDTA) supplemented with 1mM PMSF, 1 mM Na3VO4, 10 mM NaF, 1X Complete Protease Inhibitors Cocktail (Roche, Basel, Switzerland). Lysates were centrifuged at 14000 x g for 30 min at 4°C and protein concentration was measured using the Bradford assay (Bio-Rad, Hercules, CA, USA). Lysates were diluted in Laemmli buffer and boiled for 5 minutes at 95°C. Equal amounts of proteins were loaded on 4–15% Mini-PROTEAN TGX Precast Protein Gels (Bio-Rad) and transferred to PVALBDF Transfer Membrane (MerckMillipore, Billerica, MA, USA). Membranes were blocked in 5% non-fat dry milk (Santa Cruz Biotechnology, Dallas, TX, USA) in Tris-buffer saline, 0.1% Tween20 and incubated with the indicated antibodies following he manufacturer's instructions. The following antibodies were used: rabbit anti-Cool2/αPix (C23D2) (Cell Signaling Technology, 4573), mouse anti-GAPDH (Invitrogen, AM4300). Horseradish peroxidase-conjugated secondary antibodies from Sigma-Aldrich. Immunoblots were developed by chemiluminescence with ECL (Clarity Western ECLSubstrate, Bio-Rad), acquired with the molecular imager ChemiDoc XRS, and quantified by densitometricanalysis using the Image-lab software (Bio-Rad). All comparative images of immunoblots were obtained byexposure of the same membranes

3.6.3 Brain preparation for histological analysis

For the collection of postnatal brains, mice were anesthetized with Avertin (30 µl of pure Avertin in 400 µl of PBS) and transcardially perfused with 10 ml of PBS (pH 7.4) and 10 ml of 4% (w/v) PFA in PBS (pH 7.4, adjusted with NaOH). Brains were removed, post-fixed overnight at 4°C in 4% PFA, placed overnight at 4°C in 30% (w/v) sucrose in PBS for cryoprotection, embedded in OCT blocks, and stored at −80° C until analysis. OCT blocks were cut into 30 µm-thick coronal sections using a cryotome (Leica CM 1950). Free-floating sections were collected in PBS in multiwell plates and stored at −20°C in a cryoprotectant solution (30% (v/v) glycerol and 30% (v/v) ethylene glycol in 0.2 M phosphate buffer, pH 7.4) until processed. The range of sections used for analysis corresponds to coronal sections 67–74 (anterior hippocampus), 75-78 (middle hippocampus), 79-82 (posterior hippocampus) of the reference Allen Brain Atlas (Allen Reference Atlas–Mouse Brain [brain atlas]; available from atlas.brainmap.org). For the analysis, we selected neurons in the hippocampal region. For the collection of embryonic brains, embryos were obtained through cesarean section at E14.5 (considering the day of the vaginal plug as E0.5) from anesthetized pregnant dams and transferred in PBS. Embryonic brains used for immunohistochemistry were dissected and fixed overnight at 4°C in 4% PFA, then placed overnight at 4°C in 30% (w/v) sucrose in PBS for cryoprotection, embedded in OCT blocks, and stored at -80°C until analysis. OCT blocks were cut into 15 µm-thick coronal sections and collected on super-adhesive glass slides.

3.6.4 Spatial transcriptomic

Brains of WT adult mice (P60) were collected and fixed as mentioned above. After PFA-fixation, they were placed in 70% ethanol overnight and processed to be included in paraffin. Brains were cut as mentioned above, selecting slides corresponding to section 79 of the Allen Brain Atlas. Sections were placed on Visium Tissue Optimization Slides (catalog no. 3000394, 10x Genomics) and Visium Spatial Gene Expression Slides (catalog no. 2000233, 10x Genomics). Tissue sections were then processed according to the Visium Spatial Gene Expression User Guide (catalog no. CG000239 Rev A, 10x Genomics) or Visium Spatial Tissue Optimization User Guide (catalog no. CG000238 Rev A, 10x Genomics). Brightfield histology images were taken using a 10× objective on a Leica DM6 microscope. Libraries preparation was followed by sequencing on a NovaSeq6000 The acquired data were overlaid onto the brightfield brain images (hematoxylin and eosin stain).

3.6.5 *In situ* hybridization

Mouse *Arhgef6* antisense probe was synthetized from mouse cDNA by two round of end-point PCR (Phusion High Fidelity DNA polymerase, New England Biolabs), using specific primers recognizing all Arhgef6 isoforms (forward 5'-CCTCGATTCTCCAGTAACCATC-3' and reverse 5'-GGCCACTGATGAGTCCAACT-3'; Primer 3 Plus: http://biotools.umassmed.edu/cgi-bin/primer3plus/primer3plus.cgi) in order to obtain a 902 bp amplicon; the reverse primer was modified by adding the sequence T7 polymerase promoter (5'-GGTAATACGACTCACTATAGGG-3') at its 5'-end. PCR reaction was caried out using the following thermal protocol: 98°C, 30 s, 98°C 10 s for 35 cycles, 60°C 20 s per 35 cycles, 72°C 20 s for 35 cycles, 72°C 7 min. The product of PCR #1 was run on a 1% agarose gel and the band corresponding to the desired amplicon was extracted using the Gel Extraction Kit (Qiagen) and employed as template for a second run of PCR. Then, the product of PCR #2 was purified using the PCR Purification Kit (Qiagen), quantified by OD (Nanodrop2000, Thermo Scientific) and checked on a 1% agarose gel. For probe synthesis, 1 µg of PCR #2 product was used as template for T7 RNA polymerase *in vitro* transcription following manufacturer instructions (DIG RNA labelling kit, Roche). The probe was checked on 1% agarose gel and purified by glycogen/LiCl precipitation. Hybridization and detection. 20 µm-thick cryosections from PFA-fixed mouse embryonic tissues were incubated with DIG-labelled antisense riboprobes (2 µg/mL). Hybridization step was performed in hybridization buffer (50% formamide, 0.3 M NaCl, 20 mM Tris-HCl, 5mM EDTA, 10% Dextran sulphate, 1x Denhardt's solution, 0.25 mg/mL Torula yeast tRNA) overnight at 65°C. Sections were then washed with saline sodium citrate (SSC) buffer (50% Formamide, 1X Saline Sodium Citrate buffer, 0,1% Tween20), blocked with blocking buffer (100 mM Maleic acid, 150 mM NaCl, 0.1% Tween20, 2% blocking reagent (Roche), 10% Normal Goat Serum (Sigma-Aldrich)) and finally incubated overnight with alkaline phosphatase (AP)-conjugated anti-DIG antibody (1:1500; Roche). mRNA expression was revealed by colorimetric staining using 4-Nitro blue tetrazolium chloride solution and 5-Bromo-4-chloro-3-indolyl phosphate disodium salt (NBT/BCIP, Roche) in a staining solution (100 mM NaCl, 50 mM MgCl 2 , 100 mM Tris-HCl pH 9.8, 1% Tween20, 50% poly-vinyl-alcohol) at 37°C. Colorimetric reaction was checked after 6 hours and if no colored precipitate was detected, new staining solution was added overnight. The reaction was stopped with MilliQ H_2O and slides were mounted with aqueous mounting media Mowiol 4-88 (Sigma-Aldrich).

3.6.6 Primary cultures of hippocampal neurons

µ-slides 2-well Ibidi were coated with 0.1 mg/ml poly-L-lysine (Sigma) in borate buffer (pH 8.5) and washed with deionized water. One day before establishing the culture, µ-slides were rinsed in a MEM (Gibco) solution with 1% (v/v) pyruvate 100X (Gibco), 20% (w/v) glucose, 1% (v/v) Penicillin-Streptomycin, and 10% (v/v) horse serum (Gibco). *GAD67-eGFP* and *Arhgef6-KO;GAD67-eGFP* pups at P0 were used to establish primary cultures of hippocampal neurons. Hippocampi were dissected free from the brain, after depriving of the meninges, in sterile conditions in a cold solution of 1% (v/v) HEPES in HBSS with calcium and magnesium (Gibco). Hippocampi were washed with a cold solution containing 1% Penicillin-Streptomycin and 1% HEPES in HBSS with calcium and magnesium (Gibco) and incubated in 1 ml HBSS with 25% of Trypsine 0.25% (Gibco). Hippocampi were washed 2 times in HBSS at 37°C for 10 minutes each. Hippocampi were disaggregated in a solution containing DNAase (used 1:1,000; Promega) by pipetting. Cells were counted and 430.000 cells were plated on each well containing Neurobasal medium (Gibco) added with 1% Penicillin-Streptomycin, 2% (v/v) B27 (Gibco), and 0.25% (v/v) GlutaMAX (Gibco). Neurons were incubated at 37° C in a 5% CO2 saturation atmosphere.

3.6.7 Brain sections and primary cultures immunostaining

Brain sections were washed three times in PBS, incubated for 1 h at room temperature with a blocking solution (10% goat or donkey serum and 0.2% Triton X-100 in PBS), and incubated overnight at 4°C with the primary antibodies diluted in a solution composed of 0.5% Triton X-100 and 5% goat or donkey serum. Then, sections were incubated for 2 h at room temperature with fluorophore-conjugated secondary antibodies diluted in a solution composed of 0.2% Triton X-100 and 3% goat or donkey serum and washed three times in PBS. Finally, sections were counterstained with DAPI and mounted with Mowiol onto super-adhesive glass slides. Primary cortical cultures were fixed at 10 days *in vitro* (10 DIV) with 4% PFA in PBS for 20 min at room temperature. Neurons were incubated for 1 h at room temperature with a blocking solution containing 5% goat serum and 0.1% Triton X-100 in PBS. The primary antibody (anti-GFP) was diluted in a solution containing 3% goat serum and 0.1% Triton X-100 in PBS and incubated overnight at 4°C. Secondary antibodies were incubated for 1 h at room temperature. Coverslips were mounted with Mowiol onto glass slides. Primary antibodies: rabbit anti-GFP. Secondary antibodies: Alexa Fluor 488 donkey antirabbit IgG (used 1:500; Invitrogen). Slides were examined with a Leica SP8 confocal microscope.

Raw images were digitally processed to normalize the background and optimize the contrast, rotated, and sized with ImageJ (NIH, Bethesda, Maryland; http://imagej.nih.gov/ij/). For the strata analysis, hippocampi were divided into stratum oriens (SO), stratum pyramidale (SP), stratum radiatum (SR), stratum lacunosum-moleculare (SLM), molecular layer of dentate gyrus (ML), granule cell layer (GL), hilus of dentate gyrus (H). For tangential migration analysis, polar plots were generated by using matplotlib Python library (https://matplotlib. org/stable/#). Morphological analysis on primary cultures was performed using ImageJ (NIH, Bethesda, Maryland; http://imagej.nih.gov/ij/); arborization of each neuron was quantified by performing Sholl analysis (Sholl, 1953) by ImageJ plugin Sholl Analysis Plugin (v1.0) (Ghosh Lab Software; http://ghoshlab.org/ software/index.html).

3.6.8 Whole-cell patch-clamp recording

For acute slices, 4 *GAD67-eGFP* and 4 *Arhgef6-KO;GAD67-eGFP* P90 mice were killed by cervical dislocation. Brains were removed and placed at 4°C in oxygenated (95% O2–5%CO2) adapted artificial cerebrospinal fluid (ACSF), containing 120 mM choline chloride, 3.5 mM KCl, 0.5 mM $CaCl_2$, 6 mM $MgSO_4$, 1.25 mM NaH_2PO_4, 25 mM D-glucose and 25 mM NaHCO3. somatosensory cortex coronal slices (300 μm) were cut in ice-cold ACSF using a vibratome (Microm HM 650 V, Thermo Scientific) and subsequently placed for 30 min in ACSF containing 120 mM NaCl, 3.5 mM KCl, 25 mM, $NaHCO_3$, 25 mM D-glucose, 2.5 mM $CaCl_2$, 1.3 mM $MgSO_4$, and 1.25 mM NaH_2PO_4, at 32 °C. Slices were kept at room temperature for at least 1 h before recording. Patch electrodes of borosilicate glasses (Hilgenberg, Mansfield, Germany) were pulled to a final resistance of 5–9 MΩ. For current-clamp recordings in both brain slice and primary cultured neurons, the internal solution contained: 135 mM gluconic acid (potassium salt: K-gluconate), 5 mM NaCl, 2 mM $MgCl_2$, 10 mM HEPES, 0.5 mM EGTA, 2 mM ATP Tris, and 0.4 mM Tris-GTP. Patch-clamp recordings from CINs (somatosensory cortex, layer IV-VI) were performed in whole-cell configuration using an EPC-10 amplifier (HEKA Elektronic, Lambrecht, Germany). Traces were sampled at 10 kHz and filtered using a low-pass Bessel filter set at 2 kHz. All the experiments were performed at room temperature (22–24°C). Resting membrane potential (V_{rest}) and membrane capacitance (C_m) were routinely acquired when the whole-cell patch-clamp configuration was established. The membrane time constant (tm) was calculated by Clampfit software following a step current injection of −30 pA. C_m was calculated by applying the formula $C_m = \tau_m/R_{in}$. The action potential (AP) parameters were obtained by analyzing a series of spikes recorded during tonic

firing of 1–2 min duration. Tonic firing was elicited by depolarizing membranes with a minimum amount of current corresponding to the rheobase value (Marcantoni et al., 2014). After reaching steady-state condition during tonic firing, at least five APs were selected and averaged for each cell, then the measures of AP peak amplitude, half-width, maximum rising slope, and maximum repolarizing slope were performed with Clampfit software (Axon Instruments). The peak amplitude of AP was measured from the threshold to the AP peak and the halfwidth was calculated at half-maximal AP height. To analyze the relationship between firing frequency and injected current, the membrane potential was adjusted to −70 mV and then 20 pulses of increasing intensity (from -30–160 pA, 500 ms duration) were injected. The mean firing frequency of each current step was calculated as the number of spikes per second. The rheobase was determined as the minimum amount of current required to trigger one spike. Input resistance (R_{in}) was calculated in a linear region of the membrane voltage injected current curve centered at the holding potential (−70 mV), through the injection of hyperpolarizing and depolarizing current steps (from −30 to 30 pA; 10 pA steps). For primary neuronal cultures, the extracellular solution for current recordings (Tyrode's solution) contained: 2 mM $CaCl_2$, 10 mM HEPES, 130 mM NaCl, 4 mM KCl, 2 mM $MgCl_2$, and 10 mM D-glucose (Tomagra et al., 2019). Patch-clamp recordings were performed using an EPC-9 amplifier (HEKA Elektronic, Lambrecht, Germany) and pClamp software (Molecular Devices, Silicon Valley, CA, United States). Analysis of firing activity was performed with Clampfit software (Axon Instruments).

3.6.9 hiPSC mutagenesis

hiPSCs DYS0100 (ATCC) were dissociated using TrypLE Select Enzyme (Gibco) electroporated on a Lonza Nucleofector 4-D (program CM-113, solution P3) according to manufacturer's instructions. Briefly, equal amount of 100-µM crRNA and tracrRNA (Integrated DNA Technologies) were mixed to form gRNAs. 150 pmol of gRNAs were complexed with 120 pmol of Cas9 proteins (Integrated DNA Technologies) to form ribonucleoprotein complex (RNPs). Electroporation mix was prepared as previously described (Ghetti et al., 2021). After the electroporation, cells were plated in a Geltrex (Gibco)-coaeted plate and maintained in Stemflex medium supplemented with RevitaCell Supplement (Gibco) for 48 h. Monoclonal cell lines were established by single-cell sorting into 96-well plates followed by expansion. Off-targets for gRNA + 4 were analyzed by Cas-OFFinder online algorithm, by selecting: SpCas9 from Streptococcus pyogenes: 5'-NGG-3', mismatch number ≤ 4, DNA bulge size $= 0$, RNA bulge size $= 0$ and as a target genome the Homo sapiens (GRCh38/hg38). Genomic DNA was extracted using

QuickExtract DNA extraction solution (Epicentre) and the target locus amplified by PCR using Phusion High Fidelity DNA Polymerase (Thermo Fisher). Oligos used to evaluate InDels resulting from cleavage of one crRNA are listed below. (Table1) Purified PCR products were sequenced and analyzed using TIDE, EditR, or SYNTHEGO ICE software (Brinkman et al., 2014, 2018; Conant et al., 2022; Kluesner et al., 2018).

Table 1. *ARHGEF6* editing and off-targets sequencing details.

Sequence	Primers for sequencing			
	forward	reverse	amplicon (bp)	Tm (°C)
TAAAAGAGTACTC AGTACCT target *Arhgef6* **(chrX:+136747529)**	ATCACGAGAACA ATCCTGGC	GAGTGGGTCTG AGTATGCAC	480	58
TGACAGAAGTAC TCAGTACCT off-target #1 (chrX:+106959275)	GAAATGGTGGTTC CAGACAGC	GAACCGCACCA CTCTGTTG	343	59
TACTAGGTACTCA GTACCT off-target #2 (chr6:-67012633)	TCTGTAGCAAAA CAACCTGGC	TCACCTGCTAA TGACCAAACAC	447	58.55
TTAAAGAACTCTC AGTACCT off-target #3 (chr4:+168535958)	TGAACACCCATTG CATCCCTC	AGGTGCCCAGA GACCTTTATC	640	59.16

3.6.10 hiPSC differentiation in neural progenitors, singular rosettes, and embryoid bodies

hiPSCs were expanded by culturing them in Geltrex (Gibco)-coated 6-well plates with Essential 8 (E8; Gibco) medium. The medium was changed every day. When passed, cultures were washed with DPBS and then exposed to 0.5 mM EDTA dissociation solution and incubated at 37°C until the cells and the colonies appeared round and not completely detached from the well. When the cells were ready to be detached, dissociation buffer was eliminated, and the colonies were picked up and

transferred in a 15 ml falcon tube. The cells were centrifuged at 200 x g for 5 minutes, the supernatant discarded, and cells resuspended in E8 medium and plated in a 6-well plate. The cells were incubated at 37°C with 5% CO_2 and the medium was replaced every day.

For the embryoid bodies (EBs) formation, hiPSCs were collected from a well of a 6-well plate at 70-80% confluence, centrifuged at 200xg for 5 minutes and the pellet was gently resuspended in complete E8 medium. Cells of each clone were plated in 4 ml of E8 complete medium supplemented with 5 μM of ROCK inhibitor Y-27632 into a 6-well plate previously treated with Pluronic Acid. The treatment of the well was performed by incubating the plate with Pluronic Acid solution 50 mg/ml at room temperature for 1 hour. The plate was tilted several times to distribute the cell suspension and then the cells were cultured in standard conditions (at 37°C; 5% CO2; 21% O2). EBs were checked every day and medium replaced every second day. It is necessary to check every day for the presence of non-adherent regular cell clumps and the plate must be tilt in order to distribute the cell aggregates. The medium was replaced every other day by collecting the EBs in a 15 ml falcon tube and letting them to settle down to the bottom part of the tube. The medium was changed by replacing the supernatant and the EBs were transferred in the original wells. From day 2 to day 7, EBs were cultured by shifting from E8 medium to Essential 6 (E6; Gibco) medium until EBs were maintained only in complete E6 medium. At day 7, EBs were collected and transferred on Geltrex-coated in μ-slides 2-well Ibidi to allow the growth in adhesion and perform imaging analysis. E6 medium was replaced every other day. Neuronal induction (*i.e.*, the conversion of hiPSCs into neural progenitor cells, NPCs) was performed by using the PSC Neural Induction Medium (Gibco), following manufacturer instructions.

For the single rosette assay, hiPSCs were maintained in Essential 8 Medium (Gibco) on Geltrex (Gibco)-coated tissue culture plates and routinely passaged with the ReLeSR reagent (STEMCELL Technologies). RGC derivation from human pluripotent stem cells was performed using Essential 6 Medium (E6) (Gibco). To generate micropatterned RGCs, cells were first rinsed with PBS, dissociated with Accutase (STEMCELL Technologies) for 5 min at 37 °C and collected by centrifugation at 200g for 5 min. Singularized RGCs were resuspended in E6 medium with 10 μM ROCK inhibitor (Y-27632; STEMCELL Technologies) and seeded onto micropatterned substrates at 75,000 cells per cm^2 in 2 ml of medium per well. The following day, the medium was replaced with 2 ml E6 medium, and 50% medium changes were performed daily thereafter. Ninety-six-well plates were custom made with micropatterning of polyethylene-glycol-methyl-ether-grafted

substrates, presenting arrays of circular regions 250 μm in diameter (Knight et al., 2018), and were coated with Geltrex overnight.

3.6.11 hiPSC and hiPSC-derived cells staining

Cells plated into the Geltrex-coated in μ-slides 2-well Ibidi were fixed with 4% PFA for 30 min at room temperature and washed with PBS before a 1 h incubation in PBS 0.3% Triton X-100 (Sigma, T9284) and 6% BSA (Sigma, AA0281). Overnight incubation at 4 °C with a primary antibody solution was followed by a 2 h incubation at room temperature with a secondary antibody solution, both consisting of PBS 0.1% Triton X-100 and 2.5% BSA with three washes before and after the secondary antibody incubation. Primary antibodies: mouse anti-OCT3/4 (1:1000; Santa Cruz Biotechnology, sc-5279), rabbit anti-SOX2 (1:1000, Abcam, AB97959), mouse anti-GATA4 (1:1000; Santa Cruz Biotechnology, sc-25310), rabbit anti-TUJ1 (1:1000; GeneTex, GTX130245), mouse anti-ACTA2 (1:1000; Antibodies, A279072), mouse anti-NESTIN (1:1000; R&D Systems, MAB1259), mouse anti-PAX6 (1:1000; BD Pharmigen, 561462), rabbit anti-FABP7 (Millipore, ABN14). For the phalloidin staining, cells were washed in PBS and fixed in formaldehyde 4% PBS for 30 minutes. Cells were permeabilized with 0.1% Triton X-100 PBS for 5 minutes and blocked in 3% non-fat dry milk PBS for 30 min. 200 uL of phalloidin-FITC (1:500 in BSA 10X PBS) were added to each well for 90 minutes. Mowiol was used as mounting media to preserve fluorescence. Cover-slips were examined with the Leica laser scanning confocal microscope SP8 under excitation wavelengths of 488 nm. Images were analyzed for their corrected total cell fluorescence (CTCF) calculated by Integrated Density (Area of selected cell x Mean fluorescence of background readings) and with ImageJ software. Singular rosettes were imaged using a ×20 objective with the Leica Thunder Microscope for 14 h under bright-field light. CO_2 and temperature were maintained at 5% and 37 °C throughout the recording using a recording chamber. Anisotropy was automatically calculated by using the FibrilTool plugin in Image-J (Boudaoud et al., 2014).

3.6.12 Differentiation and assembly of cortical and ventral organoids

Cortical and ventral differentiations from hiPSCs were performed as previously described (Birey et al., 2017; Sloan et al., 2018). For cortical and ventral differentiations from feeder-free maintained hiPSCs, cells were maintained on Geltrex (Gibco)-coated plates (Costar) in Essential 8 (E8) medium (Gibco) in a 5% CO2 humidified atmosphere. Cells were passaged every 4-5 days with UltraPure

0.5 mM EDTA, pH 8.0 (Thermo Fisher Scientific, 15575020). On day 0, feeder-free cultured human pluripotent stem cells, 80–90% confluent, were dissociated to single cells with Accutase (Gibco), and 9,000 cells per well were reaggregated in ultra-low-cell-adhesion 96-well plates with V-bottomed conical wells (sBio PrimeSurface plate; Sumitomo Bakelite) in Essential 6 (E6) medium (Gibco) supplemented with the SMAD pathway inhibitors dorsomorphin (2.5 mM, Sigma-Aldrich, P5499) and SB431542 (10 mM, R&D Systems, 1614). Feeder-free cortical differentiation was performed as previously described (Yoon et al., 2019) using the recipe variant without XAV299. Feeder-free ventral differentiation protocol was based on the Feeder-free cortical differentiation protocol with the following modifications (added on top of small molecules/growth factors specified in the cortical recipe): day 3–6; XAV-939 (2.5mM, Tocris, 3748), day 7–24; IWP-2 (2.5mM, Selleck Chemicals, S7085), day 13–24; SAG (100nM, EMD Millipore, 566660). To promote progenitor differentiation, BDNF (20 ng/mL) and NT-3 (20 ng/mL) were added starting on day 25 with media changes every other day. After day 43, media changes every 4-5 days were performed only with neural media (NM) without growth factors. Assembly of cortical and ventral organoids to generate forebrain assembloids was performed as previously described (Birey et al., 2017; Sloan et al., 2018). 2M ventral organoids were transduced with lentivirus LV-Dlxi1/2-eGFP (gift from S. Pasca and J. Rubenstein) as described in ref. (Paulsen et al., 2022). Bright-field microscopy was used to capture images of all organoids from day 3 to day 60. ImageJ software was then used to measure the area and the perimeter of each single organoid. Prism software was then used to plot the average size of the organoids of each differentiation.

3.6.13 Organoids staining

Organoids were fixed with 4% PFA for 30 min at room temperature before overnight incubation at 4 °C in 30% sucrose solution. Organoids were then embedded in Tissue-Tek O.C.T. compound (Sakura, 62550) and sectioned at 25 µm with a cryostat onto glass slides (Globe Scientific, 1354W). Slides were washed 3× with a PBS 0.1% Tween-20 (Sigma, P9416) solution before a 1 h incubation in PBS 0.3% Triton X-100 (Sigma, T9284) and 6% BSA (Sigma, AA0281). Overnight incubation at 4 °C with a primary antibody solution was followed by a 2 h incubation at room temperature with a secondary antibody solution, both consisting of PBS 0.1% Triton X-100 and 2.5% BSA with three washes before and after the secondary antibody incubation. Slides were coverslipped using Fluoromount-G (EMS, 50-259-73). Primary antibodies: goat anti-SOX2 (1:1000; R&D Systems, AF2018), rabbit NKX2.1 (1:500; Abcam ab76013), rabbit anti-NEUN (1.200;

Abcam, ab177487), mouse anti-MKI67 (1:1000, BD Biosciences, 550609), chicken anti-MAP2 (1:5000; Abcam, ab5392), rabbit anti-FOXG1 (1:1000; Abcam, ab18259), mouse anti-SATB2 (1:100; Abcam, ab51502), rabbit anti-PAX6 (1:400; BioLegend, 901301). Terminal deoxynucleotidyl transferase dUTP nick end labeling (TUNEL) (Click-iT™ TUNEL Alexa Fluor Imaging Assays for Microscopy & HCS, Invitrogen) was performed according to manufacturer instructions. Organoids stained were imaged with x10 objective with Leica Thunder Microscope and used for quantification. Images were opened in ImageJ software, and the background noise was reduced. To count all cells, DAPI-positive cells were initially counted. The lowest and maximum threshold values were set at 30 and 250, respectively. The proportion of nuclear markers-positive cells was calculated by normalization to the number of DAPI-positive cells.

3.6.14 Statistical analysis

For the statistical comparisons, GraphPad Prism software (GraphPad Software Inc.) was used. For each experiment, the statistical test used is reported in the figure legends. Shapiro-Wilk and Kolmogorov-Smirnov tests were used to test for normality, F test was used to test for equality of variance, and results were evaluated to choose the appropriate statistical test. The results are shown as mean ± Standard Error of Mean (SEM). The threshold for statistical significance was set at $p < 0.05$.

References

Adachi, M., Autry, A. E., Covington III, H. E., & Monteggia, L. M. (2009). MeCP2-mediated transcription repression in the basolateral amygdala may underlie heightened anxiety in a mouse model of Rett syndrome. *The Journal of Neuroscience*, *29*(13), 4218–4227. https://doi.org/10.1523/JNEUROSCI.4225-08.2009

Agnew, B. J., Minamide, L. S., & Bamburg, J. R. (1995). Reactivation of phosphorylated actin depolymerizing factor and identification of the regulatory site. *The Journal of Biological Chemistry*, *270*(29), 17582–17587. https://doi.org/10.1074/jbc.270.29.17582

Akbarian, S., Kim, J. J., Potkin, S. G., Hagman, J. O., Tafazzoli, A., Bunney, W. E., & Jones, E. G. (1995). Gene expression for glutamic acid decarboxylase is reduced without loss of neurons in prefrontal cortex of schizophrenics. *Archives of General Psychiatry*, *52*(4), 258–266. https://doi.org/10.1001/archpsyc.1995.03950160008002

Alber, M., Kalscheuer, V. M., Marco, E., Sherr, E., Lesca, G., Till, M., Gradek, G., Wiesener, A., Korenke, C., Mercier, S., Becker, F., Yamamoto, T., Scherer, S. W., Marshall, C. R., Walker, S., Dutta, U. R., Dalal, A. B., Suckow, V., Jamali, P., … Minassian, B. A. (2017). ARHGEF9 disease: Phenotype clarification and genotype-phenotype correlation. *Neurology. Genetics*, *3*(3), e148. https://doi.org/10.1212/NXG.0000000000000148

Alfonso, J., Penkert, H., Duman, C., Zuccotti, A., & Monyer, H. (2015). Downregulation of Sphingosine 1-Phosphate Receptor 1 Promotes the Switch from Tangential to Radial Migration in the OB. *Journal of Neuroscience*, *35*(40), 13659–13672. https://doi.org/10.1523/JNEUROSCI.1353-15.2015

Allison, D. W., Gelfand, V. I., Spector, I., & Craig, A. M. (1998). Role of Actin in Anchoring Postsynaptic Receptors in Cultured Hippocampal Neurons: Differential Attachment of NMDA versus AMPA Receptors. *The Journal of Neuroscience*, *18*(7), 2423. https://doi.org/10.1523/JNEUROSCI.18-07-02423.1998

Amano, M., Ito, M., Kimura, K., Fukata, Y., Chihara, K., Nakano, T., Matsuura, Y., & Kaibuchi, K. (1996). Phosphorylation and activation of myosin by Rho-associated kinase (Rho-kinase). *The Journal of Biological Chemistry*, *271*(34), 20246–20249. https://doi.org/10.1074/jbc.271.34.20246

Anastasiadis, P. Z., Moon, S. Y., Thoreson, M. A., Mariner, D. J., Crawford, H. C., Zheng, Y., & Reynolds, A. B. (2000). Inhibition of RhoA by p120 catenin. *Nature Cell Biology*, *2*(9), 637–644. https://doi.org/10.1038/35023588

Anderson, S. A., Eisenstat, D. D., Shi, L., & Rubenstein, J. L. (1997). Interneuron migration from basal forebrain to neocortex: Dependence on Dlx genes. *Science (New York, N.Y.)*, *278*(5337), 474–476. https://doi.org/10.1126/science.278.5337.474

Andrews, W. D., Zito, A., Memi, F., Jones, G., Tamamaki, N., & Parnavelas, J. G. (2013). Limk2 mediates semaphorin signalling in cortical interneurons migrating through the subpallium. *Biology Open*, *2*(3), 277–282. https://doi.org/10.1242/bio.20133202

Arber, S., Barbayannis, F. A., Hanser, H., Schneider, C., Stanyon, C. A., Bernard, O., & Caroni, P. (1998). Regulation of actin dynamics through phosphorylation of cofilin by LIM-kinase. *Nature*, *393*(6687), 805–809. https://doi.org/10.1038/31729

Asrar, S., Meng, Y., Zhou, Z., Todorovski, Z., Huang, W. W., & Jia, Z. (2009). Regulation of hippocampal long-term potentiation by p21-activated protein kinase 1 (PAK1). *Neuropharmacology*, *56*(1), 73–80. https://doi.org/10.1016/j.neuropharm.2008.06.055

Assoum, M., Bruel, A.-L., Crenshaw, M. L., Delanne, J., Wentzensen, I. M., McWalter, K., Dent, K. M., Vitobello, A., Kuentz, P., Thevenon, J., Duffourd, Y., Thauvin-Robinet, C., & Faivre, L. (2020). Novel KIAA1033/WASHC4 mutations in three patients with syndromic intellectual disability and a review of the literature. *American Journal of Medical Genetics Part A*, *182*(4), 792–797. https://doi.org/10.1002/ajmg.a.61487

Ba, W., van der Raadt, J., & Nadif Kasri, N. (2013). Rho GTPase signaling at the synapse: Implications for intellectual disability. *Experimental Cell Research*, *319*(15), 2368–2374. https://doi.org/10.1016/j.yexcr.2013.05.033

Ba, W., Yan, Y., Reijnders, M. R. F., Schuurs-Hoeijmakers, J. H. M., Feenstra, I., Bongers, E. M. H. F., Bosch, D. G. M., De Leeuw, N., Pfundt, R., Gilissen, C., De Vries, P. F., Veltman, J. A., Hoischen, A., Mefford, H. C., Eichler, E. E., Vissers, L. E. L. M., Nadif Kasri, N., & De Vries, B. B. A. (2016). TRIO loss of function is associated with mild intellectual disability and affects dendritic branching and synapse function. *Human Molecular Genetics*, *25*(5), 892–902. https://doi.org/10.1093/hmg/ddv618

Bagley, J. A., Reumann, D., Bian, S., Lévi-Strauss, J., & Knoblich, J. A. (2017). Fused dorsal-ventral cerebral organoids model complex interactions between diverse brain regions. *Nature Methods*, *14*(7), 743. https://doi.org/10.1038/nmeth.4304

Bardoni, B., & Abekhoukh, S. (2014). CYFIP family proteins between autism and intellectual disability: Links with Fragile X syndrome. *Frontiers in Cellular Neuroscience*, *8*. https://doi.org/10.3389/fncel.2014.00081

Bartolini, G., Sánchez-Alcañiz, J. A., Osório, C., Valiente, M., García-Frigola, C., & Marín, O. (2017). Neuregulin 3 Mediates Cortical Plate Invasion and Laminar Allocation of GABAergic Interneurons. *Cell Reports*, *18*(5), 1157–1170. https://doi.org/10.1016/j.celrep.2016.12.089

Baudoin, J.-P., Viou, L., Launay, P.-S., Luccardini, C., Espeso Gil, S., Kiyasova, V., Irinopoulou, T., Alvarez, C., Rio, J.-P., Boudier, T., Lechaire, J.-P., Kessaris, N., Spassky, N., & Métin, C. (2012). Tangentially migrating neurons assemble a primary cilium that promotes their reorientation to the cortical plate. *Neuron*, *76*(6), 1108–1122. https://doi.org/10.1016/j.neuron.2012.10.027

Begemann, A., Sticht, H., Begtrup, A., Vitobello, A., Faivre, L., Banka, S., Alhaddad, B., Asadollahi, R., Becker, J., Bierhals, T., Brown, K. E., Bruel, A.-L., Brunet, T., Carneiro, M., Cremer, K., Day, R., Denommé-Pichon, A.-S., Dyment, D. A., Engels, H., … Rauch, A. (2021). New insights into the clinical and molecular spectrum of the novel CYFIP2-related neurodevelopmental disorder and impairment of the WRC-mediated actin dynamics. *Genetics in Medicine: Official Journal of the American College of Medical Genetics*, *23*(3), 543–554. https://doi.org/10.1038/s41436-020-01011-x

Belforte, J. E., Zsiros, V., Sklar, E. R., Jiang, Z., Yu, G., Li, Y., Quinlan, E. M., & Nakazawa, K. (2010). Postnatal NMDA receptor ablation in corticolimbic

interneurons confers schizophrenia-like phenotypes. *Nature Neuroscience*, *13*(1), 76–83. https://doi.org/10.1038/nn.2447

Belichenko, P. V., Kleschevnikov, A. M., Masliah, E., Wu, C., Takimoto-Kimura, R., Salehi, A., & Mobley, W. C. (2009). Excitatory-inhibitory relationship in the fascia dentata in the Ts65Dn mouse model of Down syndrome. *The Journal of Comparative Neurology*, *512*(4), 453–466. https://doi.org/10.1002/cne.21895

Ben-Ari, Y. (2002). Excitatory actions of gaba during development: The nature of the nurture. *Nature Reviews Neuroscience*, *3*(9), 728–739. https://doi.org/10.1038/nrn920

Bergmann, C., Zerres, K., Senderek, J., Rudnik-Schoneborn, S., Eggermann, T., Häusler, M., Mull, M., & Ramaekers, V. T. (2003). Oligophrenin 1 (OPHN1) gene mutation causes syndromic X-linked mental retardation with epilepsy, rostral ventricular enlargement and cerebellar hypoplasia. *Brain: A Journal of Neurology*, *126*(Pt 7), 1537–1544. https://doi.org/10.1093/brain/awg173

Besson, A., Gurian-West, M., Schmidt, A., Hall, A., & Roberts, J. M. (2004). p27Kip1 modulates cell migration through the regulation of RhoA activation. *Genes & Development*, *18*(8), 862–876. https://doi.org/10.1101/gad.1185504

Billuart, P., Bienvenu, T., Ronce, N., des Portes, V., Vinet, M. C., Zemni, R., Roest Crollius, H., Carrié, A., Fauchereau, F., Cherry, M., Briault, S., Hamel, B., Fryns, J. P., Beldjord, C., Kahn, A., Moraine, C., & Chelly, J. (1998). Oligophrenin-1 encodes a rhoGAP protein involved in X-linked mental retardation. *Nature*, *392*(6679), 923–926. https://doi.org/10.1038/31940

Birey, F., Andersen, J., Makinson, C. D., Islam, S., Wei, W., Huber, N., Fan, H. C., Metzler, K. R. C., Panagiotakos, G., Thom, N., O'Rourke, N. A., Steinmetz, L. M., Bernstein, J. A., Hallmayer, J., Huguenard, J. R., & Paşca, S. P. (2017). Assembly of functionally integrated human forebrain spheroids. *Nature*, *545*(7652), 54–59. https://doi.org/10.1038/nature22330

Birey, F., Li, M.-Y., Gordon, A., Thete, M. V., Valencia, A. M., Revah, O., Paşca, A. M., Geschwind, D. H., & Paşca, S. P. (2022). Dissecting the molecular basis of human interneuron migration in forebrain assembloids from Timothy syndrome. *Cell Stem Cell*, *29*(2), 248-264.e7. https://doi.org/10.1016/j.stem.2021.11.011

Birtele, M., Del Dosso, A., Xu, T., Nguyen, T., Wilkinson, B., Hosseini, N., Nguyen, S., Urenda, J.-P., Knight, G., Rojas, C., Flores, I., Atamian, A., Moore, R., Sharma, R., Pirrotte, P., Ashton, R. S., Huang, E. J., Rumbaugh, G., Coba, M. P., & Quadrato, G. (2023). Non-synaptic function of the autism spectrum disorder-associated gene SYNGAP1 in cortical neurogenesis. *Nature Neuroscience*, *26*(12), 2090–2103. https://doi.org/10.1038/s41593-023-01477-3

Borovac, J., Bosch, M., & Okamoto, K. (2018). Regulation of actin dynamics during structural plasticity of dendritic spines: Signaling messengers and actin-binding proteins. *Molecular and Cellular Neurosciences*, *91*, 122–130. https://doi.org/10.1016/j.mcn.2018.07.001

Boudaoud, A., Burian, A., Borowska-Wykręt, D., Uyttewaal, M., Wrzalik, R., Kwiatkowska, D., & Hamant, O. (2014). FibrilTool, an ImageJ plug-in to quantify fibrillar structures in raw microscopy images. *Nature Protocols*, *9*(2), 457–463. https://doi.org/10.1038/nprot.2014.024

Bowling, K. M., Thompson, M. L., Amaral, M. D., Finnila, C. R., Hiatt, S. M., Engel, K. L., Cochran, J. N., Brothers, K. B., East, K. M., Gray, D. E., Kelley, W. V., Lamb, N. E., Lose, E. J., Rich, C. A., Simmons, S., Whittle, J. S., Weaver, B. T., Nesmith, A. S., Myers, R. M., … Cooper, G. M. (2017). Genomic diagnosis for children with intellectual disability and/or developmental delay. *Genome Medicine*, *9*(1), 43. https://doi.org/10.1186/s13073-017-0433-1

Bozdagi, O., Sakurai, T., Dorr, N., Pilorge, M., Takahashi, N., & Buxbaum, J. D. (2012). Haploinsufficiency of Cyfip1 produces fragile X-like phenotypes in mice. *PloS One*, *7*(8), e42422. https://doi.org/10.1371/journal.pone.0042422

Bravo-Cordero, J. J., Magalhaes, M. A. O., Eddy, R. J., Hodgson, L., & Condeelis, J. (2013). Functions of cofilin in cell locomotion and invasion. *Nature Reviews Molecular Cell Biology*, *14*(7), 405–415. https://doi.org/10.1038/nrm3609

Brinkman, E. K., Chen, T., Amendola, M., & van Steensel, B. (2014). Easy quantitative assessment of genome editing by sequence trace decomposition. *Nucleic Acids Research*, *42*(22), e168. https://doi.org/10.1093/nar/gku936

Brinkman, E. K., Kousholt, A. N., Harmsen, T., Leemans, C., Chen, T., Jonkers, J., & van Steensel, B. (2018). Easy quantification of template-directed CRISPR/Cas9 editing. *Nucleic Acids Research*, *46*(10), e58. https://doi.org/10.1093/nar/gky164

Brown, J. A., & Bridgman, P. C. (2009). Disruption of the cytoskeleton during Semaphorin 3A induced growth cone collapse correlates with differences in actin organization and associated binding proteins. *Developmental Neurobiology*, *69*(10), 633–646. https://doi.org/10.1002/dneu.20732

Burridge, K., & Wennerberg, K. (2004). Rho and Rac Take Center Stage. *Cell*, *116*(2), 167–179. https://doi.org/10.1016/S0092-8674(04)00003-0

Busti, I., Allegra, M., Spalletti, C., Panzi, C., Restani, L., Billuart, P., & Caleo, M. (2020). ROCK/PKA Inhibition Rescues Hippocampal Hyperexcitability and GABAergic Neuron Alterations in a Oligophrenin-1 Knock-Out Mouse Model of X-Linked Intellectual Disability. *The Journal of Neuroscience: The Official Journal of the Society for Neuroscience*, *40*(13), 2776–2788. https://doi.org/10.1523/JNEUROSCI.0462-19.2020

Cammarota, M., Losi, G., Chiavegato, A., Zonta, M., & Carmignoto, G. (2013). Fast spiking interneuron control of seizure propagation in a cortical slice model of focal epilepsy. *The Journal of Physiology*, *591*(4), 807–822. https://doi.org/10.1113/jphysiol.2012.238154

Campa, C. C., Germena, G., Ciraolo, E., Copperi, F., Sapienza, A., Franco, I., Ghigo, A., Camporeale, A., Di Savino, A., Martini, M., Perino, A., Megens, R. T. A., Kurz, A. R. M., Scheiermann, C., Sperandio, M., Gamba, A., & Hirsch, E. (2016). Rac signal adaptation controls neutrophil mobilization from the bone marrow. *Science Signaling*, *9*(459), ra124–ra124. https://doi.org/10.1126/scisignal.aah5882

Carlén, M., Meletis, K., Siegle, J. H., Cardin, J. A., Futai, K., Vierling-Claassen, D., Rühlmann, C., Jones, S. R., Deisseroth, K., Sheng, M., Moore, C. I., & Tsai, L.-H. (2012). A critical role for NMDA receptors in parvalbumin interneurons for gamma rhythm induction and behavior. *Molecular Psychiatry*, *17*(5), 537–548. https://doi.org/10.1038/mp.2011.31

Carlsson, L., Nyström, L.-E., Sundkvist, I., Markey, F., & Lindberg, U. (1977). Actin polymerizability is influenced by profilin, a low molecular weight protein in non-muscle cells. *Journal of Molecular Biology*, *115*(3), 465–483. https://doi.org/10.1016/0022-2836(77)90166-8

Castillon, C., Gonzalez, L., Domenichini, F., Guyon, S., Da Silva, K., Durand, C., Lestaevel, P., Vaillend, C., Laroche, S., Barnier, J.-V., & Poirier, R. (2020). The

intellectual disability PAK3 R67C mutation impacts cognitive functions and adult hippocampal neurogenesis. *Human Molecular Genetics*, *29*(12), 1950–1968. https://doi.org/10.1093/hmg/ddz296

Causeret, F., Jacobs, T., Terao, M., Heath, O., Hoshino, M., & Nikolic, M. (2007). Neurabin-I is phosphorylated by Cdk5: Implications for neuronal morphogenesis and cortical migration. *Molecular Biology of the Cell*, *18*(11), 4327–4342. https://doi.org/10.1091/mbc.e07-04-0372

Causeret, F., Terao, M., Jacobs, T., Nishimura, Y. V., Yanagawa, Y., Obata, K., Hoshino, M., & Nikolic, M. (2009). The p21-activated kinase is required for neuronal migration in the cerebral cortex. *Cerebral Cortex (New York, N.Y.: 1991)*, *19*(4), 861–875. https://doi.org/10.1093/cercor/bhn133

Centonze, D., Rossi, S., Mercaldo, V., Napoli, I., Ciotti, M. T., De Chiara, V., Musella, A., Prosperetti, C., Calabresi, P., Bernardi, G., & Bagni, C. (2008). Abnormal striatal GABA transmission in the mouse model for the fragile X syndrome. *Biological Psychiatry*, *63*(10), 963–973. https://doi.org/10.1016/j.biopsych.2007.09.008

Chadman, K. K., Gong, S., Scattoni, M. L., Boltuck, S. E., Gandhy, S. U., Heintz, N., & Crawley, J. N. (2008). Minimal aberrant behavioral phenotypes of neuroligin-3 R451C knockin mice. *Autism Research: Official Journal of the International Society for Autism Research*, *1*(3), 147–158. https://doi.org/10.1002/aur.22

Chao, H.-T., Chen, H., Samaco, R. C., Xue, M., Chahrour, M., Yoo, J., Neul, J. L., Gong, S., Lu, H.-C., Heintz, N., Ekker, M., Rubenstein, J. L. R., Noebels, J. L., Rosenmund, C., & Zoghbi, H. Y. (2010). Dysfunction in GABA signalling mediates autism-like stereotypies and Rett syndrome phenotypes. *Nature*, *468*(7321), 263–269. https://doi.org/10.1038/nature09582

Chen, L., Liao, G., Waclaw, R. R., Burns, K. A., Linquist, D., Campbell, K., Zheng, Y., & Kuan, C.-Y. (2007). Rac1 controls the formation of midline commissures and the competency of tangential migration in ventral telencephalic neurons. *The Journal of Neuroscience: The Official Journal of the Society for Neuroscience*, *27*(14), 3884–3893. https://doi.org/10.1523/JNEUROSCI.3509-06.2007

Chen, L., Melendez, J., Campbell, K., Kuan, C.-Y., & Zheng, Y. (2009). Rac1 deficiency in the forebrain results in neural progenitor reduction and microcephaly. *Developmental Biology*, *325*(1), 162–170. https://doi.org/10.1016/j.ydbio.2008.10.023

Chen, R. Z., Akbarian, S., Tudor, M., & Jaenisch, R. (2001). Deficiency of methyl-CpG binding protein-2 in CNS neurons results in a Rett-like phenotype in mice. *Nature Genetics*, *27*(3), 327–331. https://doi.org/10.1038/85906

Chen, Y., Yang, Z., Meng, M., Zhao, Y., Dong, N., Yan, H., Liu, L., Ding, M., Peng, H. B., & Shao, F. (2009). Cullin mediates degradation of RhoA through evolutionarily conserved BTB adaptors to control actin cytoskeleton structure and cell movement. *Molecular Cell*, *35*(6), 841–855. https://doi.org/10.1016/j.molcel.2009.09.004

Chen, Z., Borek, D., Padrick, S. B., Gomez, T. S., Metlagel, Z., Ismail, A. M., Umetani, J., Billadeau, D. D., Otwinowski, Z., & Rosen, M. K. (2010). Structure and control of the actin regulatory WAVE complex. *Nature*, *468*(7323), 533–538. https://doi.org/10.1038/nature09623

Cheng, J., Scala, F., Blanco, F. A., Niu, S., Firozi, K., Keehan, L., Mulherkar, S., Froudarakis, E., Li, L., Duman, J. G., Jiang, X., & Tolias, K. F. (2021). The Rac-GEF Tiam1 Promotes Dendrite and Synapse Stabilization of Dentate Granule Cells and Restricts Hippocampal-Dependent Memory Functions. *The Journal of Neuroscience: The Official Journal of the Society for Neuroscience*, *41*(6), 1191–1206. https://doi.org/10.1523/JNEUROSCI.3271-17.2020

Cherfils, J., & Zeghouf, M. (2013). Regulation of small GTPases by GEFs, GAPs, and GDIs. *Physiological Reviews*, *93*(1), 269–309. https://doi.org/10.1152/physrev.00003.2012

Cheung, Z. H., Chin, W. H., Chen, Y., Ng, Y. P., & Ip, N. Y. (2007). Cdk5 is involved in BDNF-stimulated dendritic growth in hippocampal neurons. *PLoS Biology*, *5*(4), e63. https://doi.org/10.1371/journal.pbio.0050063

Chiaradia, I., Imaz-Rosshandler, I., Nilges, B. S., Boulanger, J., Pellegrini, L., Das, R., Kashikar, N. D., & Lancaster, M. A. (2023). Tissue morphology influences the temporal program of human brain organoid development. *Cell Stem Cell*, *30*(10), 1351-1367.e10. https://doi.org/10.1016/j.stem.2023.09.003

Chou, F.-S., & Wang, P.-S. (2016). The Arp2/3 complex is essential at multiple stages of neural development. *Neurogenesis (Austin, Tex.)*, *3*(1), e1261653. https://doi.org/10.1080/23262133.2016.1261653

Clowry, G. J. (2015). An enhanced role and expanded developmental origins for gamma-aminobutyric acidergic interneurons in the human cerebral cortex. *Journal of Anatomy*, *227*(4), 384–393. https://doi.org/10.1111/joa.12198

Clynen, E., Swijsen, A., Raijmakers, M., Hoogland, G., & Rigo, J.-M. (2014). Neuropeptides as Targets for the Development of Anticonvulsant Drugs. *Molecular Neurobiology*, *50*(2), 626–646. https://doi.org/10.1007/s12035-014-8669-x

Cobos, I., Borello, U., & Rubenstein, J. L. R. (2007). *Dlx* Transcription Factors Promote Migration through Repression of Axon and Dendrite Growth. *Neuron*, *54*(6), 873–888. https://doi.org/10.1016/j.neuron.2007.05.024

Cobos, I., Calcagnotto, M. E., Vilaythong, A. J., Thwin, M. T., Noebels, J. L., Baraban, S. C., & Rubenstein, J. L. R. (2005). Mice lacking Dlx1 show subtype-specific loss of interneurons, reduced inhibition and epilepsy. *Nature Neuroscience*, *8*(8), 1059–1068. https://doi.org/10.1038/nn1499

Compagnucci, C., Barresi, S., Petrini, S., Billuart, P., Piccini, G., Chiurazzi, P., Alfieri, P., Bertini, E., & Zanni, G. (2016). Rho Kinase Inhibition Is Essential During In Vitro Neurogenesis and Promotes Phenotypic Rescue of Human Induced Pluripotent Stem Cell-Derived Neurons With Oligophrenin-1 Loss of Function. *Stem Cells Translational Medicine*, *5*(7), 860–869. https://doi.org/10.5966/sctm.2015-0303

Conant, D., Hsiau, T., Rossi, N., Oki, J., Maures, T., Waite, K., Yang, J., Joshi, S., Kelso, R., Holden, K., Enzmann, B. L., & Stoner, R. (2022). Inference of CRISPR Edits from Sanger Trace Data. *The CRISPR Journal*, *5*(1), 123–130. https://doi.org/10.1089/crispr.2021.0113

Cooper, J. A. (2008). A mechanism for inside-out lamination in the neocortex. *Trends in Neurosciences*, *31*(3), 113–119. https://doi.org/10.1016/j.tins.2007.12.003

Cooper, J. A. (2013). Cell biology in neuroscience: Mechanisms of cell migration in the nervous system. *The Journal of Cell Biology*, *202*(5), 725–734. https://doi.org/10.1083/jcb.201305021

Corbetta, S., D'Adamo, P., Gualdoni, S., Braschi, C., Berardi, N., & de Curtis, I. (2008). Hyperactivity and novelty-induced hyperreactivity in mice lacking Rac3. *Behavioural Brain Research*, *186*(2), 246–255. https://doi.org/10.1016/j.bbr.2007.08.019

Corbetta, S., Gualdoni, S., Ciceri, G., Monari, M., Zuccaro, E., Tybulewicz, V. L. J., & de Curtis, I. (2009). Essential role of Rac1 and Rac3 GTPases in neuronal development. *FASEB Journal: Official Publication of the Federation of American Societies for Experimental Biology*, *23*(5), 1347–1357. https://doi.org/10.1096/fj.08-121574

Costa, C., Germena, G., Martin-Conte, E. L., Molineris, I., Bosco, E., Marengo, S., Azzolino, O., Altruda, F., Ranieri, V. M., & Hirsch, E. (2011). The RacGAP ArhGAP15 is a master negative regulator of neutrophil functions. *Blood*, *118*(4), 1099–1108. https://doi.org/10.1182/blood-2010-12-324756

Costa, R. M., Federov, N. B., Kogan, J. H., Murphy, G. G., Stern, J., Ohno, M., Kucherlapati, R., Jacks, T., & Silva, A. J. (2002). Mechanism for the learning deficits in a mouse model of neurofibromatosis type 1. *Nature*, *415*(6871), 526–530. https://doi.org/10.1038/nature711

Curia, G., Longo, D., Biagini, G., Jones, R. S. G., & Avoli, M. (2008). The pilocarpine model of temporal lobe epilepsy. *Journal of Neuroscience Methods*, *172*(2), 143–157. https://doi.org/10.1016/j.jneumeth.2008.04.019

Curia, G., Papouin, T., Séguéla, P., & Avoli, M. (2009). Downregulation of tonic GABAergic inhibition in a mouse model of fragile X syndrome. *Cerebral Cortex (New York, N.Y.: 1991)*, *19*(7), 1515–1520. https://doi.org/10.1093/cercor/bhn159

Davenport, E. C., Szulc, B. R., Drew, J., Taylor, J., Morgan, T., Higgs, N. F., López-Doménech, G., & Kittler, J. T. (2019). Autism and Schizophrenia-Associated CYFIP1 Regulates the Balance of Synaptic Excitation and Inhibition. *Cell Reports*, *26*(8), 2037-2051.e6. https://doi.org/10.1016/j.celrep.2019.01.092

de Carlos, J. A., López-Mascaraque, L., & Valverde, F. (1996). Dynamics of cell migration from the lateral ganglionic eminence in the rat. *The Journal of Neuroscience: The Official Journal of the Society for Neuroscience*, *16*(19), 6146–6156. https://doi.org/10.1523/JNEUROSCI.16-19-06146.1996

de Curtis, I. (2014). Roles of Rac1 and Rac3 GTPases during the development of cortical and hippocampal GABAergic interneurons. *Frontiers in Cellular Neuroscience, 8*, 307. https://doi.org/10.3389/fncel.2014.00307

De Marco García, N. V., Karayannis, T., & Fishell, G. (2011). Neuronal activity is required for the development of specific cortical interneuron subtypes. *Nature*, *472*(7343), 351–355. https://doi.org/10.1038/nature09865

Debant, A., Serra-Pagès, C., Seipel, K., O'Brien, S., Tang, M., Park, S. H., & Streuli, M. (1996). The multidomain protein Trio binds the LAR transmembrane tyrosine phosphatase, contains a protein kinase domain, and has separate rac-specific and rho-specific guanine nucleotide exchange factor domains. *Proceedings of the National Academy of Sciences of the United States of America*, *93*(11), 5466–5471. https://doi.org/10.1073/pnas.93.11.5466

DeDiego, I., Smith-Fernández, A., & Fairén, A. (1994). Cortical cells that migrate beyond area boundaries: Characterization of an early neuronal population in the lower intermediate zone of prenatal rats. *The European Journal of Neuroscience*, *6*(6), 983–997. https://doi.org/10.1111/j.1460-9568.1994.tb00593.x

DeFelipe, J. (1993). Neocortical neuronal diversity: Chemical heterogeneity revealed by colocalization studies of classic neurotransmitters, neuropeptides, calcium-binding proteins, and cell surface molecules. *Cerebral Cortex (New York, N.Y.: 1991)*, *3*(4), 273–289. https://doi.org/10.1093/cercor/3.4.273

Duarte, K., Heide, S., Poëa-Guyon, S., Rousseau, V., Depienne, C., Rastetter, A., Nava, C., Attié-Bitach, T., Razavi, F., Martinovic, J., Moutard, M. L., Cherfils, J., Mignot, C., Héron, D., & Barnier, J.-V. (2020). PAK3 mutations responsible for severe intellectual disability and callosal agenesis inhibit cell migration. *Neurobiology of Disease*, *136*, 104709. https://doi.org/10.1016/j.nbd.2019.104709

Duffney, L. J., Wei, J., Cheng, J., Liu, W., Smith, K. R., Kittler, J. T., & Yan, Z. (2013). Shank3 deficiency induces NMDA receptor hypofunction via an actin-dependent mechanism. *The Journal of Neuroscience: The Official Journal of the Society for Neuroscience*, *33*(40), 15767–15778. https://doi.org/10.1523/JNEUROSCI.1175-13.2013

Eden, S., Rohatgi, R., Podtelejnikov, A. V., Mann, M., & Kirschner, M. W. (2002). Mechanism of regulation of WAVE1-induced actin nucleation by Rac1 and Nck. *Nature*, *418*(6899), 790–793. https://doi.org/10.1038/nature00859

Edwards, D. C., Sanders, L. C., Bokoch, G. M., & Gill, G. N. (1999). Activation of LIM-kinase by Pak1 couples Rac/Cdc42 GTPase signalling to actin cytoskeletal dynamics. *Nature Cell Biology*, *1*(5), 253–259. https://doi.org/10.1038/12963

Ehler, E., van Leeuwen, F., Collard, J. G., & Salinas, P. C. (1997). Expression of*Tiam-1*in the Developing Brain Suggests a Role for the Tiam-1–Rac Signaling Pathway in Cell Migration and Neurite Outgrowth. *Molecular and Cellular Neuroscience*, *9*(1), 1–12. https://doi.org/10.1006/mcne.1997.0602

Elliott, A. M., Simard, L. R., Coghlan, G., Chudley, A. E., Chodirker, B. N., Greenberg, C. R., Burch, T., Ly, V., Hatch, G. M., & Zelinski, T. (2013). A novel mutation in KIAA0196: Identification of a gene involved in Ritscher–Schinzel/3C syndrome in a First Nations cohort. *Journal of Medical Genetics*, *50*(12), 819–822. https://doi.org/10.1136/jmedgenet-2013-101715

Endo, M., Ohashi, K., & Mizuno, K. (2007). LIM kinase and slingshot are critical for neurite extension. *The Journal of Biological Chemistry*, *282*(18), 13692–13702. https://doi.org/10.1074/jbc.M610873200

Erbayat-Altay, E., Yamada, K. A., Wong, M., & Thio, L. L. (2008). Increased severity of pentylenetetrazol induced seizures in leptin deficient *ob*/*ob* mice. *Neuroscience Letters*, *433*(2), 82–86. https://doi.org/10.1016/j.neulet.2007.12.051

Escamilla, C. O., Filonova, I., Walker, A. K., Xuan, Z. X., Holehonnur, R., Espinosa, F., Liu, S., Thyme, S. B., López-García, I. A., Mendoza, D. B., Usui, N., Ellegood, J., Eisch, A. J., Konopka, G., Lerch, J. P., Schier, A. F., Speed, H. E., & Powell, C. M. (2017). Kctd13 deletion reduces synaptic transmission via increased RhoA. *Nature*, *551*(7679), 227–231. https://doi.org/10.1038/nature24470

Fauchereau, F., Herbrand, U., Chafey, P., Eberth, A., Koulakoff, A., Vinet, M.-C., Ahmadian, M. R., Chelly, J., & Billuart, P. (2003). The RhoGAP activity of OPHN1, a new F-actin-binding protein, is negatively controlled by its amino-terminal domain. *Molecular and Cellular Neurosciences*, *23*(4), 574–586. https://doi.org/10.1016/s1044-7431(03)00078-2

Feldt, J., Schicht, M., Garreis, F., Welss, J., Schneider, U. W., & Paulsen, F. (2018). Structure, regulation and related diseases of the actin-binding protein gelsolin. *Expert Reviews in Molecular Medicine*, *20*, e7. https://doi.org/10.1017/erm.2018.7

Fishell, G., & Rudy, B. (2011). Mechanisms of inhibition within the telencephalon: “where the wild things are.” *Annual Review of Neuroscience*, *34*, 535–567. https://doi.org/10.1146/annurev-neuro-061010-113717

Flames, N., Long, J. E., Garratt, A. N., Fischer, T. M., Gassmann, M., Birchmeier, C., Lai, C., Rubenstein, J. L. R., & Marín, O. (2004). Short- and long-range attraction of cortical GABAergic interneurons by neuregulin-1. *Neuron*, *44*(2), 251–261. https://doi.org/10.1016/j.neuron.2004.09.028

Froemke, R. C. (2015). Plasticity of cortical excitatory-inhibitory balance. *Annual Review of Neuroscience*, *38*, 195–219. https://doi.org/10.1146/annurev-neuro-071714-034002

Fu, W.-Y., Chen, Y., Sahin, M., Zhao, X.-S., Shi, L., Bikoff, J. B., Lai, K.-O., Yung, W.-H., Fu, A. K. Y., Greenberg, M. E., & Ip, N. Y. (2007). Cdk5 regulates EphA4-mediated dendritic spine retraction through an ephexin1-dependent mechanism. *Nature Neuroscience*, *10*(1), 67–76. https://doi.org/10.1038/nn1811

Galanopoulou, A. S. (2010). Mutations affecting GABAergic signaling in seizures and epilepsy. *Pflugers Archiv: European Journal of Physiology*, *460*(2), 505–523. https://doi.org/10.1007/s00424-010-0816-2

Garvalov, B. K., Flynn, K. C., Neukirchen, D., Meyn, L., Teusch, N., Wu, X., Brakebusch, C., Bamburg, J. R., & Bradke, F. (2007). Cdc42 Regulates Cofilin during the Establishment of Neuronal Polarity. *The Journal of Neuroscience*, *27*(48), 13117. https://doi.org/10.1523/JNEUROSCI.3322-07.2007

Gelman, D. M., Marín, O., & Rubenstein, J. L. R. (2012). The Generation of Cortical Interneurons. In J. L. Noebels, M. Avoli, M. A. Rogawski, R. W. Olsen, & A. V. Delgado-Escueta (Eds.), *Jasper’s Basic Mechanisms of the Epilepsies* (4th ed.). National Center for Biotechnology Information (US). http://www.ncbi.nlm.nih.gov/books/NBK98190/

Gemelli, T., Berton, O., Nelson, E. D., Perrotti, L. I., Jaenisch, R., & Monteggia, L. M. (2006). Postnatal loss of methyl-CpG binding protein 2 in the forebrain is sufficient to mediate behavioral aspects of Rett syndrome in mice. *Biological Psychiatry*, *59*(5), 468–476. https://doi.org/10.1016/j.biopsych.2005.07.025

Ghetti, S., Burigotto, M., Mattivi, A., Magnani, G., Casini, A., Bianchi, A., Cereseto, A., & Fava, L. L. (2021). CRISPR/Cas9 ribonucleoprotein-mediated knockin generation in hTERT-RPE1 cells. *STAR Protocols*, *2*(2), 100407. https://doi.org/10.1016/j.xpro.2021.100407

Gibson, J. R., Bartley, A. F., Hays, S. A., & Huber, K. M. (2008). Imbalance of neocortical excitation and inhibition and altered UP states reflect network hyperexcitability in the mouse model of fragile X syndrome. *Journal of Neurophysiology*, *100*(5), 2615–2626. https://doi.org/10.1152/jn.90752.2008

Gohla, A., & Bokoch, G. M. (2002). 14-3-3 Regulates Actin Dynamics by Stabilizing Phosphorylated Cofilin. *Current Biology*, *12*(19), 1704–1710. https://doi.org/10.1016/S0960-9822(02)01184-3

Gomez, T. M., & Letourneau, P. C. (2014). Actin dynamics in growth cone motility and navigation. *Journal of Neurochemistry*, *129*(2), 221–234. https://doi.org/10.1111/jnc.12506

Gonzalez-Billault, C., Muñoz-Llancao, P., Henriquez, D. R., Wojnacki, J., Conde, C., & Caceres, A. (2012). The role of small GTPases in neuronal morphogenesis and polarity. *Cytoskeleton (Hoboken, N.J.)*, *69*(7), 464–485. https://doi.org/10.1002/cm.21034

Govek, E.-E., Hatten, M. E., & Van Aelst, L. (2011). The role of Rho GTPase proteins in CNS neuronal migration. *Developmental Neurobiology*, *71*(6), 528–553. https://doi.org/10.1002/dneu.20850

Guo, H., Zhang, Q., Dai, R., Yu, B., Hoekzema, K., Tan, J., Tan, S., Jia, X., Chung, W. K., Hernan, R., Alkuraya, F. S., Alsulaiman, A., Al-Muhaizea, M. A., Lesca, G., Pons, L., Labalme, A., Laux, L., Bryant, E., Brown, N. J., … Xia, K. (2020). *NCKAP1* Disruptive Variants Lead to a Neurodevelopmental Disorder with Core Features of Autism. *The American Journal of Human Genetics*, *107*(5), 963–976. https://doi.org/10.1016/j.ajhg.2020.10.002

Guo, J., & Anton, E. S. (2014). Decision making during interneuron migration in the developing cerebral cortex. *Trends in Cell Biology*, *24*(6), 342–351. https://doi.org/10.1016/j.tcb.2013.12.001

Guy, J., Hendrich, B., Holmes, M., Martin, J. E., & Bird, A. (2001). A mouse Mecp2-null mutation causes neurological symptoms that mimic Rett syndrome. *Nature Genetics*, *27*(3), 322–326. https://doi.org/10.1038/85899

Hall, A., & Lalli, G. (2010). Rho and Ras GTPases in Axon Growth, Guidance, and Branching. *Cold Spring Harbor Perspectives in Biology*, *2*(2), a001818. https://doi.org/10.1101/cshperspect.a001818

Hall, A., & Nobes, C. D. (2000). Rho GTPases: Molecular switches that control the organization and dynamics of the actin cytoskeleton. *Philosophical Transactions of the Royal Society of London. Series B: Biological Sciences*. https://doi.org/10.1098/rstb.2000.0632

Hansen, D. V., Lui, J. H., Flandin, P., Yoshikawa, K., Rubenstein, J. L., Alvarez-Buylla, A., & Kriegstein, A. R. (2013). Non-epithelial stem cells and cortical interneuron production in the human ganglionic eminences. *Nature Neuroscience*, *16*(11), 1576–1587. https://doi.org/10.1038/nn.3541

Harripaul, R., Vasli, N., Mikhailov, A., Rafiq, M. A., Mittal, K., Windpassinger, C., Sheikh, T. I., Noor, A., Mahmood, H., Downey, S., Johnson, M., Vleuten, K., Bell, L., Ilyas, M., Khan, F. S., Khan, V., Moradi, M., Ayaz, M., Naeem, F., … Vincent, J. B. (2018). Mapping autosomal recessive intellectual disability: Combined microarray and exome sequencing identifies 26 novel candidate genes in 192 consanguineous families. *Molecular Psychiatry*, *23*(4), 973–984. https://doi.org/10.1038/mp.2017.60

Hashimoto, T., Volk, D. W., Eggan, S. M., Mirnics, K., Pierri, J. N., Sun, Z., Sampson, A. R., & Lewis, D. A. (2003). Gene expression deficits in a subclass of GABA neurons in the prefrontal cortex of subjects with schizophrenia. *The Journal of Neuroscience: The Official Journal of the Society for Neuroscience*, *23*(15), 6315–6326. https://doi.org/10.1523/JNEUROSCI.23-15-06315.2003

Hatanaka, Y., Zhu, Y., Torigoe, M., Kita, Y., & Murakami, F. (2016). From migration to settlement: The pathways, migration modes and dynamics of neurons in the developing brain. *Proceedings of the Japan Academy. Series B, Physical and Biological Sciences*, *92*(1), 1–19. https://doi.org/10.2183/pjab.92.1

Hawasli, A. H., Benavides, D. R., Nguyen, C., Kansy, J. W., Hayashi, K., Chambon, P., Greengard, P., Powell, C. M., Cooper, D. C., & Bibb, J. A. (2007). Cyclin-dependent kinase 5 governs learning and synaptic plasticity via control of

NMDAR degradation. *Nature Neuroscience*, *10*(7), 880–886. https://doi.org/10.1038/nn1914

Haydon, P. G., & Drapeau, P. (1995). From contact to connection: Early events during synaptogenesis. *Trends in Neurosciences*, *18*(4), 196–201. https://doi.org/10.1016/0166-2236(95)93901-9

He, L., Zhang, Z., Yu, Y., Ahmed, S., Cheung, N. S., & Qi, R. Z. (2011). The neuronal p35 activator of Cdk5 is a novel F-actin binding and bundling protein. *Cellular and Molecular Life Sciences: CMLS*, *68*(9), 1633–1643. https://doi.org/10.1007/s00018-010-0562-9

Heasman, S. J., & Ridley, A. J. (2008). Mammalian Rho GTPases: New insights into their functions from in vivo studies. *Nature Reviews. Molecular Cell Biology*, *9*(9), 690–701. https://doi.org/10.1038/nrm2476

Hirose, M., Ishizaki, T., Watanabe, N., Uehata, M., Kranenburg, O., Moolenaar, W. H., Matsumura, F., Maekawa, M., Bito, H., & Narumiya, S. (1998). Molecular dissection of the Rho-associated protein kinase (p160ROCK)-regulated neurite remodeling in neuroblastoma N1E-115 cells. *The Journal of Cell Biology*, *141*(7), 1625–1636. https://doi.org/10.1083/jcb.141.7.1625

Hisanaga, S., & Endo, R. (2010). Regulation and role of cyclin-dependent kinase activity in neuronal survival and death. *Journal of Neurochemistry*, *115*(6), 1309–1321. https://doi.org/10.1111/j.1471-4159.2010.07050.x

Hlushchenko, I., & Hotulainen, P. (2019). Chemical LTD, but not LTP, induces transient accumulation of gelsolin in dendritic spines. *Biological Chemistry*, *400*(9), 1129–1139. https://doi.org/10.1515/hsz-2019-0110

Homanics, G. E., DeLorey, T. M., Firestone, L. L., Quinlan, J. J., Handforth, A., Harrison, N. L., Krasowski, M. D., Rick, C. E., Korpi, E. R., Mäkelä, R., Brilliant, M. H., Hagiwara, N., Ferguson, C., Snyder, K., & Olsen, R. W. (1997). Mice devoid of gamma-aminobutyrate type A receptor beta3 subunit have epilepsy, cleft palate, and hypersensitive behavior. *Proceedings of the National Academy of Sciences of the United States of America*, *94*(8), 4143–4148. https://doi.org/10.1073/pnas.94.8.4143

Hoogenraad, C. C., Akhmanova, A., Galjart, N., & De Zeeuw, C. I. (2004). LIMK1 and CLIP-115: Linking cytoskeletal defects to Williams syndrome.

BioEssays: News and Reviews in Molecular, Cellular and Developmental Biology, *26*(2), 141–150. https://doi.org/10.1002/bies.10402

Horn, S., Au, M., Basel-Salmon, L., Bayrak-Toydemir, P., Chapin, A., Cohen, L., Elting, M. W., Graham, J. M., Gonzaga-Jauregui, C., Konen, O., Holzer, M., Lemke, J., Miller, C. E., Rey, L. K., Wolf, N. I., Weiss, M. M., Waisfisz, Q., Mirzaa, G. M., Wieczorek, D., … Abou Jamra, R. (2019). De novo variants in PAK1 lead to intellectual disability with macrocephaly and seizures. *Brain: A Journal of Neurology*, *142*(11), 3351–3359. https://doi.org/10.1093/brain/awz264

Hua, J. Y., Smear, M. C., Baier, H., & Smith, S. J. (2005). Regulation of axon growth in vivo by activity-based competition. *Nature*, *434*(7036), 1022–1026. https://doi.org/10.1038/nature03409

Huganir, R. L., & Nicoll, R. A. (2013). AMPARs and synaptic plasticity: The last 25 years. *Neuron*, *80*(3), 704–717. https://doi.org/10.1016/j.neuron.2013.10.025

Huo, H.-Q., Qu, Z.-Y., Yuan, F., Ma, L., Yao, L., Xu, M., Hu, Y., Ji, J., Bhattacharyya, A., Zhang, S.-C., & Liu, Y. (2018). Modeling Down Syndrome with Patient iPSCs Reveals Cellular and Migration Deficits of GABAergic Neurons. *Stem Cell Reports*, *10*(4), 1251–1266. https://doi.org/10.1016/j.stemcr.2018.02.001

InanlooRahatloo, K., Peymani, F., Kahrizi, K., & Najmabadi, H. (2019). Whole-Transcriptome Analysis Reveals Dysregulation of Actin-Cytoskeleton Pathway in Intellectual Disability Patients. *Neuroscience*, *404*, 423–444. https://doi.org/10.1016/j.neuroscience.2019.01.029

Irwin, S. A., Galvez, R., & Greenough, W. T. (2000). Dendritic spine structural anomalies in fragile-X mental retardation syndrome. *Cerebral Cortex (New York, N.Y.: 1991)*, *10*(10), 1038–1044. https://doi.org/10.1093/cercor/10.10.1038

Isaacson, J. S., & Scanziani, M. (2011). How inhibition shapes cortical activity. *Neuron*, *72*(2), 231–243. https://doi.org/10.1016/j.neuron.2011.09.027

Ishizaki, T., Maekawa, M., Fujisawa, K., Okawa, K., Iwamatsu, A., Fujita, A., Watanabe, N., Saito, Y., Kakizuka, A., Morii, N., & Narumiya, S. (1996). The small GTP-binding protein Rho binds to and activates a 160 kDa Ser/Thr protein kinase homologous to myotonic dystrophy kinase. *The EMBO Journal*, *15*(8), 1885–1893.

Jaffe, A. B., & Hall, A. (2005). Rho GTPases: Biochemistry and biology. *Annual Review of Cell and Developmental Biology*, *21*, 247–269. https://doi.org/10.1146/annurev.cellbio.21.020604.150721

Jalink, K., van Corven, E. J., Hengeveld, T., Morii, N., Narumiya, S., & Moolenaar, W. H. (1994). Inhibition of lysophosphatidate- and thrombin-induced neurite retraction and neuronal cell rounding by ADP ribosylation of the small GTP-binding protein Rho. *Journal of Cell Biology*, *126*(3), 801–810. https://doi.org/10.1083/jcb.126.3.801

Jiang, Y.-H., Pan, Y., Zhu, L., Landa, L., Yoo, J., Spencer, C., Lorenzo, I., Brilliant, M., Noebels, J., & Beaudet, A. L. (2010). Altered ultrasonic vocalization and impaired learning and memory in Angelman syndrome mouse model with a large maternal deletion from Ube3a to Gabrb3. *PloS One*, *5*(8), e12278. https://doi.org/10.1371/journal.pone.0012278

Johnson, G. V., & Jope, R. S. (1992). The role of microtubule-associated protein 2 (MAP-2) in neuronal growth, plasticity, and degeneration. *Journal of Neuroscience Research*, *33*(4), 505–512. https://doi.org/10.1002/jnr.490330402

Juarez, P., & Martínez Cerdeño, V. (2022). Parvalbumin and parvalbumin chandelier interneurons in autism and other psychiatric disorders. *Frontiers in Psychiatry*, *13*. https://doi.org/10.3389/fpsyt.2022.913550

Kahn, O. I., & Baas, P. W. (2016). Microtubules and Growth Cones: Motors Drive the Turn. *Trends in Neurosciences*, *39*(7), 433–440. https://doi.org/10.1016/j.tins.2016.04.009

Kato, M. (2015). Genotype-phenotype correlation in neuronal migration disorders and cortical dysplasias. *Frontiers in Neuroscience*, *9*. https://doi.org/10.3389/fnins.2015.00181

Katoh, K., Kano, Y., Amano, M., Kaibuchi, K., & Fujiwara, K. (2001). Stress fiber organization regulated by MLCK and Rho-kinase in cultured human fibroblasts. *American Journal of Physiology. Cell Physiology*, *280*(6), C1669-1679. https://doi.org/10.1152/ajpcell.2001.280.6.C1669

Katrancha, S. M., Shaw, J. E., Zhao, A. Y., Myers, S. A., Cocco, A. R., Jeng, A. T., Zhu, M., Pittenger, C., Greer, C. A., Carr, S. A., Xiao, X., & Koleske, A. J. (2019). Trio Haploinsufficiency Causes Neurodevelopmental Disease-Associated

Deficits. *Cell Reports*, *26*(10), 2805-2817.e9. https://doi.org/10.1016/j.celrep.2019.02.022

Kawauchi, T. (2015). Cellullar insights into cerebral cortical development: Focusing on the locomotion mode of neuronal migration. *Frontiers in Cellular Neuroscience*, *9*. https://doi.org/10.3389/fncel.2015.00394

Kelsom, C., & Lu, W. (2013). Development and specification of GABAergic cortical interneurons. *Cell & Bioscience*, *3*(1), 19. https://doi.org/10.1186/2045-3701-3-19

Kesavapany, S., Amin, N., Zheng, Y.-L., Nijhara, R., Jaffe, H., Sihag, R., Gutkind, J. S., Takahashi, S., Kulkarni, A., Grant, P., & Pant, H. C. (2004). P35/cyclin-dependent kinase 5 phosphorylation of ras guanine nucleotide releasing factor 2 (RasGRF2) mediates Rac-dependent Extracellular Signal-regulated kinase 1/2 activity, altering RasGRF2 and microtubule-associated protein 1b distribution in neurons. *The Journal of Neuroscience: The Official Journal of the Society for Neuroscience*, *24*(18), 4421–4431. https://doi.org/10.1523/JNEUROSCI.0690-04.2004

Kessaris, N., Magno, L., Rubin, A. N., & Oliveira, M. G. (2014). Genetic programs controlling cortical interneuron fate. *Current Opinion in Neurobiology*, *26*(100), 79–87. https://doi.org/10.1016/j.conb.2013.12.012

Khaitlina, S., & Hinssen, H. (2002). Ca-dependent binding of actin to gelsolin. *FEBS Letters*, *521*(1–3), 14–18. https://doi.org/10.1016/S0014-5793(02)02657-1

Khelfaoui, M., Denis, C., van Galen, E., de Bock, F., Schmitt, A., Houbron, C., Morice, E., Giros, B., Ramakers, G., Fagni, L., Chelly, J., Nosten-Bertrand, M., & Billuart, P. (2007). Loss of X-linked mental retardation gene oligophrenin1 in mice impairs spatial memory and leads to ventricular enlargement and dendritic spine immaturity. *The Journal of Neuroscience: The Official Journal of the Society for Neuroscience*, *27*(35), 9439–9450. https://doi.org/10.1523/JNEUROSCI.2029-07.2007

Kim, A. S., Kakalis, L. T., Abdul-Manan, N., Liu, G. A., & Rosen, M. K. (2000). Autoinhibition and activation mechanisms of the Wiskott–Aldrich syndrome protein. *Nature*, *404*(6774), 151–158. https://doi.org/10.1038/35004513

Kim, C. H., & Lisman, J. E. (1999). A role of actin filament in synaptic transmission and long-term potentiation. *The Journal of Neuroscience: The Official Journal of the Society for Neuroscience*, *19*(11), 4314–4324. https://doi.org/10.1523/JNEUROSCI.19-11-04314.1999

Kim, I. H., Racz, B., Wang, H., Burianek, L., Weinberg, R., Yasuda, R., Wetsel, W. C., & Soderling, S. H. (2013). Disruption of Arp2/3 results in asymmetric structural plasticity of dendritic spines and progressive synaptic and behavioral abnormalities. *The Journal of Neuroscience: The Official Journal of the Society for Neuroscience*, *33*(14), 6081–6092. https://doi.org/10.1523/JNEUROSCI.0035-13.2013

Kim, I. H., Wang, H., Soderling, S. H., & Yasuda, R. (2014). Loss of Cdc42 leads to defects in synaptic plasticity and remote memory recall. *eLife*, *3*, e02839. https://doi.org/10.7554/eLife.02839

Kimura, K., Ito, M., Amano, M., Chihara, K., Fukata, Y., Nakafuku, M., Yamamori, B., Feng, J., Nakano, T., Okawa, K., Iwamatsu, A., & Kaibuchi, K. (1996). Regulation of myosin phosphatase by Rho and Rho-associated kinase (Rho-kinase). *Science (New York, N.Y.)*, *273*(5272), 245–248. https://doi.org/10.1126/science.273.5272.245

Kleschevnikov, A. M., Belichenko, P. V., Villar, A. J., Epstein, C. J., Malenka, R. C., & Mobley, W. C. (2004). Hippocampal long-term potentiation suppressed by increased inhibition in the Ts65Dn mouse, a genetic model of Down syndrome. *The Journal of Neuroscience: The Official Journal of the Society for Neuroscience*, *24*(37), 8153–8160. https://doi.org/10.1523/JNEUROSCI.1766-04.2004

Kluesner, M. G., Nedveck, D. A., Lahr, W. S., Garbe, J. R., Abrahante, J. E., Webber, B. R., & Moriarity, B. S. (2018). EditR: A Method to Quantify Base Editing from Sanger Sequencing. *The CRISPR Journal*, *1*(3), 239–250. https://doi.org/10.1089/crispr.2018.0014

Knight, G. T., Lundin, B. F., Iyer, N., Ashton, L. M., Sethares, W. A., Willett, R. M., & Ashton, R. S. (2018). Engineering induction of singular neural rosette emergence within hPSC-derived tissues. *eLife*, *7*, e37549. https://doi.org/10.7554/eLife.37549

Kojima, H., Rosendale, M., Sugiyama, Y., Hayashi, M., Horiguchi, Y., Yoshihara, T., Ikegaya, Y., Saneyoshi, T., & Hayashi, Y. (2019). The role of

CaMKII-Tiam1 complex on learning and memory. *Neurobiology of Learning and Memory*, *166*, 107070. https://doi.org/10.1016/j.nlm.2019.107070

Kollins, K. M., Hu, J., Bridgman, P. C., Huang, Y. Q., & Gallo, G. (2009). Myosin-II negatively regulates minor process extension and the temporal development of neuronal polarity. *Developmental Neurobiology*, *69*(5), 279–298. https://doi.org/10.1002/dneu.20704

Korobova, F., & Svitkina, T. (2010). Molecular architecture of synaptic actin cytoskeleton in hippocampal neurons reveals a mechanism of dendritic spine morphogenesis. *Molecular Biology of the Cell*, *21*(1), 165–176. https://doi.org/10.1091/mbc.e09-07-0596

Korotkova, T., Fuchs, E. C., Ponomarenko, A., von Engelhardt, J., & Monyer, H. (2010). NMDA receptor ablation on parvalbumin-positive interneurons impairs hippocampal synchrony, spatial representations, and working memory. *Neuron*, *68*(3), 557–569. https://doi.org/10.1016/j.neuron.2010.09.017

Kozma, R., Sarner, S., Ahmed, S., & Lim, L. (1997). Rho family GTPases and neuronal growth cone remodelling: Relationship between increased complexity induced by Cdc42Hs, Rac1, and acetylcholine and collapse induced by RhoA and lysophosphatidic acid. *Molecular and Cellular Biology*, *17*(3), 1201–1211. https://doi.org/10.1128/MCB.17.3.1201

Kreis, P., Thévenot, E., Rousseau, V., Boda, B., Muller, D., & Barnier, J.-V. (2007). The p21-activated kinase 3 implicated in mental retardation regulates spine morphogenesis through a Cdc42-dependent pathway. *The Journal of Biological Chemistry*, *282*(29), 21497–21506. https://doi.org/10.1074/jbc.M703298200

Kubo, T., Endo, M., Hata, K., Taniguchi, J., Kitajo, K., Tomura, S., Yamaguchi, A., Mueller, B. K., & Yamashita, T. (2008). Myosin IIA is required for neurite outgrowth inhibition produced by repulsive guidance molecule. *Journal of Neurochemistry*, *105*(1), 113–126. https://doi.org/10.1111/j.1471-4159.2007.05125.x

Kunda, P., Paglini, G., Quiroga, S., Kosik, K., & Cáceres, A. (2001). Evidence for the Involvement of Tiam1 in Axon Formation. *Journal of Neuroscience*, *21*(7), 2361–2372. https://doi.org/10.1523/JNEUROSCI.21-07-02361.2001

Kutsche, K., Yntema, H., Brandt, A., Jantke, I., Nothwang, H. G., Orth, U., Boavida, M. G., David, D., Chelly, J., Fryns, J. P., Moraine, C., Ropers, H. H., Hamel, B. C., van Bokhoven, H., & Gal, A. (2000). Mutations in ARHGEF6, encoding a guanine nucleotide exchange factor for Rho GTPases, in patients with X-linked mental retardation. *Nature Genetics*, *26*(2), 247–250. https://doi.org/10.1038/80002

Kwon, Y., Lee, S. J., Lee, E., Kim, D., & Park, D. (2019). βPix heterozygous mice have defects in neuronal morphology and social interaction. *Biochemical and Biophysical Research Communications*, *516*(4), 1204–1210. https://doi.org/10.1016/j.bbrc.2019.07.001

Lambrechts, A., Jonckheere, V., Peleman, C., Polet, D., De Vos, W., Vandekerckhove, J., & Ampe, C. (2006). Profilin-I-ligand interactions influence various aspects of neuronal differentiation. *Journal of Cell Science*, *119*(8), 1570–1578. https://doi.org/10.1242/jcs.02884

Lappalainen, P., & Drubin, D. G. (1997). Cofilin promotes rapid actin filament turnover in vivo. *Nature*, *388*(6637), 78–82. https://doi.org/10.1038/40418

Law, R., Dixon-Salazar, T., Jerber, J., Cai, N., Abbasi, A. A., Zaki, M. S., Mittal, K., Gabriel, S. B., Rafiq, M. A., Khan, V., Nguyen, M., Ali, G., Copeland, B., Scott, E., Vasli, N., Mikhailov, A., Khan, M. N., Andrade, D. M., Ayaz, M., … Gleeson, J. G. (2014). Biallelic Truncating Mutations in *FMN2*, Encoding the Actin-Regulatory Protein Formin 2, Cause Nonsyndromic Autosomal-Recessive Intellectual Disability. *The American Journal of Human Genetics*, *95*(6), 721–728. https://doi.org/10.1016/j.ajhg.2014.10.016

Le Magueresse, C., & Monyer, H. (2013). GABAergic Interneurons Shape the Functional Maturation of the Cortex. *Neuron*, *77*(3), 388–405. https://doi.org/10.1016/j.neuron.2013.01.011

Leeuwen, F. N. van, Kain, H. E. T., Kammen, R. A. van der, Michiels, F., Kranenburg, O. W., & Collard, J. G. (1997). The Guanine Nucleotide Exchange Factor Tiam1 Affects Neuronal Morphology; Opposing Roles for the Small GTPases Rac and Rho. *Journal of Cell Biology*, *139*(3), 797–807. https://doi.org/10.1083/jcb.139.3.797

Lein, E. S., Hawrylycz, M. J., Ao, N., Ayres, M., Bensinger, A., Bernard, A., Boe, A. F., Boguski, M. S., Brockway, K. S., Byrnes, E. J., Chen, L., Chen, L.,

Chen, T.-M., Chin, M. C., Chong, J., Crook, B. E., Czaplinska, A., Dang, C. N., Datta, S., … Jones, A. R. (2007). Genome-wide atlas of gene expression in the adult mouse brain. *Nature*, *445*(7124), 168–176. https://doi.org/10.1038/nature05453

Lelieveld, S. H., Reijnders, M. R. F., Pfundt, R., Yntema, H. G., Kamsteeg, E.-J., de Vries, P., de Vries, B. B. A., Willemsen, M. H., Kleefstra, T., Löhner, K., Vreeburg, M., Stevens, S. J. C., van der Burgt, I., Bongers, E. M. H. F., Stegmann, A. P. A., Rump, P., Rinne, T., Nelen, M. R., Veltman, J. A., … Gilissen, C. (2016). Meta-analysis of 2,104 trios provides support for 10 new genes for intellectual disability. *Nature Neuroscience*, *19*(9), 1194–1196. https://doi.org/10.1038/nn.4352

Levitt, P. (2005). Developmental Neurobiology and Clinical Disorders: Lost in Translation? *Neuron*, *46*(3), 407–412. https://doi.org/10.1016/j.neuron.2005.04.015

Levitt, P., Eagleson, K. L., & Powell, E. M. (2004). Regulation of neocortical interneuron development and the implications for neurodevelopmental disorders. *Trends in Neurosciences*, *27*(7), 400–406. https://doi.org/10.1016/j.tins.2004.05.008

Lewis, S. A., Tian, G., & Cowan, N. J. (1997). The alpha- and beta-tubulin folding pathways. *Trends in Cell Biology*, *7*(12), 479–484. https://doi.org/10.1016/S0962-8924(97)01168-9

Li, A., Zhu, H.-M., Chen, Y., Yan, F., Liu, Z.-Y., Li, Z.-L., Dong, W.-R., Zhang, L., & Wang, H.-H. (2021). Cdc42 Facilitates Axonogenesis by Enhancing Microtubule Stabilization in Primary Hippocampal Neurons. *Cellular and Molecular Neurobiology*, *41*(7), 1599–1610. https://doi.org/10.1007/s10571-021-01051-0

Liaci, C., Camera, M., Caslini, G., Rando, S., Contino, S., Romano, V., & Merlo, G. R. (2021). Neuronal Cytoskeleton in Intellectual Disability: From Systems Biology and Modeling to Therapeutic Opportunities. *International Journal of Molecular Sciences*, *22*(11), 6167. https://doi.org/10.3390/ijms22116167

Liaci, C., Camera, M., Zamboni, V., Sarò, G., Ammoni, A., Parmigiani, E., Ponzoni, L., Hidisoglu, E., Chiantia, G., Marcantoni, A., Giustetto, M., Tomagra, G., Carabelli, V., Torelli, F., Sala, M., Yanagawa, Y., Obata, K., Hirsch, E., &

Merlo, G. R. (2022). Loss of ARHGAP15 affects the directional control of migrating interneurons in the embryonic cortex and increases susceptibility to epilepsy. *Frontiers in Cell and Developmental Biology*, *10*, 875468. https://doi.org/10.3389/fcell.2022.875468

Lim, L., Mi, D., Llorca, A., & Marín, O. (2018). Development and Functional Diversification of Cortical Interneurons. *Neuron*, *100*(2), 294–313. https://doi.org/10.1016/j.neuron.2018.10.009

Lin, C.-H., & Forscher, P. (1995). Growth cone advance is inversely proportional to retrograde F-actin flow. *Neuron*, *14*(4), 763–771. https://doi.org/10.1016/0896-6273(95)90220-1

Lin, G. N., Corominas, R., Lemmens, I., Yang, X., Tavernier, J., Hill, D. E., Vidal, M., Sebat, J., & Iakoucheva, L. M. (2015). Spatiotemporal 16p11.2 protein network implicates cortical late mid-fetal brain development and KCTD13-Cul3-RhoA pathway in psychiatric diseases. *Neuron*, *85*(4), 742–754. https://doi.org/10.1016/j.neuron.2015.01.010

López-Bendito, G., Sturgess, K., Erdélyi, F., Szabó, G., Molnár, Z., & Paulsen, O. (2004). Preferential origin and layer destination of GAD65-GFP cortical interneurons. *Cerebral Cortex (New York, N.Y.: 1991)*, *14*(10), 1122–1133. https://doi.org/10.1093/cercor/bhh072

Lowery, L. A., & Vactor, D. V. (2009). The trip of the tip: Understanding the growth cone machinery. *Nature Reviews. Molecular Cell Biology*, *10*(5), 332. https://doi.org/10.1038/nrm2679

Lu, M., Witke, W., Kwiatkowski, D. J., & Kosik, K. S. (1997). Delayed retraction of filopodia in gelsolin null mice. *The Journal of Cell Biology*, *138*(6), 1279–1287. https://doi.org/10.1083/jcb.138.6.1279

Luo, L. (2000). RHO GTPASES in neuronal morphogenesis. *Nature Reviews Neuroscience*, *1*(3), 173–180. https://doi.org/10.1038/35044547

Ma, T., Wang, C., Wang, L., Zhou, X., Tian, M., Zhang, Q., Zhang, Y., Li, J., Liu, Z., Cai, Y., Liu, F., You, Y., Chen, C., Campbell, K., Song, H., Ma, L., Rubenstein, J. L., & Yang, Z. (2013). Subcortical origins of human and monkey neocortical interneurons. *Nature Neuroscience*, *16*(11), 1588–1597. https://doi.org/10.1038/nn.3536

Maciver, S. K., & Hussey, P. J. (2002). The ADF/cofilin family: Actin-remodeling proteins. *Genome Biology*, *3*(5), reviews3007. https://doi.org/10.1186/gb-2002-3-5-reviews3007

Maday, S., Twelvetrees, A. E., Moughamian, A. J., & Holzbaur, E. L. F. (2014). Axonal transport: Cargo-specific mechanisms of motility and regulation. *Neuron*, *84*(2), 292–309. https://doi.org/10.1016/j.neuron.2014.10.019

Maekawa, M., Ishizaki, T., Boku, S., Watanabe, N., Fujita, A., Iwamatsu, A., Obinata, T., Ohashi, K., Mizuno, K., & Narumiya, S. (1999). Signaling from Rho to the actin cytoskeleton through protein kinases ROCK and LIM-kinase. *Science (New York, N.Y.)*, *285*(5429), 895–898. https://doi.org/10.1126/science.285.5429.895

Mamula, D., Korthals, M., Hradsky, J., Gottfried, A., Fischer, K.-D., & Tedford, K. (2021). Arhgef6 (alpha-PIX) cytoskeletal regulator signals to GTPases and Cofilin to couple T cell migration speed and persistence. *Journal of Leukocyte Biology*, *110*(5), 839–852. https://doi.org/10.1002/JLB.1A1219-719R

Manfredi, I., Zani, A. D., Rampoldi, L., Pegorini, S., Bernascone, I., Moretti, M., Gotti, C., Croci, L., Consalez, G. G., Ferini-Strambi, L., Sala, M., Pattini, L., & Casari, G. (2009). Expression of mutant β2 nicotinic receptors during development is crucial for epileptogenesis. *Human Molecular Genetics*, *18*(6), 1075–1088. https://doi.org/10.1093/hmg/ddp004

Manser, E., Leung, T., Salihuddin, H., Zhao, Z., & Lim, L. (1994). A brain serine/threonine protein kinase activated by Cdc42 and Rac1. *Nature*, *367*(6458), 40–46. https://doi.org/10.1038/367040a0

Marcantoni, A., Raymond, E. F., Carbone, E., & Marie, H. (2014). Firing properties of entorhinal cortex neurons and early alterations in an Alzheimer's disease transgenic model. *Pflügers Archiv - European Journal of Physiology*, *466*(7), 1437–1450. https://doi.org/10.1007/s00424-013-1368-z

Marín, O. (2012). Interneuron dysfunction in psychiatric disorders. *Nature Reviews Neuroscience*, *13*(2), 107–120. https://doi.org/10.1038/nrn3155

Marín, O. (2013). Cellular and molecular mechanisms controlling the migration of neocortical interneurons. *The European Journal of Neuroscience*, *38*(1), 2019–2029. https://doi.org/10.1111/ejn.12225

Markram, H., Toledo-Rodriguez, M., Wang, Y., Gupta, A., Silberberg, G., & Wu, C. (2004). Interneurons of the neocortical inhibitory system. *Nature Reviews. Neuroscience*, *5*(10), 793–807. https://doi.org/10.1038/nrn1519

Martin Lorenzo, S., Nalesso, V., Chevalier, C., Birling, M.-C., & Herault, Y. (2021). Targeting the RHOA pathway improves learning and memory in adult Kctd13 and 16p11.2 deletion mouse models. *Molecular Autism*, *12*(1), 1. https://doi.org/10.1186/s13229-020-00405-7

Martinelli, S., Krumbach, O. H. F., Pantaleoni, F., Coppola, S., Amin, E., Pannone, L., Nouri, K., Farina, L., Dvorsky, R., Lepri, F., Buchholzer, M., Konopatzki, R., Walsh, L., Payne, K., Pierpont, M. E., Vergano, S. S., Langley, K. G., Larsen, D., Farwell, K. D., … Mirzaa, G. M. (2018). Functional Dysregulation of CDC42 Causes Diverse Developmental Phenotypes. *The American Journal of Human Genetics*, *102*(2), 309–320. https://doi.org/10.1016/j.ajhg.2017.12.015

Martinez, L. A., & Tejada-Simon, M. V. (2011). Pharmacological inactivation of the small GTPase Rac1 impairs long-term plasticity in the mouse hippocampus. *Neuropharmacology*, *61*(1–2), 305. https://doi.org/10.1016/j.neuropharm.2011.04.017

Martini, F. J., Valiente, M., López Bendito, G., Szabó, G., Moya, F., Valdeolmillos, M., & Marín, O. (2009). Biased selection of leading process branches mediates chemotaxis during tangential neuronal migration. *Development*, *136*(1), 41–50. https://doi.org/10.1242/dev.025502

Matsui, T., Amano, M., Yamamoto, T., Chihara, K., Nakafuku, M., Ito, M., Nakano, T., Okawa, K., Iwamatsu, A., & Kaibuchi, K. (1996). Rho-associated kinase, a novel serine/threonine kinase, as a putative target for small GTP binding protein Rho. *The EMBO Journal*, *15*(9), 2208–2216.

Meberg, P. J., & Bamburg, J. R. (2000). Increase in neurite outgrowth mediated by overexpression of actin depolymerizing factor. *The Journal of Neuroscience: The Official Journal of the Society for Neuroscience*, *20*(7), 2459–2469. https://doi.org/10.1523/JNEUROSCI.20-07-02459.2000

Medeiros, N. A., Burnette, D. T., & Forscher, P. (2006). Myosin II functions in actin-bundle turnover in neuronal growth cones. *Nature Cell Biology*, *8*(3), 216–226. https://doi.org/10.1038/ncb1367

Meng, J., Meng, Y., Hanna, A., Janus, C., & Jia, Z. (2005). Abnormal long-lasting synaptic plasticity and cognition in mice lacking the mental retardation gene Pak3. *The Journal of Neuroscience: The Official Journal of the Society for Neuroscience*, *25*(28), 6641–6650. https://doi.org/10.1523/JNEUROSCI.0028-05.2005

Meseke, M., Rosenberger, G., & Förster, E. (2013). Reelin and the Cdc42/Rac1 guanine nucleotide exchange factor αPIX/Arhgef6 promote dendritic Golgi translocation in hippocampal neurons. *The European Journal of Neuroscience*, *37*(9), 1404–1412. https://doi.org/10.1111/ejn.12153

Métin, C., Baudoin, J.-P., Rakić, S., & Parnavelas, J. G. (2006). Cell and molecular mechanisms involved in the migration of cortical interneurons. *European Journal of Neuroscience*, *23*(4), 894–900. https://doi.org/10.1111/j.1460-9568.2006.04630.x

Michiels, F., Habets, G. G. M., Stam, J. C., van der Kammen, R. A., & Collard, J. G. (1995). A role for Rac in Tiaml-induced membrane ruffling and invasion. *Nature*, *375*(6529), 338–340. https://doi.org/10.1038/375338a0

Miki, H., Suetsugu, S., & Takenawa, T. (1998). WAVE, a novel WASP-family protein involved in actin reorganization induced by Rac. *The EMBO Journal*, *17*(23), 6932–6941. https://doi.org/10.1093/emboj/17.23.6932

Miyamoto, Y., Yamauchi, J., Tanoue, A., Wu, C., & Mobley, W. C. (2006). TrkB binds and tyrosine-phosphorylates Tiam1, leading to activation of Rac1 and induction of changes in cellular morphology. *Proceedings of the National Academy of Sciences of the United States of America*, *103*(27), 10444–10449. https://doi.org/10.1073/pnas.0603914103

Moncini, S., Castronovo, P., Murgia, A., Russo, S., Bedeschi, M. F., Lunghi, M., Selicorni, A., Bonati, M. T., Riva, P., & Venturin, M. (2016). Functional characterization of CDK5 and CDK5R1 mutations identified in patients with non-syndromic intellectual disability. *Journal of Human Genetics*, *61*(4), 283–293. https://doi.org/10.1038/jhg.2015.144

Motokawa, M., Watanabe, S., Nakatomi, A., Kondoh, T., Matsumoto, T., Morifuji, K., Sawada, H., Nishimura, T., Nunoi, H., Yoshiura, K.-I., Moriuchi, H., & Dateki, S. (2018). A hot-spot mutation in CDC42 (p.Tyr64Cys) and novel

phenotypes in the third patient with Takenouchi-Kosaki syndrome. *Journal of Human Genetics*, *63*(3), 387–390. https://doi.org/10.1038/s10038-017-0396-5

Mulatinho, M. V., de Carvalho Serao, C. L., Scalco, F., Hardekopf, D., Pekova, S., Mrasek, K., Liehr, T., Weise, A., Rao, N., & Llerena, J. C. (2012). Severe intellectual disability, omphalocele, hypospadia and high blood pressure associated to a deletion at 2q22.1q22.3: Case report. *Molecular Cytogenetics*, *5*(1), 30. https://doi.org/10.1186/1755-8166-5-30

Murakoshi, H., Wang, H., & Yasuda, R. (2011). Local, persistent activation of Rho GTPases during plasticity of single dendritic spines. *Nature*, *472*(7341), 100–104. https://doi.org/10.1038/nature09823

Nadarajah, B., Brunstrom, J. E., Grutzendler, J., Wong, R. O., & Pearlman, A. L. (2001). Two modes of radial migration in early development of the cerebral cortex. *Nature Neuroscience*, *4*(2), 143–150. https://doi.org/10.1038/83967

Nakagawa, O., Fujisawa, K., Ishizaki, T., Saito, Y., Nakao, K., & Narumiya, S. (1996). ROCK-I and ROCK-II, two isoforms of Rho-associated coiled-coil forming protein serine/threonine kinase in mice. *FEBS Letters*, *392*(2), 189–193. https://doi.org/10.1016/0014-5793(96)00811-3

Nery, S., Fishell, G., & Corbin, J. G. (2002). The caudal ganglionic eminence is a source of distinct cortical and subcortical cell populations. *Nature Neuroscience*, *5*(12), 1279–1287. https://doi.org/10.1038/nn971

Niwa, R., Nagata-Ohashi, K., Takeichi, M., Mizuno, K., & Uemura, T. (2002). Control of Actin Reorganization by Slingshot, a Family of Phosphatases that Dephosphorylate ADF/Cofilin. *Cell*, *108*(2), 233–246. https://doi.org/10.1016/S0092-8674(01)00638-9

Nodé-Langlois, R., Muller, D., & Boda, B. (2006). Sequential implication of the mental retardation proteins ARHGEF6 and PAK3 in spine morphogenesis. *Journal of Cell Science*, *119*(Pt 23), 4986–4993. https://doi.org/10.1242/jcs.03273

Noren, N. K., Liu, B. P., Burridge, K., & Kreft, B. (2000). P120 Catenin Regulates the Actin Cytoskeleton via Rho Family Gtpases. *Journal of Cell Biology*, *150*(3), 567–580. https://doi.org/10.1083/jcb.150.3.567

Nuovo, S., Brankovic, V., Caputi, C., Casella, A., Nigro, V., Leuzzi, V., & Valente, E. M. (2021). Novel unconventional variants expand the allelic spectrum

of OPHN1 gene. *American Journal of Medical Genetics. Part A*, *185*(5), 1575–1581. https://doi.org/10.1002/ajmg.a.62144

O'Brien, S. P., Seipel, K., Medley, Q. G., Bronson, R., Segal, R., & Streuli, M. (2000). Skeletal muscle deformity and neuronal disorder in Trio exchange factor-deficient mouse embryos. *Proceedings of the National Academy of Sciences of the United States of America*, *97*(22), 12074–12078. https://doi.org/10.1073/pnas.97.22.12074

Oguro-Ando, A., Rosensweig, C., Herman, E., Nishimura, Y., Werling, D., Bill, B. R., Berg, J. M., Gao, F., Coppola, G., Abrahams, B. S., & Geschwind, D. H. (2015). Increased CYFIP1 dosage alters cellular and dendritic morphology and dysregulates mTOR. *Molecular Psychiatry*, *20*(9), 1069–1078. https://doi.org/10.1038/mp.2014.124

Ohashi, K., Nagata, K., Maekawa, M., Ishizaki, T., Narumiya, S., & Mizuno, K. (2000). Rho-associated kinase ROCK activates LIM-kinase 1 by phosphorylation at threonine 508 within the activation loop. *The Journal of Biological Chemistry*, *275*(5), 3577–3582. https://doi.org/10.1074/jbc.275.5.3577

Ohori, S., Mitsuhashi, S., Ben-Haim, R., Heyman, E., Sengoku, T., Ogata, K., & Matsumoto, N. (2020). A novel PAK1 variant causative of neurodevelopmental disorder with postnatal macrocephaly. *Journal of Human Genetics*, *65*(5), 481–485. https://doi.org/10.1038/s10038-020-0728-8

Okano, I., Hiraoka, J., Otera, H., Nunoue, K., Ohashi, K., Iwashita, S., Hirai, M., & Mizuno, K. (1995). Identification and characterization of a novel family of serine/threonine kinases containing two N-terminal LIM motifs. *The Journal of Biological Chemistry*, *270*(52), 31321–31330. https://doi.org/10.1074/jbc.270.52.31321

Olmos-Serrano, J. L., Paluszkiewicz, S. M., Martin, B. S., Kaufmann, W. E., Corbin, J. G., & Huntsman, M. M. (2010). Defective GABAergic neurotransmission and pharmacological rescue of neuronal hyperexcitability in the amygdala in a mouse model of fragile X syndrome. *The Journal of Neuroscience: The Official Journal of the Society for Neuroscience*, *30*(29), 9929–9938. https://doi.org/10.1523/JNEUROSCI.1714-10.2010

O'Roak, B. J., Deriziotis, P., Lee, C., Vives, L., Schwartz, J. J., Girirajan, S., Karakoc, E., MacKenzie, A. P., Ng, S. B., Baker, C., Rieder, M. J., Nickerson, D.

A., Bernier, R., Fisher, S. E., Shendure, J., & Eichler, E. E. (2011). Exome sequencing in sporadic autism spectrum disorders identifies severe de novo mutations. *Nature Genetics*, *43*(6), 585–589. https://doi.org/10.1038/ng.835

Papadopoulos, T., Korte, M., Eulenburg, V., Kubota, H., Retiounskaia, M., Harvey, R. J., Harvey, K., O'Sullivan, G. A., Laube, B., Hülsmann, S., Geiger, J. R. P., & Betz, H. (2007). Impaired GABAergic transmission and altered hippocampal synaptic plasticity in collybistin-deficient mice. *The EMBO Journal*, *26*(17), 3888–3899. https://doi.org/10.1038/sj.emboj.7601819

Park, E., Na, M., Choi, J., Kim, S., Lee, J.-R., Yoon, J., Park, D., Sheng, M., & Kim, E. (2003). The Shank family of postsynaptic density proteins interacts with and promotes synaptic accumulation of the beta PIX guanine nucleotide exchange factor for Rac1 and Cdc42. *The Journal of Biological Chemistry*, *278*(21), 19220–19229. https://doi.org/10.1074/jbc.M301052200

Paulsen, B., Velasco, S., Kedaigle, A. J., Pigoni, M., Quadrato, G., Deo, A. J., Adiconis, X., Uzquiano, A., Sartore, R., Yang, S. M., Simmons, S. K., Symvoulidis, P., Kim, K., Tsafou, K., Podury, A., Abbate, C., Tucewicz, A., Smith, S. N., Albanese, A., … Arlotta, P. (2022). Autism genes converge on asynchronous development of shared neuron classes. *Nature*, *602*(7896), 268–273. https://doi.org/10.1038/s41586-021-04358-6

Peça, J., Feliciano, C., Ting, J. T., Wang, W., Wells, M. F., Venkatraman, T. N., Lascola, C. D., Fu, Z., & Feng, G. (2011). Shank3 mutant mice display autistic-like behaviours and striatal dysfunction. *Nature*, *472*(7344), 437–442. https://doi.org/10.1038/nature09965

Peck, J., Douglas, G., Wu, C. H., & Burbelo, P. D. (2002). Human RhoGAP domain-containing proteins: Structure, function and evolutionary relationships. *FEBS Letters*, *528*(1–3), 27–34. https://doi.org/10.1016/S0014-5793(02)03331-8

Peñagarikano, O., Abrahams, B. S., Herman, E. I., Winden, K. D., Gdalyahu, A., Dong, H., Sonnenblick, L. I., Gruver, R., Almajano, J., Bragin, A., Golshani, P., Trachtenberg, J. T., Peles, E., & Geschwind, D. H. (2011). Absence of CNTNAP2 leads to epilepsy, neuronal migration abnormalities, and core autism-related deficits. *Cell*, *147*(1), 235–246. https://doi.org/10.1016/j.cell.2011.08.040

Penagarikano, O., Mulle, J. G., & Warren, S. T. (2007). The pathophysiology of fragile x syndrome. *Annual Review of Genomics and Human Genetics*, *8*, 109–129. https://doi.org/10.1146/annurev.genom.8.080706.092249

Pengelly, R. J., Greville-Heygate, S., Schmidt, S., Seaby, E. G., Jabalameli, M. R., Mehta, S. G., Parker, M. J., Goudie, D., Fagotto-Kaufmann, C., Mercer, C., DDD Study, Debant, A., Ennis, S., & Baralle, D. (2016). Mutations specific to the Rac-GEF domain of TRIO cause intellectual disability and microcephaly. *Journal of Medical Genetics*, *53*(11), 735–742. https://doi.org/10.1136/jmedgenet-2016-103942

Pennucci, R., Tavano, S., Tonoli, D., Gualdoni, S., & de Curtis, I. (2011). Rac1 and Rac3 GTPases regulate the development of hilar mossy cells by affecting the migration of their precursors to the hilus. *PloS One*, *6*(9), e24819. https://doi.org/10.1371/journal.pone.0024819

Pensold, D., Symmank, J., Hahn, A., Lingner, T., Salinas-Riester, G., Downie, B. R., Ludewig, F., Rotzsch, A., Haag, N., Andreas, N., Schubert, K., Hübner, C. A., Pieler, T., & Zimmer, G. (2017). The DNA Methyltransferase 1 (DNMT1) Controls the Shape and Dynamics of Migrating POA-Derived Interneurons Fated for the Murine Cerebral Cortex. *Cerebral Cortex*, *27*(12), 5696–5714. https://doi.org/10.1093/cercor/bhw341

Penzes, P., Buonanno, A., Passafaro, M., Sala, C., & Sweet, R. A. (2013). Developmental vulnerability of synapses and circuits associated with neuropsychiatric disorders. *Journal of Neurochemistry*, *126*(2), 165–182. https://doi.org/10.1111/jnc.12261

Pilpel, Y., & Segal, M. (2004). Activation of PKC induces rapid morphological plasticity in dendrites of hippocampal neurons via Rac and Rho-dependent mechanisms. *The European Journal of Neuroscience*, *19*(12), 3151–3164. https://doi.org/10.1111/j.0953-816X.2004.03380.x

Piton, A., Redin, C., & Mandel, J.-L. (2013). XLID-causing mutations and associated genes challenged in light of data from large-scale human exome sequencing. *American Journal of Human Genetics*, *93*(2), 368–383. https://doi.org/10.1016/j.ajhg.2013.06.013

Pizzarelli, R., Griguoli, M., Zacchi, P., Petrini, E. M., Barberis, A., Cattaneo, A., & Cherubini, E. (2020). Tuning GABAergic Inhibition: Gephyrin Molecular

Organization and Functions. *Neuroscience*, *439*, 125–136. https://doi.org/10.1016/j.neuroscience.2019.07.036

Pleasure, S. J., Anderson, S., Hevner, R., Bagri, A., Marin, O., Lowenstein, D. H., & Rubenstein, J. L. (2000). Cell migration from the ganglionic eminences is required for the development of hippocampal GABAergic interneurons. *Neuron*, *28*(3), 727–740. https://doi.org/10.1016/s0896-6273(00)00149-5

Poduri, A., & Lowenstein, D. (2011). Epilepsy genetics—Past, present, and future. *Current Opinion in Genetics & Development*, *21*(3), 325–332. https://doi.org/10.1016/j.gde.2011.01.005

Pollard, T. D. (2007). Regulation of actin filament assembly by Arp2/3 complex and formins. *Annual Review of Biophysics and Biomolecular Structure*, *36*, 451–477. https://doi.org/10.1146/annurev.biophys.35.040405.101936

Pollard, T. D. (2016). Actin and Actin-Binding Proteins. *Cold Spring Harbor Perspectives in Biology*, *8*(8), a018226. https://doi.org/10.1101/cshperspect.a018226

Pollard, T. D., & Borisy, G. G. (2003). Cellular motility driven by assembly and disassembly of actin filaments. *Cell*, *112*(4), 453–465. https://doi.org/10.1016/s0092-8674(03)00120-x

Pollard, T. D., & Cooper, J. A. (1984). Quantitative analysis of the effect of Acanthamoeba profilin on actin filament nucleation and elongation. *Biochemistry*, *23*(26), 6631–6641. https://doi.org/10.1021/bi00321a054

Polleux, F., Whitford, K. L., Dijkhuizen, P. A., Vitalis, T., & Ghosh, A. (2002). Control of cortical interneuron migration by neurotrophins and PI3-kinase signaling. *Development (Cambridge, England)*, *129*(13), 3147–3160. https://doi.org/10.1242/dev.129.13.3147

Powell, E. M., Campbell, D. B., Stanwood, G. D., Davis, C., Noebels, J. L., & Levitt, P. (2003). Genetic disruption of cortical interneuron development causes region- and GABA cell type-specific deficits, epilepsy, and behavioral dysfunction. *The Journal of Neuroscience: The Official Journal of the Society for Neuroscience*, *23*(2), 622–631. https://doi.org/10.1523/JNEUROSCI.23-02-00622.2003

Pröschel, C., Blouin, M. J., Gutowski, N. J., Ludwig, R., & Noble, M. (1995). Limk1 is predominantly expressed in neural tissues and phosphorylates serine, threonine and tyrosine residues in vitro. *Oncogene*, *11*(7), 1271–1281.

Purtell, H., Dhamne, S. C., Gurnani, S., Bainbridge, E., Modi, M. E., Lammers, S. H. T., Super, C. E., Hameed, M. Q., Johnson, E. L., Sahin, M., & Rotenberg, A. (2018). Electrographic spikes are common in wildtype mice. *Epilepsy & Behavior*, *89*, 94–98. https://doi.org/10.1016/j.yebeh.2018.09.003

Qian, Y., Wu, B., Lu, Y., Zhou, W., Wang, S., & Wang, H. (2020). Novel PAK3 gene missense variant associated with two Chinese siblings with intellectual disability: A case report. *BMC Medical Genetics*, *21*(1), 31. https://doi.org/10.1186/s12881-020-0957-x

Racine, R. J. (1972). Modification of seizure activity by electrical stimulation: I. after-discharge threshold. *Electroencephalography and Clinical Neurophysiology*, *32*(3), 269–279. https://doi.org/10.1016/0013-4694(72)90176-9

Radu, M., Rawat, S. J., Beeser, A., Iliuk, A., Tao, W. A., & Chernoff, J. (2013). ArhGAP15, a Rac-specific GTPase-activating Protein, Plays a Dual Role in Inhibiting Small GTPase Signaling*. *Journal of Biological Chemistry*, *288*(29), 21117–21125. https://doi.org/10.1074/jbc.M113.459719

Radyushkin, K., Hammerschmidt, K., Boretius, S., Varoqueaux, F., El-Kordi, A., Ronnenberg, A., Winter, D., Frahm, J., Fischer, J., Brose, N., & Ehrenreich, H. (2009). Neuroligin-3-deficient mice: Model of a monogenic heritable form of autism with an olfactory deficit. *Genes, Brain, and Behavior*, *8*(4), 416–425. https://doi.org/10.1111/j.1601-183X.2009.00487.x

Ramakers, G. J. A., Wolfer, D., Rosenberger, G., Kuchenbecker, K., Kreienkamp, H.-J., Prange-Kiel, J., Rune, G., Richter, K., Langnaese, K., Masneuf, S., Bösl, M. R., Fischer, K.-D., Krugers, H. J., Lipp, H.-P., van Galen, E., & Kutsche, K. (2012). Dysregulation of Rho GTPases in the αPix/Arhgef6 mouse model of X-linked intellectual disability is paralleled by impaired structural and synaptic plasticity and cognitive deficits. *Human Molecular Genetics*, *21*(2), 268–286. https://doi.org/10.1093/hmg/ddr457

Rao, S., Kay, Y., & Herring, B. E. (2019). Tiam1 is Critical for Glutamatergic Synapse Structure and Function in the Hippocampus. *The Journal of Neuroscience:*

The Official Journal of the Society for Neuroscience, *39*(47), 9306–9315. https://doi.org/10.1523/JNEUROSCI.1566-19.2019

Reijnders, M. R. F., Ansor, N. M., Kousi, M., Yue, W. W., Tan, P. L., Clarkson, K., Clayton-Smith, J., Corning, K., Jones, J. R., Lam, W. W. K., Mancini, G. M. S., Marcelis, C., Mohammed, S., Pfundt, R., Roifman, M., Cohn, R., Chitayat, D., Deciphering Developmental Disorders Study, Millard, T. H., … Banka, S. (2017). RAC1 Missense Mutations in Developmental Disorders with Diverse Phenotypes. *American Journal of Human Genetics*, *101*(3), 466–477. https://doi.org/10.1016/j.ajhg.2017.08.007

Renaud, J., & Chédotal, A. (2014). Time-lapse analysis of tangential migration in Sema6A and PlexinA2 knockouts. *Molecular and Cellular Neurosciences*, *63*, 49–59. https://doi.org/10.1016/j.mcn.2014.09.005

Repetto, D., Camera, P., Melani, R., Morello, N., Russo, I., Calcagno, E., Tomasoni, R., Bianchi, F., Berto, G., Giustetto, M., Berardi, N., Pizzorusso, T., Matteoli, M., Di Stefano, P., Missler, M., Turco, E., Di Cunto, F., & Defilippi, P. (2014). p140Cap regulates memory and synaptic plasticity through Src-mediated and citron-N-mediated actin reorganization. *The Journal of Neuroscience: The Official Journal of the Society for Neuroscience*, *34*(4), 1542–1553. https://doi.org/10.1523/JNEUROSCI.2341-13.2014

Ropers, F., Derivery, E., Hu, H., Garshasbi, M., Karbasiyan, M., Herold, M., Nürnberg, G., Ullmann, R., Gautreau, A., Sperling, K., Varon, R., & Rajab, A. (2011). Identification of a novel candidate gene for non-syndromic autosomal recessive intellectual disability: The WASH complex member SWIP. *Human Molecular Genetics*, *20*(13), 2585–2590. https://doi.org/10.1093/hmg/ddr158

Rosário, M., Franke, R., Bednarski, C., & Birchmeier, W. (2007). The neurite outgrowth multiadaptor RhoGAP, NOMA-GAP, regulates neurite extension through SHP2 and Cdc42. *The Journal of Cell Biology*, *178*(3), 503–516. https://doi.org/10.1083/jcb.200609146

Rosário, M., Schuster, S., Jüttner, R., Parthasarathy, S., Tarabykin, V., & Birchmeier, W. (2012). Neocortical dendritic complexity is controlled during development by NOMA-GAP-dependent inhibition of Cdc42 and activation of cofilin. *Genes & Development*, *26*(15), 1743–1757. https://doi.org/10.1101/gad.191593.112

Rossignol, E. (2011). Genetics and Function of Neocortical GABAergic Interneurons in Neurodevelopmental Disorders. *Neural Plasticity*, *2011*(1), 649325. https://doi.org/10.1155/2011/649325

Rotty, J. D., Wu, C., & Bear, J. E. (2013). New insights into the regulation and cellular functions of the ARP2/3 complex. *Nature Reviews Molecular Cell Biology*, *14*(1), 7–12. https://doi.org/10.1038/nrm3492

Sahasrabudhe, A., Ghate, K., Mutalik, S., Jacob, A., & Ghose, A. (2016). Formin 2 regulates the stabilization of filopodial tip adhesions in growth cones and affects neuronal outgrowth and pathfinding in vivo. *Development (Cambridge, England)*, *143*(3), 449–460. https://doi.org/10.1242/dev.130104

Sakai, K., & Miyazaki, J. (1997). A Transgenic Mouse Line That Retains Cre Recombinase Activity in Mature Oocytes Irrespective of the*cre*Transgene Transmission. *Biochemical and Biophysical Research Communications*, *237*(2), 318–324. https://doi.org/10.1006/bbrc.1997.7111

Sala, C., Piëch, V., Wilson, N. R., Passafaro, M., Liu, G., & Sheng, M. (2001). Regulation of dendritic spine morphology and synaptic function by Shank and Homer. *Neuron*, *31*(1), 115–130. https://doi.org/10.1016/s0896-6273(01)00339-7

Samaco, R. C., Mandel-Brehm, C., Chao, H.-T., Ward, C. S., Fyffe-Maricich, S. L., Ren, J., Hyland, K., Thaller, C., Maricich, S. M., Humphreys, P., Greer, J. J., Percy, A., Glaze, D. G., Zoghbi, H. Y., & Neul, J. L. (2009). Loss of MeCP2 in aminergic neurons causes cell-autonomous defects in neurotransmitter synthesis and specific behavioral abnormalities. *Proceedings of the National Academy of Sciences of the United States of America*, *106*(51), 21966–21971. https://doi.org/10.1073/pnas.0912257106

Sanacora, G., Mason, G. F., & Krystal, J. H. (2000). Impairment of GABAergic Transmission in Depression: New Insights from Neuroimaging Studies. *Critical Reviews™ in Neurobiology*, *14*(1). https://doi.org/10.1615/CritRevNeurobiol.v14.i1.20

Sanders, L. C., Matsumura, F., Bokoch, G. M., & de Lanerolle, P. (1999). Inhibition of myosin light chain kinase by p21-activated kinase. *Science (New York, N.Y.)*, *283*(5410), 2083–2085. https://doi.org/10.1126/science.283.5410.2083

Saneyoshi, T., Matsuno, H., Suzuki, A., Murakoshi, H., Hedrick, N. G., Agnello, E., O'Connell, R., Stratton, M. M., Yasuda, R., & Hayashi, Y. (2019). Reciprocal Activation within a Kinase-Effector Complex Underlying Persistence of Structural LTP. *Neuron*, *102*(6), 1199-1210.e6. https://doi.org/10.1016/j.neuron.2019.04.012

Santiago-Medina, M., Gregus, K. A., & Gomez, T. M. (2013). PAK-PIX interactions regulate adhesion dynamics and membrane protrusion to control neurite outgrowth. *Journal of Cell Science*, *126*(Pt 5), 1122–1133. https://doi.org/10.1242/jcs.112607

Sayyad, W. A., Fabris, P., & Torre, V. (2016). The Role of Rac1 in the Growth Cone Dynamics and Force Generation of DRG Neurons. *PLOS ONE*, *11*(1), e0146842. https://doi.org/10.1371/journal.pone.0146842

Schaks, M., Reinke, M., Witke, W., & Rottner, K. (2020). Molecular Dissection of Neurodevelopmental Disorder-Causing Mutations in CYFIP2. *Cells*, *9*(6), 1355. https://doi.org/10.3390/cells9061355

Schlau, M., Terheyden-Keighley, D., Theis, V., Mannherz, H. G., & Theiss, C. (2018). VEGF Triggers the Activation of Cofilin and the Arp2/3 Complex within the Growth Cone. *International Journal of Molecular Sciences*, *19*(2), Article 2. https://doi.org/10.3390/ijms19020384

Schmidt, S., & Debant, A. (2014). Function and regulation of the Rho guanine nucleotide exchange factor Trio. *Small GTPases*, *5*, e29769. https://doi.org/10.4161/sgtp.29769

Selby, L., Zhang, C., & Sun, Q.-Q. (2007). Major defects in neocortical GABAergic inhibitory circuits in mice lacking the fragile X mental retardation protein. *Neuroscience Letters*, *412*(3), 227–232. https://doi.org/10.1016/j.neulet.2006.11.062

Seoh, M. L., Ng, C. H., Yong, J., Lim, L., & Leung, T. (2003). ArhGAP15, a novel human RacGAP protein with GTPase binding property. *FEBS Letters*, *539*(1–3), 131–137. https://doi.org/10.1016/S0014-5793(03)00213-8

Sessolo, M., Marcon, I., Bovetti, S., Losi, G., Cammarota, M., Ratto, G. M., Fellin, T., & Carmignoto, G. (2015). Parvalbumin-Positive Inhibitory Interneurons Oppose Propagation But Favor Generation of Focal Epileptiform Activity. *Journal*

of Neuroscience, *35*(26), 9544–9557. https://doi.org/10.1523/JNEUROSCI.5117-14.2015

Shao, L.-R., Habela, C. W., & Stafstrom, C. E. (2019). Pediatric Epilepsy Mechanisms: Expanding the Paradigm of Excitation/Inhibition Imbalance. *Children*, *6*(2), Article 2. https://doi.org/10.3390/children6020023

Shimada, T., Toriyama, M., Uemura, K., Kamiguchi, H., Sugiura, T., Watanabe, N., & Inagaki, N. (2008). Shootin1 interacts with actin retrograde flow and L1-CAM to promote axon outgrowth. *Journal of Cell Biology*, *181*(5), 817–829. https://doi.org/10.1083/jcb.200712138

Silva, C. G., Peyre, E., & Nguyen, L. (2019). Cell migration promotes dynamic cellular interactions to control cerebral cortex morphogenesis. *Nature Reviews. Neuroscience*, *20*(6), 318–329. https://doi.org/10.1038/s41583-019-0148-y

Sloan, S. A., Andersen, J., Paşca, A. M., Birey, F., & Paşca, S. P. (2018). Generation and assembly of human brain region–specific three-dimensional cultures. *Nature Protocols*, *13*(9), 2062–2085. https://doi.org/10.1038/s41596-018-0032-7

Smigiel, R., Szafranska, A., Czyzewska, M., Rauch, A., Zweier, C., & Patkowski, D. (2010). Severe clinical course of Hirschsprung disease in a Mowat-Wilson syndrome patient. *Journal of Applied Genetics*, *51*(1), 111–113. https://doi.org/10.1007/BF03195718

Smith, C. L. (1994). Cytoskeletal movements and substrate interactions during initiation of neurite outgrowth by sympathetic neurons in vitro. *The Journal of Neuroscience: The Official Journal of the Society for Neuroscience*, *14*(1), 384–398. https://doi.org/10.1523/JNEUROSCI.14-01-00384.1994

Soosairajah, J., Maiti, S., Wiggan, O., Sarmiere, P., Moussi, N., Sarcevic, B., Sampath, R., Bamburg, J. R., & Bernard, O. (2005). Interplay between components of a novel LIM kinase–slingshot phosphatase complex regulates cofilin. *The EMBO Journal*, *24*(3), 473–486. https://doi.org/10.1038/sj.emboj.7600543

Spence, E. F., Kanak, D. J., Carlson, B. R., & Soderling, S. H. (2016). The Arp2/3 Complex Is Essential for Distinct Stages of Spine Synapse Maturation, Including Synapse Unsilencing. *The Journal of Neuroscience: The Official Journal*

of the Society for Neuroscience, *36*(37), 9696–9709. https://doi.org/10.1523/JNEUROSCI.0876-16.2016

Spence, E. F., & Soderling, S. H. (2015). Actin Out: Regulation of the Synaptic Cytoskeleton. *The Journal of Biological Chemistry*, *290*(48), 28613–28622. https://doi.org/10.1074/jbc.R115.655118

Südhof, T. C. (2018). Towards an Understanding of Synapse Formation. *Neuron*, *100*(2), 276–293. https://doi.org/10.1016/j.neuron.2018.09.040

Sultan, K. T., Brown, K. N., & Shi, S.-H. (2013). Production and organization of neocortical interneurons. *Frontiers in Cellular Neuroscience*, *7*, 221. https://doi.org/10.3389/fncel.2013.00221

Sumi, T., Matsumoto, K., Takai, Y., & Nakamura, T. (1999). Cofilin phosphorylation and actin cytoskeletal dynamics regulated by rho- and Cdc42-activated LIM-kinase 2. *The Journal of Cell Biology*, *147*(7), 1519–1532. https://doi.org/10.1083/jcb.147.7.1519

Sun, X., Wang, L., Wei, C., Sun, M., Li, Q., Meng, H., Yue, W., Zhang, D., & Li, J. (2021). Dysfunction of Trio GEF1 involves in excitatory/inhibitory imbalance and autism-like behaviors through regulation of interneuron migration. *Molecular Psychiatry*, *26*(12), 7621–7640. https://doi.org/10.1038/s41380-021-01109-x

Svitkina, T. M., & Borisy, G. G. (1999). Arp2/3 Complex and Actin Depolymerizing Factor/Cofilin in Dendritic Organization and Treadmilling of Actin Filament Array in Lamellipodia. *Journal of Cell Biology*, *145*(5), 1009–1026. https://doi.org/10.1083/jcb.145.5.1009

Tahirovic, S., Hellal, F., Neukirchen, D., Hindges, R., Garvalov, B. K., Flynn, K. C., Stradal, T. E., Chrostek-Grashoff, A., Brakebusch, C., & Bradke, F. (2010). Rac1 Regulates Neuronal Polarization through the WAVE Complex. *Journal of Neuroscience*, *30*(20), 6930–6943. https://doi.org/10.1523/JNEUROSCI.5395-09.2010

Tai, C., Abe, Y., Westenbroek, R. E., Scheuer, T., & Catterall, W. A. (2014). Impaired excitability of somatostatin- and parvalbumin-expressing cortical interneurons in a mouse model of Dravet syndrome. *Proceedings of the National Academy of Sciences*, *111*(30), E3139–E3148. https://doi.org/10.1073/pnas.1411131111

Takenouchi, T., Okamoto, N., Ida, S., Uehara, T., & Kosaki, K. (2016). Further evidence of a mutation in CDC42 as a cause of a recognizable syndromic form of thrombocytopenia. *American Journal of Medical Genetics. Part A*, *170A*(4), 852–855. https://doi.org/10.1002/ajmg.a.37526

Tallent, M. K., & Siggins, G. R. (1999). Somatostatin Acts in CA1 and CA3 to Reduce Hippocampal Epileptiform Activity. *Journal of Neurophysiology*. https://doi.org/10.1152/jn.1999.81.4.1626

Tamamaki, N., Fujimori, K. E., & Takauji, R. (1997). Origin and route of tangentially migrating neurons in the developing neocortical intermediate zone. *The Journal of Neuroscience: The Official Journal of the Society for Neuroscience*, *17*(21), 8313–8323. https://doi.org/10.1523/JNEUROSCI.17-21-08313.1997

Tamamaki, N., Yanagawa, Y., Tomioka, R., Miyazaki, J.-I., Obata, K., & Kaneko, T. (2003). Green fluorescent protein expression and colocalization with calretinin, parvalbumin, and somatostatin in the GAD67-GFP knock-in mouse. *Journal of Comparative Neurology*, *467*(1), 60–79. https://doi.org/10.1002/cne.10905

Tan, H. O., Reid, C. A., Single, F. N., Davies, P. J., Chiu, C., Murphy, S., Clarke, A. L., Dibbens, L., Krestel, H., Mulley, J. C., Jones, M. V., Seeburg, P. H., Sakmann, B., Berkovic, S. F., Sprengel, R., & Petrou, S. (2007). Reduced cortical inhibition in a mouse model of familial childhood absence epilepsy. *Proceedings of the National Academy of Sciences*, *104*(44), 17536–17541. https://doi.org/10.1073/pnas.0708440104

Tanaka, D. H., & Nakajima, K. (2012). Migratory pathways of GABAergic interneurons when they enter the neocortex. *The European Journal of Neuroscience*, *35*(11), 1655–1660. https://doi.org/10.1111/j.1460-9568.2012.08111.x

Tanaka, D. H., Oiwa, R., Sasaki, E., & Nakajima, K. (2011). Changes in cortical interneuron migration contribute to the evolution of the neocortex. *Proceedings of the National Academy of Sciences of the United States of America*, *108*(19), 8015–8020. https://doi.org/10.1073/pnas.1102153108

Tanaka, E., & Sabry, J. (1995). Making the connection: Cytoskeletal rearrangements during growth cone guidance. *Cell*, *83*(2), 171–176. https://doi.org/10.1016/0092-8674(95)90158-2

Tang, D., Yeung, J., Lee, K. Y., Matsushita, M., Matsui, H., Tomizawa, K., Hatase, O., & Wang, J. H. (1995). An isoform of the neuronal cyclin-dependent kinase 5 (Cdk5) activator. *The Journal of Biological Chemistry*, *270*(45), 26897–26903. https://doi.org/10.1074/jbc.270.45.26897

Taniuchi, K., Nakagawa, H., Hosokawa, M., Nakamura, T., Eguchi, H., Ohigashi, H., Ishikawa, O., Katagiri, T., & Nakamura, Y. (2005). Overexpressed P-Cadherin/CDH3 Promotes Motility of Pancreatic Cancer Cells by Interacting with p120ctn and Activating Rho-Family GTPases. *Cancer Research*, *65*(8), 3092–3099. https://doi.org/10.1158/0008.5472.CAN-04-3646

Tashiro, A., Minden, A., & Yuste, R. (2000). Regulation of dendritic spine morphology by the rho family of small GTPases: Antagonistic roles of Rac and Rho. *Cerebral Cortex (New York, N.Y.: 1991)*, *10*(10), 927–938. https://doi.org/10.1093/cercor/10.10.927

Tastet, J., Vourc'h, P., Laumonnier, F., Vallée, B., Michelle, C., Duittoz, A., Bénédetti, H., & Andres, C. R. (2012). LIMK2d, a truncated isoform of Lim kinase 2 regulates neurite growth in absence of the LIM kinase domain. *Biochemical and Biophysical Research Communications*, *420*(2), 247–252. https://doi.org/10.1016/j.bbrc.2012.02.134

Tcherkezian, J., & Lamarche-Vane, N. (2007). Current knowledge of the large RhoGAP family of proteins. *Biology of the Cell*, *99*(2), 67–86. https://doi.org/10.1042/BC20060086

ten Klooster, J. P., Jaffer, Z. M., Chernoff, J., & Hordijk, P. L. (2006). Targeting and activation of Rac1 are mediated by the exchange factor beta-Pix. *The Journal of Cell Biology*, *172*(5), 759–769. https://doi.org/10.1083/jcb.200509096

Tian, C., Kay, Y., Sadybekov, A., Rao, S., Katritch, V., & Herring, B. E. (2018). An Intellectual Disability-Related Missense Mutation in Rac1 Prevents LTP Induction. *Frontiers in Molecular Neuroscience*, *11*, 223. https://doi.org/10.3389/fnmol.2018.00223

Tivodar, S., Kalemaki, K., Kounoupa, Z., Vidaki, M., Theodorakis, K., Denaxa, M., Kessaris, N., de Curtis, I., Pachnis, V., & Karagogeos, D. (2015). Rac-GTPases Regulate Microtubule Stability and Axon Growth of Cortical GABAergic Interneurons. *Cerebral Cortex (New York, N.Y.: 1991)*, *25*(9), 2370–2382. https://doi.org/10.1093/cercor/bhu037

Tobacman, L. S., & Korn, E. D. (1982). The regulation of actin polymerization and the inhibition of monomeric actin ATPase activity by Acanthamoeba profilin. *Journal of Biological Chemistry*, *257*(8), 4166–4170. https://doi.org/10.1016/S0021-9258(18)34701-X

Tolias, K. F., Bikoff, J. B., Kane, C. G., Tolias, C. S., Hu, L., & Greenberg, M. E. (2007). The Rac1 guanine nucleotide exchange factor Tiam1 mediates EphB receptor-dependent dendritic spine development. *Proceedings of the National Academy of Sciences of the United States of America*, *104*(17), 7265–7270. https://doi.org/10.1073/pnas.0702044104

Tomasevic, N., Jia, Z., Russell, A., Fujii, T., Hartman, J. J., Clancy, S., Wang, M., Beraud, C., Wood, K. W., & Sakowicz, R. (2007). Differential Regulation of WASP and N-WASP by Cdc42, Rac1, Nck, and PI(4,5)P2. *Biochemistry*, *46*(11), 3494–3502. https://doi.org/10.1021/bi062152y

Toriyama, M., Kozawa, S., Sakumura, Y., & Inagaki, N. (2013). Conversion of a Signal into Forces for Axon Outgrowth through Pak1-Mediated Shootin1 Phosphorylation. *Current Biology*, *23*(6), 529–534. https://doi.org/10.1016/j.cub.2013.02.017

Tóth, K., & Maglóczky, Z. (2014). The vulnerability of calretinin-containing hippocampal interneurons to temporal lobe epilepsy. *Frontiers in Neuroanatomy*, *8*. https://doi.org/10.3389/fnana.2014.00100

Toyo-oka, K., Wachi, T., Hunt, R. F., Baraban, S. C., Taya, S., Ramshaw, H., Kaibuchi, K., Schwarz, Q. P., Lopez, A. F., & Wynshaw-Boris, A. (2014). 14-3-3ε and ζ Regulate Neurogenesis and Differentiation of Neuronal Progenitor Cells in the Developing Brain. *Journal of Neuroscience*, *34*(36), 12168–12181. https://doi.org/10.1523/JNEUROSCI.2513-13.2014

Tsai, L. H., Delalle, I., Caviness, V. S., Chae, T., & Harlow, E. (1994). P35 is a neural-specific regulatory subunit of cyclin-dependent kinase 5. *Nature*, *371*(6496), 419–423. https://doi.org/10.1038/371419a0

Tyagarajan, S. K., Ghosh, H., Harvey, K., & Fritschy, J.-M. (2011). Collybistin splice variants differentially interact with gephyrin and Cdc42 to regulate gephyrin clustering at GABAergic synapses. *Journal of Cell Science*, *124*(Pt 16), 2786–2796. https://doi.org/10.1242/jcs.086199

Vadlamudi, R. K., Li, F., Barnes, C. J., Bagheri-Yarmand, R., & Kumar, R. (2004). P41-Arc subunit of human Arp2/3 complex is a p21-activated kinase-1-interacting substrate. *EMBO Reports*, *5*(2), 154–160. https://doi.org/10.1038/sj.embor.7400079

Vaghi, V., Pennucci, R., Talpo, F., Corbetta, S., Montinaro, V., Barone, C., Croci, L., Spaiardi, P., Consalez, G. G., Biella, G., & Curtis, I. de. (2012). Rac1 and Rac3 GTPases Control Synergistically the Development of Cortical and Hippocampal GABAergic Interneurons. *Cerebral Cortex (New York, NY)*, *24*(5), 1247. https://doi.org/10.1093/cercor/bhs402

Vezzani, A., Serafini, R., Stasi, M. A., Viganò, G., Rizzi, M., & Samanin, R. (1991). A peptidase-resistant cyclic octapeptide analogue of somatostatin (SMS 201–995) modulates seizures induced by quinolinic and kainic acids differently in the rat hippocampus. *Neuropharmacology*, *30*(4), 345–352. https://doi.org/10.1016/0028-3908(91)90059-K

Vidaki, M., Tivodar, S., Doulgeraki, K., Tybulewicz, V., Kessaris, N., Pachnis, V., & Karagogeos, D. (2012). Rac1-Dependent Cell Cycle Exit of MGE Precursors and GABAergic Interneuron Migration to the Cortex. *Cerebral Cortex*, *22*(3), 680–692. https://doi.org/10.1093/cercor/bhr145

Vitriol, E. A., & Zheng, J. Q. (2012). Growth cone travel in space and time: The cellular ensemble of cytoskeleton, adhesion, and membrane. *Neuron*, *73*(6), 1068–1081. https://doi.org/10.1016/j.neuron.2012.03.005

Wang, J. Y., Wigston, D. J., Rees, H. D., Levey, A. I., & Falls, D. L. (2000). LIM kinase 1 accumulates in presynaptic terminals during synapse maturation. *The Journal of Comparative Neurology*, *416*(3), 319–334. https://doi.org/10.1002/(sici)1096-9861(20000117)416:3<319::aid-cne4>3.0.co;2-q

Wang, J.-Y., Zhou, P., Wang, J., Tang, B., Su, T., Liu, X.-R., Li, B.-M., Meng, H., Shi, Y.-W., Yi, Y.-H., He, N., & Liao, W.-P. (2018). ARHGEF9 mutations in epileptic encephalopathy/intellectual disability: Toward understanding the mechanism underlying phenotypic variation. *Neurogenetics*, *19*(1), 9–16. https://doi.org/10.1007/s10048-017-0528-2

Wang, T., Guo, H., Xiong, B., Stessman, H. A. F., Wu, H., Coe, B. P., Turner, T. N., Liu, Y., Zhao, W., Hoekzema, K., Vives, L., Xia, L., Tang, M., Ou, J., Chen,

B., Shen, Y., Xun, G., Long, M., Lin, J., … Eichler, E. E. (2016). De novo genic mutations among a Chinese autism spectrum disorder cohort. *Nature Communications*, *7*(1), 13316. https://doi.org/10.1038/ncomms13316

Watabe-Uchida, M., Govek, E.-E., & Aelst, L. V. (2006). Regulators of Rho GTPases in Neuronal Development. *Journal of Neuroscience*, *26*(42), 10633–10635. https://doi.org/10.1523/JNEUROSCI.4084-06.2006

Wichterle, H., Turnbull, D. H., Nery, S., Fishell, G., & Alvarez-Buylla, A. (2001). In utero fate mapping reveals distinct migratory pathways and fates of neurons born in the mammalian basal forebrain. *Development (Cambridge, England)*, *128*(19), 3759–3771. https://doi.org/10.1242/dev.128.19.3759

Williams, R. H., & Riedemann, T. (2021). Development, Diversity, and Death of MGE-Derived Cortical Interneurons. *International Journal of Molecular Sciences*, *22*(17), 9297. https://doi.org/10.3390/ijms22179297

Winder, S. J., & Ayscough, K. R. (2005). Actin-binding proteins. *Journal of Cell Science*, *118*(4), 651–654. https://doi.org/10.1242/jcs.01670

Wong, K., Ren, X. R., Huang, Y. Z., Xie, Y., Liu, G., Saito, H., Tang, H., Wen, L., Brady-Kalnay, S. M., Mei, L., Wu, J. Y., Xiong, W. C., & Rao, Y. (2001). Signal transduction in neuronal migration: Roles of GTPase activating proteins and the small GTPase Cdc42 in the Slit-Robo pathway. *Cell*, *107*(2), 209–221. https://doi.org/10.1016/s0092-8674(01)00530-x

Woo, S., & Gomez, T. M. (2006). Rac1 and RhoA promote neurite outgrowth through formation and stabilization of growth cone point contacts. *The Journal of Neuroscience: The Official Journal of the Society for Neuroscience*, *26*(5), 1418–1428. https://doi.org/10.1523/JNEUROSCI.4209-05.2006

Woo, T. U., Whitehead, R. E., Melchitzky, D. S., & Lewis, D. A. (1998). A subclass of prefrontal gamma-aminobutyric acid axon terminals are selectively altered in schizophrenia. *Proceedings of the National Academy of Sciences of the United States of America*, *95*(9), 5341–5346. https://doi.org/10.1073/pnas.95.9.5341

Xin, X., Wang, Y., Ma, X., Rompolas, P., Keutmann, H. T., Mains, R. E., & Eipper, B. A. (2008). Regulation of Kalirin by Cdk5. *Journal of Cell Science*, *121*(Pt 15), 2601. https://doi.org/10.1242/jcs.016089

Xu, X., Jaehne, E. J., Greenberg, Z., McCarthy, P., Saleh, E., Parish, C. L., Camera, D., Heng, J., Haas, M., Baune, B. T., Ratnayake, U., van den Buuse, M., Lopez, A. F., Ramshaw, H. S., & Schwarz, Q. (2015). 14-3-3ζ deficient mice in the BALB/c background display behavioural and anatomical defects associated with neurodevelopmental disorders. *Scientific Reports*, *5*, 12434. https://doi.org/10.1038/srep12434

Yamada, M. K., Nakanishi, K., Ohba, S., Nakamura, T., Ikegaya, Y., Nishiyama, N., & Matsuki, N. (2002). Brain-derived neurotrophic factor promotes the maturation of GABAergic mechanisms in cultured hippocampal neurons. *The Journal of Neuroscience: The Official Journal of the Society for Neuroscience*, *22*(17), 7580–7585. https://doi.org/10.1523/JNEUROSCI.22-17-07580.2002

Yamaguchi, Y., Katoh, H., Yasui, H., Mori, K., & Negishi, M. (2001). RhoA inhibits the nerve growth factor-induced Rac1 activation through Rho-associated kinase-dependent pathway. *The Journal of Biological Chemistry*, *276*(22), 18977–18983. https://doi.org/10.1074/jbc.M100254200

Yang, N., Higuchi, O., Ohashi, K., Nagata, K., Wada, A., Kangawa, K., Nishida, E., & Mizuno, K. (1998). Cofilin phosphorylation by LIM-kinase 1 and its role in Rac-mediated actin reorganization. *Nature*, *393*(6687), 809–812. https://doi.org/10.1038/31735

Yang, T., Sun, Y., Zhang, F., Zhu, Y., Shi, L., Li, H., & Xu, Z. (2012). POSH localizes activated Rac1 to control the formation of cytoplasmic dilation of the leading process and neuronal migration. *Cell Reports*, *2*(3), 640–651. https://doi.org/10.1016/j.celrep.2012.08.007

Yao, R., Zhang, Y., Liu, J., Wang, J., Xu, Y., Li, N., Wang, J., & Yu, T. (2020). Clinical and Molecular Characterization of Three Novel ARHGEF9 Mutations in Patients with Developmental Delay and Epilepsy. *Journal of Molecular Neuroscience: MN*, *70*(6), 908–915. https://doi.org/10.1007/s12031-019-01465-y

Yao, Z., Liu, H., Xie, F., Fischer, S., Adkins, R. S., Aldridge, A. I., Ament, S. A., Bartlett, A., Behrens, M. M., Van den Berge, K., Bertagnolli, D., de Bézieux, H. R., Biancalani, T., Booeshaghi, A. S., Bravo, H. C., Casper, T., Colantuoni, C., Crabtree, J., Creasy, H., … Mukamel, E. A. (2021). A transcriptomic and epigenomic cell atlas of the mouse primary motor cortex. *Nature*, *598*(7879), 103–110. https://doi.org/10.1038/s41586-021-03500-8

Yntema, H. G., Hamel, B. C., Smits, A. P., van Roosmalen, T., van den Helm, B., Kremer, H., Ropers, H. H., Smeets, D. F., & van Bokhoven, H. (1998). Localisation of a gene for non-specific X linked mental retardation (MRX46) to Xq25-q26. *Journal of Medical Genetics*, *35*(10), 801–805. https://doi.org/10.1136/jmg.35.10.801

Yoshihara, Y., De Roo, M., & Muller, D. (2009a). Dendritic spine formation and stabilization. *Current Opinion in Neurobiology*, *19*(2), 146–153. https://doi.org/10.1016/j.conb.2009.05.013

Yoshihara, Y., De Roo, M., & Muller, D. (2009b). Dendritic spine formation and stabilization. *Current Opinion in Neurobiology*, *19*(2), 146–153. https://doi.org/10.1016/j.conb.2009.05.013

Yusifov, R., Tippmann, A., Staiger, J. F., Schlüter, O. M., & Löwel, S. (2021). Spine dynamics of PSD-95-deficient neurons in the visual cortex link silent synapses to structural cortical plasticity. *Proceedings of the National Academy of Sciences of the United States of America*, *118*(10), e2022701118. https://doi.org/10.1073/pnas.2022701118

Zamboni, V., Armentano, M., Berto, G., Ciraolo, E., Ghigo, A., Garzotto, D., Umbach, A., DiCunto, F., Parmigiani, E., Boido, M., Vercelli, A., El-Assawy, N., Mauro, A., Priano, L., Ponzoni, L., Murru, L., Passafaro, M., Hirsch, E., & Merlo, G. R. (2018). Hyperactivity of Rac1-GTPase pathway impairs neuritogenesis of cortical neurons by altering actin dynamics. *Scientific Reports*, *8*(1), 7254. https://doi.org/10.1038/s41598-018-25354-3

Zamboni, V., Armentano, M., Sarò, G., Ciraolo, E., Ghigo, A., Germena, G., Umbach, A., Valnegri, P., Passafaro, M., Carabelli, V., Gavello, D., Bianchi, V., D'Adamo, P., de Curtis, I., El-Assawi, N., Mauro, A., Priano, L., Ferri, N., Hirsch, E., & Merlo, G. R. (2016). Disruption of ArhGAP15 results in hyperactive Rac1, affects the architecture and function of hippocampal inhibitory neurons and causes cognitive deficits. *Scientific Reports*, *6*, 34877. https://doi.org/10.1038/srep34877

Zamboni, V., Jones, R., Umbach, A., Ammoni, A., Passafaro, M., Hirsch, E., & Merlo, G. R. (2018). Rho GTPases in Intellectual Disability: From Genetics to Therapeutic Opportunities. *International Journal of Molecular Sciences*, *19*(6), 1821. https://doi.org/10.3390/ijms19061821

Zechel, S., Nakagawa, Y., & Ibáñez, C. F. (2016). Thalamo-cortical axons regulate the radial dispersion of neocortical GABAergic interneurons. *eLife*, *5*, e20770. https://doi.org/10.7554/eLife.20770

Zhang, K., Wang, Y., Fan, T., Zeng, C., & Sun, Z. S. (2022). The p21-activated kinases in neural cytoskeletal remodeling and related neurological disorders. *Protein & Cell*, *13*(1), 6–25. https://doi.org/10.1007/s13238-020-00812-9

Zhou, Q., Xiao, M., & Nicoll, R. A. (2001). Contribution of cytoskeleton to the internalization of AMPA receptors. *Proceedings of the National Academy of Sciences of the United States of America*, *98*(3), 1261–1266. https://doi.org/10.1073/pnas.98.3.1261